The Dissertation Committee for Craig William Cone Certifies that this is the approved version of the following dissertation:

Analyzing photochemical and physical processes for organic materials

Committee:

David A Vanden Bout, Supervisor

Keith J. Stevenson

Peter J. Rossky

Lauren J. Webb

Thomas M. Truskett

Analyzing photochemical and physical processes for organic materials

by

Craig William Cone, BS

Dissertation

Presented to the Faculty of the Graduate School of

The University of Texas at Austin

in Partial Fulfillment

of the Requirements

for the Degree of

Doctor of Philosophy

The University of Texas at Austin

December, 2010

Dedication

To my wife, for being the yin to my yang.

Also, to my family and friends. I love you equally in R^2 but uniquely in θ and ϕ.

Acknowledgements

This work represents a collaboration that involves many people that are both great intellectual colleagues and good friends. First and foremost I would like to thank Dr. David Vanden Bout for his guidance, thoughtful analysis, support and leadership throughout the entire graduate school process. Having him advise me was one of the single best choices I made. I worked directly with David Ostrowski on numerous sections of this manuscript. He was invaluable and took all but one AFM that is featured in this manuscript and has been my kind hearted alter ego all along. Dr. Lynn Rozanski was helpful in regards to doing lots of the fundamental work in the green emission of polyfluorene section. I published a paper with two of my best friends Dr. Lilia Kondrachova and Dr. R. Alan May where I fit data associated with insertion of lithium atoms into metal oxides to extract diffusion coefficients. I worked with Dr. Sangik Cho on ZINDO/S calculations for different species that were extracted from J-Aggregate oxidation chemistry. Dr. Jennifer Lyon and Dr. Dorthe Eisele were also necessary for any of that work to ever see the light of day. Ryan Cheng was good enough to calculate the Langevin dynamics of homopolymers for the beta phase polyfluorene work. I had the pleasure of working with the Welch summer scholar program, Abigail Wolf and Samuel Lee who were both integral help during their short but productive times. Josh Biberdorf synthesized all of the polymers and block copolymers for the glass transition measurements.

People with whom I worked in some capacity but never published any work, still merit recognition. I could write paragraphs about how each of them was supremely helpful but that would wander and be overly mushy. Katie A. Clark, Micah S Glaz, Jon J.

Analyzing photochemical and physical processes for organic materials

Publication No._____

Craig William Cone, Ph. D.

The University of Texas at Austin, 2010

Supervisor: David A Vanden Bout, Ph. D.

Since their discovery, organic electronic materials have been of great interest as an alternative active layer material for active area materials in electronic applications. Initially studied as probes or lasing material the field has progressed to the point where both conjugated polymers and small organics have become fashionable objects of current device oriented solid state research. Organic electronic materials are liquid crystalline materials, packing into well-ordered domains when annealed thermally or via solvent annealing. The macromolecular orientation of the molecules in the solid state causes a shift in the electronic properties due to coupling of the dipoles. The amount of interaction between molecules can be correlated to different nanoscale morphologies. Such morphologies can be measured using microscopy techniques and compared to the spectroscopic results. This can then be extrapolated out to infer how the charges move within a film. Cyanine dyes represent an interesting form class of dyes as the molecular packing is strongly affected by hydrophilic and hydrophobic pendent groups, which cause the dye to arrange into a tubular bilayer. Spectroelectrochemistry is used to monitor and

controllably oxidize the samples. Using singular value decomposition (SVD) it is possible to extract each electronic species formed during electrochemical oxidation and model the proposed species using semi empirical quantum mechanical calculations. Polyfluorene is a blue luminescent polymer of interest for its high quantum yield. The solution and solid-state conformation has shown two distinct phases. The formation of the secondary phase shows a dependence on the molecular weight. In a poor solvent, as the molecular weight increases, the secondary phase forms easier. In the solid state, the highly efficient blue emission from polyfluorene is degraded by ketone defects. The energy transfer to preexisting ketone defects is increased as the filmed is thermally ordered. Glass transitions of block copolymers are studied using synthetically novel polymers where an environmentally sensitive fluorescent reporter is placed within various regions of a self-assembled film. Different dynamics are observed within the block of the film then specifically at the interface of two blocks.

Table of Contents

List of Tables

List of Figures

Chapter 1: Introduction to Disertation: Analysis of photochemical and physical processes for organic semi-conducting materials using singular value decomposition

CHAPTER 1: DISSERTATION OVERVIEW

As society increases in complexity, the range of energy demands also increases. Currently the most feasible way to meet current and future energy problems is moderate increases in current systems through material design and implementation of new materials to compete with current systems. Organic semi-conducting materials represent a great opportunity to meet a specific portion of the energy demand of a modern society. This is attainable since as organic electronic materials have specific inherent advantages over their inorganic counterparts; specifically, organic materials are cheaper to fabricate. Organic semi-conducting devices can be created from solution and do not require expensive ultra-high vacuum techniques to fabricate. One application of organic semi-conducting materials is as a photovoltaic material. Traditional materials for photovoltaic materials are silicon based, though many materials have been proposed and implemented with some success. As an alternative to silicon based materials there are specific advantages of organic materials. Organic materials have a higher molar absorptivity than silicon materials; as such, fewer materials are required to generate the same amount of excited states. The exact levels of the highest occupied molecular levels (HOMOs) and lowest unoccupied molecular levels (LUMOs) can be specifically modulated to maximize the amount of potential energy extractable from any given system. The mixing of donor/acceptor materials enables an area of study that is not easily attainable in

traditional inorganic devices. Of specific interest is the interfacial region where charge separation occurs. The difference in, as well as the absolute, energies are both important. Energy differences greater than the Coulombic binding energy (~0.1-0.3 eV) are required to make charge separation energetically favorable but contrasting that with loss of potential power as the donor HOMO and acceptor LUMO which limit the potential energy which can be extracted from any functional device. The last important factor is morphology. Not only do excited states need to be created and separated, they need to be collected at electrodes via an interpenetrating network from the point of charge separation. All three of these important factors interplay to determine the overall efficiency of the organic solar cell.

The failure mechanism for organic solar cells is very different from that of inorganic based devices. Material failure in inorganic devices is due to mechanical stress, dangling bonds and creation of electronic traps. In organic materials, there are deleterious side reactions that occur in the excited state with molecular oxygen, termed photochemistry, which alter the electronic properties of the material and inhibit charge separation. The failure of materials (or organic devices) due to oxidative processes is a vital component which needs to be further studied using nanoscale characterization techniques for semiconducting materials to positively affect the long-term economic viability of materials. The chemical and morphological changes are of specific interest for this system. Changes to the system are probed by measuring the electronic absorption spectra.

This thesis will broadly examine physical properties of organic molecules in general very different settings. The first context is understanding redox chemistry in artificial light harvesting antenna. The second context is examining chemistry and morphology changes in polyfluorene. The third context is examining mobility of

interfacial regions in block copolymer systems. Singular value decomposition will be used to examine spectral changes associated with the chemistry of each process.

Polyfluorene

Phenylene-based polymers are one of the most important classes of conjugated polymers and have been the subject of extensive research as active materials for organic electronics and polymer lasers.[1-14] Polyfluorenes are the simplest regular stepladder-type polyphenylenes in which every second ring is bridged. Polyphenylenes have been of particular interest as they are high quantum yield[15, 16] [17] (x>90%) blue light emitting materials. Polyfluorenes are also an attractive material for further research as they are easily modified synthetically and the synthesis proceeds in high yield.[18-23] The unique electronic properties arise from the conjugated backbone, whereas the solubility of the molecule comes from the hydrocarbon chains that extend from the bridge for the backbone. There are several factors that must be met for a luminescent material to function. The first point is the energy at which the material emits is primarily dependent on the HOMO/LUMO energy gap. This can be modulated synthetically by copolymerizing the repeat unit which affects the energy levels.[24-29] In the solid state, however, the energy gap is also affected by interactions between the polymer chains, which leads to shifts in energy levels. This can be controlled by modulating the chains and conjugated backbone to affect the aggregation, which causes the shift to lower energy emission. The molecular weight and defects, through synthetic methods, can drastically change the material property, which affects the total efficiency and viability of the material properties to meet specific demands of the particular usage.

While polyfluorene monomer can be synthetically copolymerized for specific applications, chain conformation and stacking effects can also be manipulated to create

specific electronic properties as well. The main electronic absorption of polyflourenes are characterized by a broad main peak in the blue region (~400nm) of the visible spectrum. The secondary electronic properties when the polymer is in a different physical conformation can clearly be observed as a red shifting of the electronic emission.[30] The beta phase of polyfluorene has had several advantageous observed physical properties compared to the primary phase. Beta phase polyfluorene has been an observed to strongly trap electrons and increase hole mobility to double the observed mobility of pristine polyfluorene.[12, 31-33] Also, the Forster energy transfer to the beta phase competes against undesirable excimer formation in pristine polyfluorene. The beta phase can be studied in solution as a function of the many available synthetic handles, as well as in the solid state using optical microscopy to individually probe disbursed nanowires of polyfluorene to build up a data set different from the bulk polyflourene values. [34]

Glass transitions of polymer materials

Glassy polymers as we know them today were developed in the 1950s and were originally considered a replacement for cellulosic esters that had been introduced substantially earlier.[35, 36] The most important glassy polymer is polystyrene (PS); although it is more brittle than its predecessors, it could be produced cheaply under simple processing conditions. Along with poly(methyl methacrylate) (PMMA), PS is the main academic system for physical properties of glassy polymer studies. Glassy polymer systems have desirable optical properties and use in thermoforming and molding applications. Many materials, not only polymers, may be found in the glassy state. The simplest way to consider the transition to the glassy state is through the rapid increase in viscosity that occurs when liquids are cooled and when crystallization does not occur.

Most organic compounds will crystallize upon cooling below their melting temperature, but in more complex materials, such as polymers, the rate of crystallization may be slow enough that a glass is formed before the material has crystallized. The glassy state of a material can be characterized through the changes that occur as it is cooled past its melting point. The viscosity of the liquid increases rapidly as the temperature decreases to the point where the rearrangement of the molecules timescale has increased beyond the timescale of the experiment.[37-39]

The physical properties of the melt material, such as the Young's Moduls, specific heat capacity and thermal expansion coefficient, have been characterized for the bulk materials and bulk values. Physical properties of polymer materials are traditionally characterized through experimental methods such as wide angle X-ray scattering, differential scanning calorimetery, small angle x-ray scattering, dynamic mechanical thermal analysis, Fourier transform IR spectroscopy, nuclear magnetic resonance spectroscopy, transmission electron microscopy and molecular dynamics simulations. [40-43]

Block copolymers are unique macromolecules that enable the structural and processing properties of distinct materials which can be combined by covalently binding two different repeat units in a polymeric material.[44, 45] Depending on the energetic interaction between the repeat units and the ratio of the repeat units within the system, the material can strongly phase segregate or form an intermixed composition material.[46-48] Block copolymer systems that self-assemble have material properties of both blocked groups. However, many deviations for the bulk values have been observed based on several known factors.[49-51] These factors include thickness of material, nanoscale ordering, edge affects, and free volume differences. However, little has been done to systematically characterize the glass transitions on the nanometer length scale. This can

be done by synthetically inserting a single fluorescent probe into a block copolymer system. The area of specific interest when studying block copolymers is the interfacial region. The fluorescent probe reports on the local dynamics it experiences, and when the reporter molecule is held exactly at the interface, it can then be compared to when the reporter is located in a region rich in either material. An experiment where only the interface is being interrogated with the possibility of monomer resolution (x= ~0.6 nm) has never been proposed previously.

Singular Value Decomposition

Singular value decomposition (SVD) is a linear algebra technique for the factorization of a rectangular matrix.[52-54] The method has several applications in signal processing and statistics where the pseudoinverse least square fitting of data and matrix approximation.[55-57] This method allows for efficient ways to analyze multivariate global data. For experiments that generate large amounts correlated data, thousands to hundreds of thousands of data points, SVD is particularly useful as it provides a quantitative value for the representation of every component to the total data. This allows for detection and characterization of very small or subtle signals to be drawn out of large sets of data.[58-62]

To complete a singular value decomposition for a given set of data. Let X denote an m x n matrix of real-valued data and rank r, where without loss of generality m≥n, and therefore $r \leq n$. In the case of microarray data, x_{ij} is the expression level of the ith spectral point in the jth measurement. The elements of the ith row of X form the n-dimensional vector $\mathbf{g}_i$, which we refer to the spectral point at i^{th} wavelength. Alternatively, the elements of the jth column of X form the m-dimensional vector $\mathbf{a}_j$, which we refer to the spectra taken at the jth time.

The equation for the singular value decomposition of X is the following: $X = USV^T$ where U is an m x n matrix, S is an n x n diagonal matrix, and V^T is also an n x n matrix. The columns of U are called the left singular vectors, $\{\mathbf{u}_k\}$, and form an orthonormal basis for the wavelength dependent spectral features, so that $\mathbf{u}_i \mathbf{x} \mathbf{u}_j = 1$ for $i = j$, and $\mathbf{u}_i \mathbf{x} \mathbf{u}_j = 0$ for $i \neq j$. The rows of V^T contain the elements of the right singular vectors, $\{\mathbf{v}_k\}$, and form an orthonormal basis for the time dependence of each spectral feature. The elements of S are only nonzero on the diagonal, and are termed the singular values.

This purely mathematical deconvolution of matrix of data allows for large data sets to be broken into time-dependent and time independent components, separately modeled using assumptions from other coupled experiments and the best possible least squared fit returned with any desired amount of accuracy. This can be obtained by adding components to the model until the accuracy criteria is met, as the sum of the squared singular values included compared to the total of the squared singular values. This is equivalent to the amount of data being represented in the model. [63, 64]

CHAPTER 2: SVD ECHEM AND SVD OF OXIDATION

In chapter 2 singular value decomposition (SVD) is used to characterize spectralelectrochemical oxidation of molecular dye aggregates. The spectroscopy of the electrochemistry of amphaphilic tubular bilayer cyanine dye aggregates is non-trivial to analyze and poorly understood. SVD can be used to correlate time dependent and wavelength kinetics since the experimental setup is designed to simultaneously collect spectroscopic and electrochemical data. Using SVD to completely model time dependent and independent traces means one of the components must be known. In this specific case, the kinetics can be directly created from the electrochemistry data. The current data

was used to directly create models of time dependent kinetics. From the time dependent models, the spectral feature associated with each modeled trace can be exactly calculated. The spectra associated with each species during the reduction oxidation cycle were previously unavailable. The product of the SVD analysis of each individual species can be verified using quantum mechanical methods. ZINDO/S was used to calculate each species' absorption that contributes scientifically to the model. The agreement between the two independent methods leads to more confidence in the conclusions.

CHAPTER 3: PFO BETA PHASE

The beta phase of polyfluorene is a topic of research interest in organic electronic materials. The beta phase of polyfluorene is poorly understood as to how it forms and what environmental and synthetic factors are required for optimum creation of beta phase in solution. With unique synthetic batches of polyfluorene, which contain different molecular weight distributions and defect concentrations, it is possible to draw correlation with the temperature dependence of the beta phase formation in poor solvents. The formation of beta phase in polyfluorene has to be measured using a poor solvent, as beta phase is never observed in freely solvated polymer. Temperature dependent excitation fluorescence spectra were collected as samples were cooled to observe the unique secondary electronic absorption and quantified as a function of temperature. Each batch of polyfluorene showed a unique temperature and total amount of beta phase formed. To isolate molecular weight as a function of beta phase formation, temperature samples were size-separated with gel permeation chromatography. The dependence of molecular weight on the formation of beta phase was then directly observed. Observation was then verified using molecular dynamics simulations of bead and spring modules

using simulated annealing to calculate the radius of gyration as the molecular weight was modulated. For the correlation of the simulated collapse of the polymer globules to formation of beta phase it can then be shown that the beta phase of polyfluorene does arise from the collapse of freely solvated chains into globules.

CHAPTER 4: PFO GREEN EMISSION

Oxidative defects which lead to failure in organic electronics are of interest. Oxygen defects at the bridge point of polyfluorene repeat unit can be identified spectroscopically by low energy fluorescence emission. The energy transfer to the low energy defects can also be measured as the morphology is measured. If the polymer is heated above the glass transition temperature and allowed to crystallize, the morphology is substantially altered. The morphology of spincast and annealed films can be verified and imaged using atomic force microscopy. If there are no defects present, the ordering of the film does not create low energy emissive defects. If defects are first present, then the films of polyfluorene are aligned and the green emission increases substantially. The amount of change in spectral features can be quantified and characterized using singular value decomposition. The excited state energy transfer length increases at a decreasing rate as the defect concentration increases, which implies that the quenching radius for the defects are beginning to overlap. The link between nanoscale morphology and electronic properties for organic electronic materials is important as the field of organic devices continues to develop and compete with inorganic silicon based devices.

9

Chapter 5: Self-assembly of Block Co Polymers and Effect on Glass Transition Measurements

Self-assembly of block copolymers and the effect on glass transition temperature with a covalently bound twist induced charge transfer (TICT) reporter molecule is the topic of this chapter. Glass transitions (T_g) in block copolymers is an important and unexplored topic of research in condensed matter physics. Several deviations from the bulk values of T_g have been observed due to several factors. In this chapter the effect of self-assembly of ….be more specific here is probed. With synthetically novel block copolymers it is possible to perform the first measurements of the local environments in specific regions of block copolymer films. Ring opening metathesis polymerizations (ROMP) were performed with unique pendant groups to create a system that had a low temperature and a higher temperature crystallizing material bound to each repeat unit in a block copolymer configuration. A fluorescent reporter molecule was covalently bound to either a certain region of each block or at the interface of the block. The films were self-assembled using solvent annealing in o-DCB for one week. The self-assembly could be imaged and visualized using AFM; films that were annealed were found to be more ordered and have smaller domains than dropcast films.

Glass transition temperatures were observed for the TICT molecule mixed with homopolymers of either pendant material. These values were then compared to the differential scanning calorimeter (DSC) results as well as the temperature when the TICT reporter was covalently bound to the homopolymer. The glass transition measurements of the block copolymer system where the dye was covalently bound in region A or B were compared to the annealed films the local environments were found to have changed in both cases. Dye is bound at the interface the unordered film is found to have very different environment than the ordered film in which the dye is found to experience both

glass transitions. The amount of intermixing of polymers can be measured through the temperature dependent dynamics that the local probe reports on for each environment.

CHAPTER 6: BLOCK CO POLYMER GLASS TRANSITION MEASUREMENTS

Self-assembled block copolymers were studied using a twist induced charge transfer reporter to report on local dynamics in chapter 6. Local molecular dynamics of unique block copolymer films were studied through synthetic placement of a molecular rotor dye onto specific locations within the block co-polymer chain. Temperature dependent fluorescence measurements were collected from the different block copolymer systems after formation of self-assembled thin film morphologies which were identified with atomic force microscopy. The dynamics of the covalently bound probe placed precisely at the interface of the polymer blocks was found to be distinct from either bulk material. The glass transition temperature for each material was determined using finite difference. Dynamics of self-assembled block copolymers with the dye bound in one specific region were found to be different than that of the dye at the interface and that of the dynamics of the dye when bound to homopolymers.
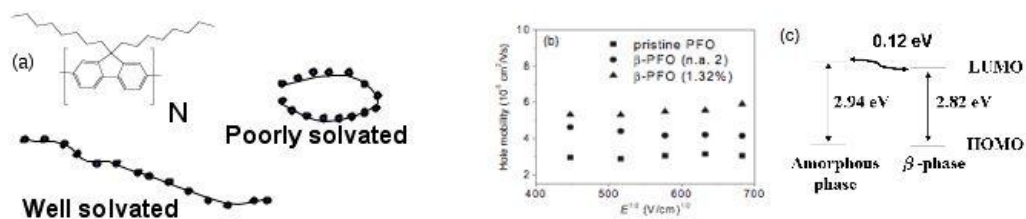
Figure 1: (a.) The chemical structure of polyfluorene is shown as well as the schematic view of the alpha and beta phase. **(b.)** Shows the increase in experimentally observed hole mobility of devices with increasing composition of beta phase. **(c.)** Shows the electronic energy level spacings and differences in alpha and beta phase polyfluorene.
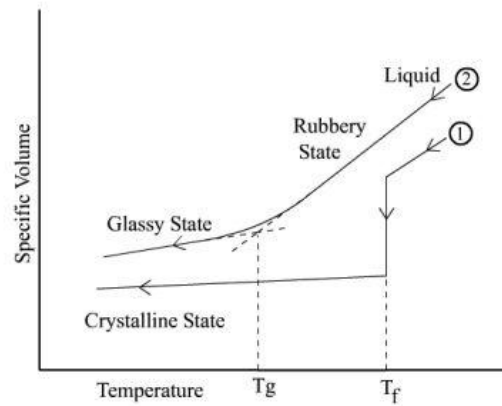
Figure 2: Shows the thermodynamic states available to a material as it cools from a high temperature above its freezing point. The material either crystallizes or forms a rubbery and then glassy state, as is the case with the many organic materials including the materials of interest.
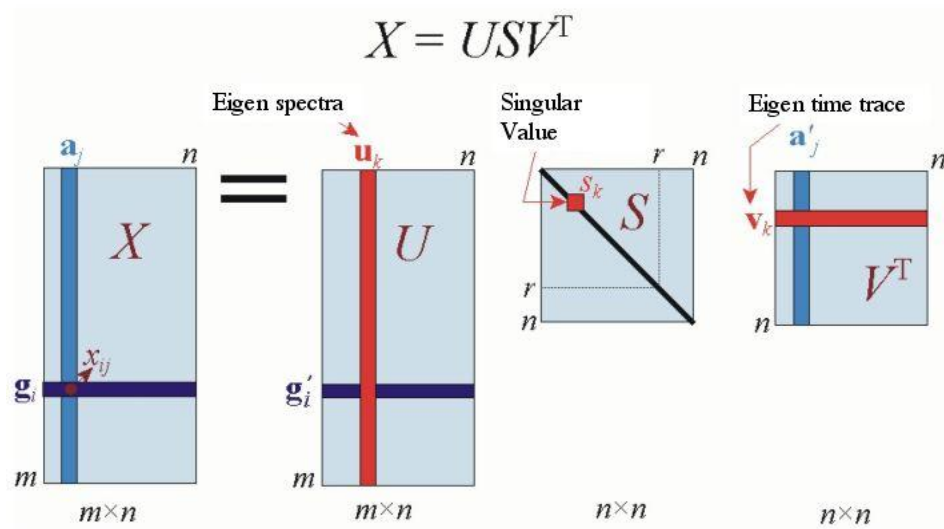
Figure 3: The general graphical representation of what occurs during a singular value decomposition.

REFERENCES

1.   Leclerc, M., *Journal of Polymer Science Part A: Polymer Chemistry* **2001,** *39* (17), 2867-2873.

2.   Grell, M.; Bradley, D. D. C.; Long, X.; Chamberlain, T.; Inbasekaran, M.; Woo, E. P.; Soliman, M., *Acta Polymerica* **1998,** *49* (8), 439-444.

3.   Liu, L.; Qiu, S.; Wang, B.; Wang, H.; Xie, Z.; Ma, Y., *J. Phys. Chem. C* **2009,** *113* (14), 5799-5804.

4.   Grell, M.; Bradley, D. D. C.; Inbasekaran, M.; Ungar, G.; Whitehead, K. S.; Woo, E. P., I *Synthetic Metals* **2000,** *111-112*, 579-581.

5.   Gadermaier, C.; Luer, L.; Gambetta, A.; Virgili, T.; Zavelani-Rossi, M.; Lanzani, G. In *Photophysics in semiconducting polymers: the case of polyfluorenes*, Wiley-VCH Verlag GmbH & Co. KGaA: 2007; pp 205-234.

6.   Barbara, P. F.; Gesquiere, A. J.; Park, S.-J.; Lee, Y. J., *Accounts of Chemical Research* **2005,** *38* (7), 602-610.

7.   Beenken, W. J. D.; Pullerits, T., *J. Phys. Chem. B* **2004,** *108* (20), 6164-6169.

8.   Chochos, C. L.; Kallitsis, J. K.; Keivanidis, P. E.; Baluschev, S.; Gregoriou, V. G., *J. Phys. Chem. B* **2006,** *110* (10), 4657-4662.

9.   Sek, D.; Iwan, A., *Recent Res. Dev. Polym. Sci.* **2004,** *8*, 67-86.

10.   Caricato, A. P.; Anni, M.; Manera, M. G.; Martino, M.; Rella, R.; Romano, F.; Tunno, T.; Valerini, D., *Applied Surface Science* **2009,** *255* (24), 9659-9664.

11.   Brookins, R. N.; Schanze, K. S.; Reynolds, J. R., *Macromolecules* **2007,** *40* (10), 3524-3526.

12.   Cadby, A.; Dean, R.; Fox, A. M.; Jones, R. A. L.; Lidzey, D. G., *Nano Lett.* **2005,** *5* (11), 2232-2237.

15

13. Janietz, S.; Bradley, D. D. C.; Grell, M.; Giebeler, C.; Inbasekaran, M.; Woo, E. P., *Applied Physics Letters* **1998,** *73* (17), 2453-2455.

14. Klaerner, G.; Miller, R. D., *Macromolecules* **1998,** *31* (6), 2007-2009.

15. Abe, M.; Yamamoto, T., *Synth. Met.* **2006,** *156* (16-17), 1118-1122.

16. Cheun, H.; Tanto, B.; Chunwaschirasiri, W.; Larson, B.; Winokur, M. J., *Applied Physics Letters* **2004,** *84* (1), 22-24.

17. Chen, P.; Yang, G.; Liu, T.; Li, T.; Wang, M.; Huang, W., *Polym. Int.* **2006,** *55* (5), 473-490.

18. Mikroyannidis, J. A.; Fenenko, L.; Adachi, C., S *J. Phys. Chem. B* **2006,** *110* (41), 20317-20326.

19. Huang, L.; Wu, S.; Qu, Y.; Geng, Y.; Wang, F., *Macromolecules* **2008,** *41* (22), 8944-8947.

20. Weinfurtner, K.; Fujikawa, H.; Tokito, S.; Taga, Y., *Applied Physics Letters* **2000,** *76* 2502.

21. Grisorio, R.; Mastrorilli, P.; Nobile, C. F.; Romanazzi, G.; Suranna, G. P.; Gigli, G.; Piliego, C.; Ciccarella, G.; Cosma, P.; Acierno, D.; Amendola, E., *Macromolecules (Washington, DC, U. S.)* **2007,** *40* (14), 4865-4873.

22. Grisorio, R.; Piliego, C.; Cosma, P.; Fini, P.; Mastrorilli, P.; Gigli, G.; Suranna, G. P.; Nobile, C. F., *Tetrahedron* **2008,** *64* (37), 8738-8745.

23. Jaramillo-Isaza, F.; Turner, M. L., S*J. Mater. Chem.* **2006,** *16* (1), 83-89.

24. Da Como, E.; Becker, K.; Feldmann, J.; Lupton, J. M., *Nano Letters* **2007,** *7* (10), 2993-2998.

25. Biagioni, P.; Celebrano, M.; Zavelani-Rossi, M.; Polli, D.; Labardi, M.; Lanzani, G.; Cerullo, G.; Finazzi, M.; Duo, L., *Appl. Phys. Lett.* **2007,** *91* (19), 191118/1-191118/3.

26. Chunwaschirasiri, W.; Tanto, B.; Huber, D. L.; Winokur, M. J., *Physical Review Letters* **2005,** *94* (10), 107402.

27. Bright, D. W.; Dias, F. B.; Galbrecht, F.; Scherf, U.; Monkman, A. P., *Advanced Functional Materials* **2009,** *19* (1), 67-73.

28. Zhou, X.-H.; Zhang, Y.; Xie, Y.-Q.; Cao, Y.; Pei, J., *Macromolecules* **2006,** *39* (11), 3830-3840.

29. Caruso, M. E.; Anni, M., *Physical Review B* **2007,** *76* (5), 054207.

30. Azuma, H.; Kobayashi, T.; Shim, Y.; Mamedov, N.; Naito, H., *Organic Electronics* **2007,** *8* (2-3), 184-188.

31. Rozanski, L. J.; Cone, C. W.; Ostrowski, D. P.; Vanden Bout, D. A., *Macromolecules* **2007,** *40* (13), 4524-4529.

32. Chochos, C. L.; Kallitsis, J. K.; Gregoriou, V. G., *J. Phys. Chem. B* **2005,** *109* (18), 8755-8760.

33. Kitts, C. C.; Vanden Bout, D. A., *Polymer* **2007,** *48* (8), 2322-2330.

34. Lupton, E. M.; Chen, L.; Liu, F., *The Journal of Physical Chemistry Letters* **2010,** *1* (9), 1326-1331.

35. Wood, L. A., *Journal of Polymer Science* **1958,** *28* (117), 319-330.

36. Allen, C.; Maysinger, D.; Eisenberg, A., *Colloids and Surfaces B: Biointerfaces* **1999,** *16* (1-4), 3-27.

37. Bates, F. S.; Fredrickson, G. H., *Annual Review of Physical Chemistry* **1990,** *41* (1), 525-557.

38. Lehn, J. M., *Angew. Chem.* **1990,** *102* (11), 1347-62 (See also Angew Chem., Int Ed Engl., 1990, 29(11), 1304-19).

39. Chiper, M.; Winter, A.; Hoogenboom, R.; Egbe, D. A. M.; Wouters, D.; Hoeppener, S.; Fustin, C.-A.; Gohy, J.-F.; Schubert, U. S., *Macromolecules (Washington, DC, U. S.)* **2008,** *41* (22), 8823-8831.

40. van Dijk, M. A.; van den Berg, R., *Macromolecules* **1995,** *28* (20), 6773-6778.

41. Khokhlov, A. R.; Grosberg, A. Y.; Pande, V. S., *Statistical Physics of Marcromolecules (Polymers and Complex Material)*. 1st ed.; American Institute of Physics: 2002; p 384.

42. Park, C.; Yoon, J.; Thomas, E. L., E*Polymer* **2003,** *44* (22), 6725-6760.

43. Segalman, R. A.; McCulloch, B.; Kirmayer, S.; Urban, J. J., *Macromolecules* **2009,** *42* (23), 9205-9216.

44. Gaur, U.; Wunderlich, B., *Macromolecules* **1980,** *13* (6), 1618-1625.

45. Leibler, L., *Macromolecules* **1980,** *13* (6), 1602-1617.

46. Ohta, T.; Kawasaki, K., *Macromolecules* **1986,** *19* (10), 2621-2632.

47. Wittkop, M.; Hˆlzl, T.; Kreitmeier, S.; Gˆritz, D., *Journal of Non-Crystalline Solids* **1996,** *201* (3), 199-210.

48. Hall, D. B.; Hooker, J. C.; Torkelson, J. M., *Macromolecules* **1997,** *30* (3), 667-669.

49. Ellison, C. J.; Torkelson, J. M., *Nat Mater* **2003,** *2* (10), 695-700.

50. Beiner, M.; Huth, H., *Nat Mater* **2003,** *2* (9), 595-599.

51. Ellison, C. J.; Kim, S. D.; Hall, D. B.; Torkelson, J. M., *The European Physical Journal E: Soft Matter and Biological Physics* **2002,** *8* (2), 155-166.

52. Gruninger, J., *Opt. Eng.* **1985,** *24* (6), 991-5.

53. Frans, S. D.; Harris, J. M., *Anal. Chem.* **1985,** *57* (8), 1718-21.

54. Sun, T.; Zhang, Z. Y.; Grattan, K. T. V.; Palmer, A. W., *Rev. Sci. Instrum.* **1998,** *69* (4), 1716-1723.

55. Pribic, R., *Anal Biochem* **1994,** *223* (1), 26-34.

56. Krittanai, C.; Johnson, W. C., *Anal Biochem* **1997,** *253* (1), 57-64.

57. Chaudhari, A. J.; Darvas, F.; Bading, J. R.; Moats, R. A.; Conti, P. S.; Smith, D. J.; Cherry, S. R.; Leahy, R. M., *Phys Med Biol* **2005,** *50* (23), 5421-41.

58. Jager, S.; Han, M.; Lewis, J. W.; Szundi, I.; Sakmar, T. P.; Kliger, D. S., *Biochemistry* **1997,** *36* (39), 11804-10.

59. Li, Y.-X.; Liu, X.-F.; Wang, W.; Zhu, Y.-C., I *Guangpu Shiyanshi* **2002,** *19* (1), 31-35.

60. Zimanyi, L., *Biopolymers* **2002,** *67* (4-5), 263-6.

61. Bai, H.; Jiang, X.; Dong, S., *Jisuanji Yu Yingyong Huaxue* **2003,** *20* (6), 731-734.

62. Kamiyoshihara, T.; Kojima, M.; Ueda, K.; Tashiro, M.; Shimotakahara, S., *Biochem Biophys Res Commun* **2007,** *355* (2), 398-403.

63. Stamatopoulos, V. G.; Karras, D. A.; Mertzios, B. G., O *Meas. Sci. Technol.* **2009,** *20* (10), 104021/1-104021/9.

64. Zhao, Y.; Schmidt, M., *J. Appl. Crystallogr.* **2009,** *42* (4), 734-740.

Chapter 2: Singular Value Decomposition Analysis of Spectroelectrochemical Redox of Molecular Nanotubes

CHAPTER SUMMARY

The oxidation of cyanine dyes nanotubes are studied using spectroelectrochemistry. The results are analyzed using singular value decomposition (SVD) and semi empirical quantum mechanical calculations. Previously unavailable absorption spectra were modeled for each species at every point throughout the oxidation and reduction process. The expected absorption wavelengths of this species present throughout the electrochemical cycles were calculated using the semi-empirical method ZINDO/S. The spectral assignments from the proposed species derived from the SVD analysis were in agreement with ZINDO/S calculations, verifying the assignment of the key species as well as the intermediates in the reaction scheme. The oxidized species have spectral positions that agree with the calculated spectral maxima of isolated species, indicating that the resulting products are not electronically perturbed by aggregation.

INTRODUCTION

Supramolecular assemblies of pi-conjugated molecules are of broad interest as they can self-assemble in solution essentially building new materials from the bottom up.[1-4] The collective properties of these new materials are fundamentally different from the simple addition of the properties of the individual molecules. In particular, self-assembled quasi one-dimensional (1-D) organic nanostructures of π-conjugated molecules[4-24] are highly attractive for nanotechnological applications due to their unidirectional nature and potential for long range energy transport. A unique class of such systems are the double walled nanotubes formed from amphiphilic cyanine

dyes.[5,7,8,25] [18,26-33]   The tubular J-aggregates closely resemble the highly efficient antennae systems of green sulfur bacteria, which contain multi-layer tubules of aggregated bacteriochlorophyll (BChl).[34,35]   These and other nanostructured cylindrical tubes with extended electronic architectures are promising for artificial light harvesting applications.[28] The spectral signature of J-aggregated cyanine dye molecule and the schematic representation of the molecular packing can be seen in Figure 1.

In order to be useful for such applications it is critical to understand the oxidative chemistry of the materials to limit the effects of photo-oxidation.   The oxidative chemistry of the tubular cyanine aggregates also has a tangential scientific relevance as an active chemical template for the photoreduction of metal ions to form metallic nanostructures.[6]   While the oxidation chemistry can be studied in a number of application settings, the most controlled manner in which to probe the redox chemistry is to study the materials using electrochemistry. This has two key advantages: first, the electrical potential can be carefully controlled, yielding an unambiguous probe of the electronic states of the aggregates.   Second, the electrochemical current provides a direct measure of the chemical kinetics for the oxidation chemistry.   The molecular changes that occur during electrochemical oxidation can be probed by simultaneously monitoring the changes in the absorption spectrum as the potential is changed.   The combined spectroelectrochemical data yields a picture of the chemical changes of the aggregates during oxidation.

Previous spectroelectrochemistry experiments on double-walled aggregates of 3,3′-bis(2-sulfopropyl)-5,5′,6,6′-tetrachloro-1,1′-dioctylbenzimida-carbocyanine (C8S3) have shown that the oxidation leads to a number of new chemical products.[8]   Based on the electrochemical and spectral data, a scheme was proposed to observe and explain spectral changes upon oxidation (Scheme I).   The initial data

analysis relied on changes in specific peak wavelengths of the spectrum; however, the analysis is complicated because spectral changes result from the simultaneous loss of aggregate absorption and increased due to products. Since these species may have overlapping transitions, it is difficult to interpret all of the spectral variations by analyzing only individual wavelengths. Another method of data analysis is required to extract whole spectral features of the key chemical species and their intermediates.

Singular value decomposition (SVD) is a linear algebra technique that is capable of extracting the key spectral components that are changing in a series of spectra. As a general method, it has been known for over seventy years [36]. The computation of a singular value decomposition is a mathematical procedure that produces orthogonal component systems. In the case of kinetic spectroscopy the goal is to decompose the kinetic data into the spectra and kinetic traces for all the relevant chemical species. Initially the method is a decomposition, so there is no loss of data, only a recollection of the values based on mathematical factorization. Thus, if there are 500 original spectra the SVD will recast into 500 new basis spectra each of which will have its own kinetics; the new basis will be categorized by a numerical importance referred to as its singular value. The advantage of SVD is that it allows the data set to be reduced in size via elimination of the basis spectra that have singular values that are not significant. In this way SVD can not only reduce the size of the data set, but determine how many independent components represent the entire set of time resolved data[37].

SVD has been utilized to model a wide variety of different types of data.[36,38,39] However, for spectroscopic measurements it has been primarily used to analyze kinetic spectra. Typically, one must assume a model for the kinetics to extract the spectra of the different species in the data set. Alternatively, one can model the spectra to extract the relevant kinetics of each species. Spectroelectrochemistry and SVD are particularly well

suited as the kinetics of the experiments are directly measured by the current in the electrochemistry experiments. As such, the kinetic model is known from the outset and the SVD analysis yields spectra associated with each electrochemical change.

In the following paper we demonstrate the power of SVD to analyze spectroelectrochemical data by examining the oxidation of the nanotubular aggregates of C8S3 to identify the chemical species in the reaction. The assignment of each chemical species is verified through the use of semi-empirical quantum mechanical calculations to describe the major optical transitions for each species. The Zerner method of intermediate neglect of differential overlap for spectroscopy (ZINDO/S)[46] was used, as it has been demonstrated to accurately determine the electronic transition energies for a wide variety of different molecules. In addition to the semi-empirical methods, time-dependent density functional theory was also used to calculate the energy and oscillator strength of each possible transition. The combination of the SVD analysis and the quantum mechanical calculations allows for the extraction of spectra of all of the chemical species in the reaction, including short lived intermediates, even in the presence of complex spectral changes from species with overlapping absorbance.

EXPERIMENTAL SECTION

C8S3 J-Aggregate Preparation

The aggregate preparation and electrochemical methods were previously described and are included again here briefly. The amphiphilic cyanine dye 3,3-bis(2-sulfopropyl)-5,5,6,6-tetrachloro-1,1-dioctylben-zimidacarbocyanine (C8S3) was obtained as a sodium salt from FEW Chemicals (Dye S 0440, FEW Chemicals, Germany) and used as received. A 3.00 mM stock solution of monomeric C8S3 was prepared by dissolving C8S3 (MW 902.8 g/mol) in pure methanol (Fisher Scientific. To prepare

C8S3 J-aggregates, 130 μL of the C8S3 stock solution was added to 500 μL of ultrapure H_2O (>18.2 MΩ cm, Barnstead). The solution was stored in the dark for 24 h before adding an additional 500 μL of H_2O to stabilize the aggregation process, which resulted in a final dye concentration of 3.36×10^{-4} M.

Electrochemical Measurements

Electrochemical experiments were conducted on J-aggregates immobilized on transparent, conductive indium tin oxide (ITO)-coated glass electrodes (Delta Technologies, Ltd); 14 Ω/0 immersed in an aqueous solution containing 1 M KNO_3 supporting electrolyte (Fisher Scientific). The pH of this supporting electrolyte was 5.78. Films of J-aggregates were prepared on ITO by drop casting 10 μL of J-aggregate solution on a 0.5 cm^2 area of ITO followed by drying in the dark for 2 h. Once dried, they remained at the ITO surface when immersed in the supporting electrolyte.

ITO working electrodes, either bare or with dried J-aggregate films, were placed in a 20 mL glass cell containing 5 mL supporting electrolyte and a Au wire counter electrode, with the ITO surface oriented perpendicular to the bottom of the cell. For aqueous measurements of J-aggregates a Hg/Hg_2SO_4 (saturated. K_2SO_4) reference electrode (CH Instruments; E^o) +0.640 V (vs NHE) was used. Electrochemical measurements were performed at room temperature 23 (±2 ºC) using an Autolab PGSTAT30 potentiostat interfaced with Autolab GPES version 4.9 software. Prior to each experiment the cell was purged with Ar for at least 5 min. All electrode potentials are reported vs. Hg/ Hg_2SO_4.

SVD method

A time dependent spectral matrix was created that contained the absorption spectrum collect at different times during three electrochemical sweeps. The baselines of

the spectra were corrected by assuming that the absorbance was constant and zero at 650nm. Time points were selected such that the spectral measurements and electrical measurements were synchronous.

The singular value decomposition was performed using Wolfram Research Inc product Mathematica7. The program uses a QRD decomposition to arrive at a numerical solution for the mathematical factorization of the time dependent data matrix. After the singular value decomposition had been performed, spectra were determined using a kinetic model extracted from the electrochemical data. The spectrum associated with each kinetic trace was determined from a linear combination of kinetic basis spectra. This fitting was accomplished using a Monte-Carlo algorithm in Mathematica7. The algorithm minimizes the residual error and was run for ten million attempts to acquire the best possible representation of the kinetics using SVD basis.

Quantum chemistry method

For the quantum mechanical calculations, all spectra were assumed to result from individual molecular species rather than coupled chromphores in an aggregate. For simplicity, all of the octyl hydrocarbon and sulfate (SO_3^-) sidechains on the cynanine dye were replaced with hydrogen atoms as these groups do not significantly affect the absorption properties of the species. It should be noted that since the negative charge of the sulfate group was replaced with neutral hydrogen the model systems have different total charges than the corresponding electrochemical species. Possible equilibrium geometries of the dimer-like model systems were determined using the following scheme. The initial geometries were generated by assigning various dihedral angles to the bonds with rotational degrees of freedom. Then, the initial geometries were optimized for all

degrees of freedom using molecular mechanics with MMFF force field.[40-44] Those MMFF equilibrium geometries were then used as the initial geometry for semi-empirical quantum chemistry AM1 geometry optimization. To locate the equilibrium geometries, SPARTAN '02 program package [45] was used, for the radical species. Unrestricted Hartree-Fock (UHF) AM1 geometries from the SPARTAN '02 were examined for sensitivity by using them as the initial geometries for a semi-empirical restricted open-shell Hartree-Fock (ROHF) AM1 geometry optimization performed with GAMESS.[46] No significant differences were found between the UHF and ROHF AM1 geometries.

The vertical excitation energies and oscillator strengths of each model system were obtained by single point ZINDO/S[46]calculations on the set of stable geometries obtained for the model systems. ZINDO/S calculations were run using ArgusLab.[47] The single excitation configuration interaction active space included the 45 highest occupied molecular orbitals (HOMOs) and 45 lowest unoccupied molecular orbitals (LUMOs) for all conformer geometries of the model systems, except for the radical cation species that was studied. For comparative purpose, time-dependent density functional theory (TD-DFT) [48] calculations were performed, using GAMESS with the B3LYP exchange correlation functional and a 6-31G* basis for all atoms (H, C, N and Cl). Among the stable geometries obtained, the geometry with the lowest ground state energy from each model system was selected for TD-DFT calculation.

RESULTS AND DISCUSSION

During electrochemical oxidation the absorption spectrum of the C8S3 aggregates undergoes distinct changes.[49] Figure 2 summarizes the key spectra acquired during spectroelectrochemistry experiments. The cyclic voltamagram shows a distinct oxidation

peak at 0.75 V as the potential is swept positive. This peak is the result of the oxidation of the aggregates. This results in a loss of absorption from the two aggregate peaks in Figure 2A (absorption before oxidation) and Figure 2B (absorption after oxidation). The oxidation is irreversible on this time scale as no significant reduction peak is observed as the potential is swept back to its initial value. However, as the potential is swept negative a new redox species is noted. This species has a characteristic absorption as can be seen in figure 2C where a new absorption grows in around 560 nm. This absorption disappears as the species is reoxidized when the potential is swept back to the starting value. The spectrum after one full CV cycle is shown in Figure 2.

To better understand the changes during the electrochemistry, spectra acquired every 0.1V were analyzed for three full sweeps of the potential. As outlined above, rather than modeling the changes at each wavelength in the spectrum, the data was analyzed with SVD to extract the key spectral components and their kinetics. SVD decomposed the data set into three distinct pieces: a basis set of spectra that represent the key independent spectral features, a kinetics trace for each of these features describing its contribution to each time point in the kinetic data, and a singular value that ranks the importance of each basis spectrum to the total data set and provide an unbiased rationale for reduction of the basis set dimension. Figure 3 shows the six highest ranked basis spectra and their associated kinetics. Column I shows the basis spectra with the largest singular values. The first spectrum has the largest singular value with the values decreasing down the column. As the spectral features are merely a mathematical representation of the data they can have both positive and negative components and amplitudes in the second column. The first spectrum resembles the spectrum before oxidation (Figure 2). The column II of Figure 3 shows the kinetic traces associated with each base. The time associated with the sweep through the oxidation potential (0.75) is

27

noted by the dotted line on the graphs. Examination of the kinetics shows that there are two dominant features. The first is the spectral change at the oxidation potential and the second is a reversible change associated with the potentials where the new redox species is formed. These are both seen most clearly in the kinetics for the first basis spectrum. There is a large change associated with the first oxidation followed by a reversible event. Then the pattern repeats for the final two sweeps of potential.

The SVD is simply a recasting of the original data into a new basis set and the desired absorption spectra for the different chemical species formed are linear combinations of these. Figure 4 shows the log of the singular values of the basis spectra plotted against the basis element number. The importance of each basis spectrum falls rapidly as expected. Hence, only the first six spectra were utilized for analysis; the sum of the squares of these six singular values represent 99.998 percent of all of the full sum.

To find the spectra of the species in the electrochemistry requires implementation of a kinetic model based on the measured kinetics of the reaction available from the CV data. The number of electrons per unit time extracted during the oxidation reaction can be obtained from the current at each potential. By integrating the current we know qualitatively how many molecules have reacted in each electrochemical step (assuming we know how many electrons are transferred per molecule). The kinetics can then be broken up into distinct electrochemical events to examine the spectral changes occurring during each reaction. For example, the kinetics of the initial oxidation can be modeled by integrating the current associated with the first oxidation peak. This will yield a plot of the total number of electrons transferred (molecules oxidized) as a function of time (potential). The time trace associated with this oxidation step is shown as the black line in Figure 5a. This line is obtained by integrating the current during regions I of the CV shown in Figure 2. Figure 5 also shows the potential as a function of time (red). When

the potential is swept through positive 0.25 V, there is a large change in the kinetics (Figure 5a).   The response is then flat until the potential is again swept to positive 0.25. The amplitude of the change is now significantly smaller; oxidation current on the second potential sweep is significantly reduced.   Finally, the third voltage sweep yields another small step at the same potential.   While the kinetic trace resembles a step function it is generated by integrating the CV peaks rather than from an idealized model.   For future reference the kinetics that models this initial oxidation step will be referred to as $\beta(t)$. The blue and gray curves on Figure 5a and 5b are the other electrochemical processes that are modeled.   The blue color curve in Figure 5a is the reduction and reversible oxidation of the new redox couple that is formed after oxidation of the aggregates.   Because this process is reversible, the specific reaction kinetics appears as a square wave.   Again, the shape is a direct integration of the current, this time in region II of the CV data, and will be labeled as $\chi(t)$.   In addition to the two main electrochemical kinetics, two more kinetic traces are included in the model in an effort to extract the spectra of any intermediates (Figure 5b).   These represent transient species that occur during the electrochemistry. The gray color curve shows a species that will be present during the oxidation or reduction of the new redox couple and is labeled $\beta'(t)$.   The dash blue curve is an intermediate in the aggregate oxidation and is labeled as $\chi'(t)$.   These kinetics were not derived from integration of the current, but rather were generated to resemble the transient peaks observed in the SVD kinetics.   A fifth model trace, $\alpha(t)$, was also included that represents the initial absorption spectrum.

Now that there is a kinetic model derived from the CV data, it can be used along with the SVD to obtain the spectra of the species that correspond to specific reaction kinetics.   The kinetics of the basis spectra can each be fit with a linear combination of the five kinetic traces in the model.   The spectra for each kinetic trace can then be

acquired in a standard fashion. The spectrum is a linear combination of the basis spectra where each is weighted by its singular value and the coefficient of the fit of that trace to the kinetics of that basis.

Figure 6 shows the spectra obtained for the each of the five kinetics traces. The top panel of Figure 6 shows the spectrum and kinetics associated with the first trace in the kinetic model $\alpha(t)$. This is the initial spectrum, the kinetics do change and is included as other of the others kinetic traces represent changes with respect to this spectrum. The second panel shows the spectrum of the changes associated with the oxidation at 0.25 V modeled as $\beta(t)$. Note this spectrum is shown as negative because it corresponds to a loss in absorption. This trace is not representative of any single species instead it is the spectrum of the changes that are occurring during oxidation of the aggregates. This kinetic trace represents the loss of the aggregate absorption simultaneous to the growth in the spectrum of any new species that is being formed. The third spectrum corresponds to the changes that are occurring during the reduction and oxidation of the new redox species with the kinetics $\chi(t)$. This is the loss of the product from the oxidation of the aggregates and the growth of the new species.

In addition to the kinetics that represent the two main electrochemistry events, there are two additions to the model that represent transient spectral changes that occur during the redox reactions. The fourth spectrum is that of the transient that is present during the initial oxidation , $\beta'(t)$. The last spectrum is the transient species that is present only during the oxidation of the aggregates, $\chi'(t)$.

Using an electrochemical scheme, we can interpret the molecular species that may give rise to these different spectra (see scheme 1). Previously it was proposed that the aggregates oxidized and formed a radical species that rapidly dimerized[49]. The new dimer was believed to have an oxidation potential that was smaller than that of the

30

aggregates and thus was rapidly oxidized itself. This second reduction was coupled to a loss of two protons from the oxidized dimer leading to a species that was referred to as the dehydrogenated oxidized dimer (DHD_{OX}). This is then the new redox active species that is subsequently reduced to DHD_{RED} when the potential is swept negative and the back to DHD_{OX} as the potential is swept positive again. The spectra associated with the kinetic traces then have the following interpretations. The static spectrum is simply the initial absorption spectrum of the aggregates. The spectrum associated with the aggregate oxidation, $\beta(t)$, is then the loss of the aggregate absorption plus the growth of any absorption that results from the DHD_{OX} species. The spectrum, $\chi(t)$, is the loss of the absorbance of DHD_{OX} and the growth of the absorbance of DHD_{RED}. The transient spectrum given by $\chi'(t)$ is the intermediate for this two electron reduction that is the one electron reduction product and the radical intermediate denoted as DHD_{INT}. Similarly the $\beta'(t)$ spectrum yields the intermediate to the aggregate oxidation step which is the spectrum of either the radical cation intermediate or the unoxidized dimer.

The spectra associated with the kinetics are always the difference between two spectra. In order to extract the spectra of the individual species we must have a starting point of the known spectrum of one species. The only species with a known absorption spectrum is the initial aggregate spectrum. Figure 7a shows an overlay of the initial aggregate spectrum and the β spectrum. The DHD_{OX} spectrum can be obtained from the difference in these two spectra and is shown in Figure 7c. The oxidation spectrum β and the initial aggregate spectrum were normalized to the peak at 590 nm that in previous work[49] was assigned to the outer wall of the aggregate. This had a result where difference spectrum had no negative features. The difference spectrum shows three key features. First there is a prominent peak remaining from the aggregate absorption at 599 nm that is generally attributed to the inner wall of the aggregate. Because the kinetic

31

model treats the aggregate as one species rather than inner and outer wall, the subtleties of the oxidation kinetics of the inner versus outer wall are not modeled here. Previously it was shown that the outer wall oxidizes more rapidly than the remaining inner wall. In addition to the inner wall, there are two new absorption peaks in the oxidized peak, one to the blue edge of the aggregate and one to the red edge. If we fit these absorbances maxima to Gaussians the fit has center wavelengths of 440 nm and 670 nm. These are the absorbances associated with the DHD^{4+} that was previously assumed to only absorb in the UV.[49]

The spectrum associated with the new redox couple DHD_{RED} can be extracted from the χ spectrum. Previously these species were shown to have an absorbance around 560 nm. The χ spectrum is the loss of the DHD_{OX} and the growth of DHD_{RED}. The absorbance of both species are modeled as Gaussians. To calculate the DHD_{OX} absorbance the same Gaussian peaks used to the fit the β spectrum are used again. For the DHD_{RED} a Gaussian at 560 nm is used. The model is shown in Figure 6a. A comparison of the model Gaussian spectra and the χ spectrum is shown in Figure 7c. The details of the inner and outer wall peaks are again not captured in detail, but the overall shape is well represented.

The other two kinetic traces in figure 7b are the absorption associated with the intermediate species. The χ' spectrum has an absorbance to the red of the aggregate at 720 nm. The the β' spectrum which is modeled with a trace that gains in intensity and immediately decreases does not have to be further decomposed as the time trace represents the oxidation from a +2 to a +3 species and then immediately from a +3 to a +4, species and vice versa on the reduction.

Semi-Emperical Calculations

In order to verify the spectral assignments, semi-empirical quantum calculations were performed to find the portions of the strong absorption lines associated with each species in the proposed electrochemical scheme. The method and modeling of compounds have been described earlier. The accuracy of the semi-empirical calculations was first tested by examining the spectrum of the unaggregated monomer dye. For the monomer, denoted as MON^+, there is only one major conformer. The single geometry ZINDO/S calculation on the optimized geometry gives an absorption band at 509 nm with strong oscillator strength (1.41), which is close to the experimentally determined absorption band peak of the unaggregated dye near 520 nm. Among the species in the proposed mechanism, this the only species for which the absorption spectrum can be measured outside the electrochemical experiment. For each species calculated various conformers were created with associated electronic transitions to more accurately model the process. Tables showing the conformer search results can be found in the supporting information while the most significant results have been summarized completely in table 1 and 2.

In the proposed mechanism, the first species to form is the radical dye generated by oxidation of the monomer. While the dye that is the source of the radical is electronically coupled to form a j-aggregate, we recall that the electronic spectrum of the radical and all subsequent species are calculated as isolated molecules. In the proposed mechanism, two of the radical that are generated for the dimer species. This is denoted in the model system as the 4+ dimer. This dimer can then go on to deprotonate to form the dehydrogenated to DHD_{ox}, which forms a reversible redox pair with DHD_{red}. However an alternative mechanism might be possible in which the DHD_{ox} species if formed without the 4+ dimer intermediate. Instead, the aggregated dye could dimerized to form a

33

dianion dimer denoted as the 2+ dimer. However, the AM1 geometry optimization on 2+ Dimer shows that it is not stable, as each monomer tends to separate. Therefore, the mechanism with intermediate *Dianion dimer* is not a feasible alternative.

Unlike the monomer, three equilibrium geometries of different conformers are located for the 4+ Dimer. However ZINDO/S calculation on each conformer revealed only small deviations in the spectra of the different geometries (See Table S2 and S5 in supporting information). For all the conformer the strongest absorption band and their wavelengths are close to the experimental absorption band of the unaggregated dye (520 nm). As such, the dimer is not readily observable in the experiment as it is both short lived and strongly overlapping any monomer component.

In the proposed mechanism the dimer is short lived as it rapidly deprotonates. Three different species were examined that correspond to the experimental species of the deprotonated dimer. In the model system, 4+ DHD corresponds to oxidized from DHD_{ox}, the 2+ DHD is the reduced form DHD_{red} and the 3+ DHD is the odd electron intermediate to these two DHD_{int}. The conformer search for 2+ DHD results in four equilibrium geometries (see table S2 in the supporting information). Of those four two of the conformers denoted as DHD^{2+}_1 and DHD^{2+}_2 are lower in energy by about 7 kcal/mol and are selected as the dominant conformers for which to calculate the spectra. Their absorption bands have several overlapping transitions that are clustered in energy. The main transitions are at 554 nm (S0$\rightarrow$S1) and 545 nm (S0$\rightarrow$S2) for DHD^{2+}_1 and 559 nm (S0$\rightarrow$S1) and 540 nm (S0$\rightarrow$S2) from DHD^{2+}_2 (see table S6). All of these transitions are of significant oscillator strengths and are close in energy to the absorption component which is experimentally assigned to *DHD_{red}* (560 nm).

The conformer search for 4+ DHD, which is the corresponding model system to *DHD_{ox}*, results in seven equilibrium geometries. The absorption bands for the

34

conformers differ slightly but the focus is again on the results for the two conformers with the lowest energies (DHD^{4+}_1 and DHD^{4+}_2) (see table S2). These two conformers are lower in energy than the others by more than 10 kcal/mol. There absorption bands with significant oscillator strength occur at 632 nm (S0$\rightarrow$S1), 496 nm (S0$\rightarrow$S3) and 423 nm (S0$\rightarrow$S7) for DHD^{4+}_1. For DHD^{4+}_2 the absorption bands at 623 nm (S0$\rightarrow$S1), 538 nm (S0$\rightarrow$S2), and 424 nm (S0$\rightarrow$S8) (see table S7 for full results). For both conformesr the spectrum predicts transitions around 625 nm as well as 425 nm. Therefore it would be reasonable to assign the experimental absorption component of 445 nm and 667 nm to *DHD_{ox}*. It would be worthwhile to note that both ZINDO/S and TD-DFT are useful for quantitatively estimating the transition energies and for qualitatively determining the strength of the electronic transition. It is not uncommon to observe that the relative intensity for two bands determined experimentally and computationally are not in agreement. The following is an example of that situation, the experimentally determined absorption component at 445 nm has stronger intensity than that at 667 nm, while the calculated oscillator strength of the 400 nm band calculated by ZINDO/S is nearly equivalent to the 600 nm band for both DHD^{4+}_1 and DHD^{4+}_2.

There are seven equilibrium geometries that emerge from the conformer search for 3+ DHD with UHF AM1. This is the species which is the corresponding model system to the odd electron intermediate species *DHD_{int}*. However, as ArgusLab does not allow ZINDO/S calculation for systems with an odd number of electrons, the spectra for this species were obtained with ZINDO/S calculations utilizing Hyperchem.[50] The calculated absorption spectra for all seven equilibrium geometries are not significantly different and the calculation results for the two conformers with the lowest ground state energies (DHD^{3+}_1 and DHD^{3+}_2) are given in SI Table 8a and 8b. It should be noted that in the table ZINDO/S calculation with active space of 15 HOMOs and 15 LUMOs are

presented in addition to ZINDO/S calculation with active space of 45 HOMOs and 45 LUMOs, which was used in the previous calculations. We focus again on the two conformer with the lowest energy which for the 3+ DHD systems are lower by more than 8 kcal/mol. (Table S2) No matter which conformer is examined, all show a transition with acceptable spin component and significant oscillator strength at a wavelength of 700 nm. The calculated results are also independent of which size of active space is used in the calculation. (see table S8)   These bands are close to the absorption component experimentally assigned to DHD_{int} (700 nm).

In summary, the semi-empirical calculations allow for verification of the assignments of chemical species to the spectra extracted in the analysis of the spectroelectrochemical data.   The calculations show excellent agreement with the experimentally derived spectra despite the fact that many of the chemical species have a range of potential conformations.   The most relevant absorptions for each conformer are shown in Table 1 along with oscillator strength and conformation.   These results are summarized in Table 2 where the experimentally assigned transitions extracted from the SVD analysis is compared with the model calculations.   Most interesting is that the spectra agree with the transitions for the individual molecular species indicating that the oxidized dye in the aggregates is not strongly coupled. This could be due to an increase in the separation between the molecules, a decrease in the strength of the individual optical transitions, or the presence of a distribution of molecules. The previous studies have also shown that after oxidation the nanotubes appear to have the same physical morphology indicating the oxidized dye remains in the nanotube and the dye remains tightly packed. However, their total oscillator strength of the transitions has diminished as noted by the decrease in the overall absorption of the sample.   Additionally, as the dye is oxidized the new species may not be packed as regularly as the unoxidized monomers because the

dimerized molecules are much less amenable to regular packing. Moreover, the chemistry may proceed in such a way as to create further oxidation products beyond the DHD$_{ox}$ as previously suggested.[7] Thus the lack of aggregated oxidized dye is likely the result of the smaller transition dipole moment, the reduced order in packing, and potential heterogeneity of the oxidized species.

CONCLUSIONS

The power of singular value decomposition to extract the spectra of different chemical species during electrochemistry is demonstrated with the analysis of the spectroelectrochemistry of nanotubular aggregates of amphiphillic cyanine dyes. The results verify the previously proposed oxidation scheme for the C8S3 nanotube system. The dye is first oxidized to a radical followed by an irreversible chemical/electrochemical step of dimerization, proton loss, and further oxidation to form the DHD$_{ox}$ species. The SVD results show several new transitions for the DHD$_{ox}$ that had been previously undetected due to strong spectral overlap with other species. Moreover, the analysis is able to extract the spectra associated with transient chemical intermediates which have been proposed but gone undetected. The assignments of all the chemical species were verified with semi-empirical quantum mechanical calculations. The key transitions calculated for all the species are in good agreement with the experimental spectra. The agreement of the calculations and the spectra also shows that the oxidized dye in the nanotubes are no longer exhibiting collective optical transitions.

Species	SVD	ZINDO/S
Monomer	520nm	509nm
DHD(4+)	442,661nm	490,630nm
DHD(2+)	560nm	540-560nm
DHD(3+)	720nm	720nm

Table 1: Shows the direct comparison of the electronic absorbances from experiment (SVD) and calculation (ZINDO/S).
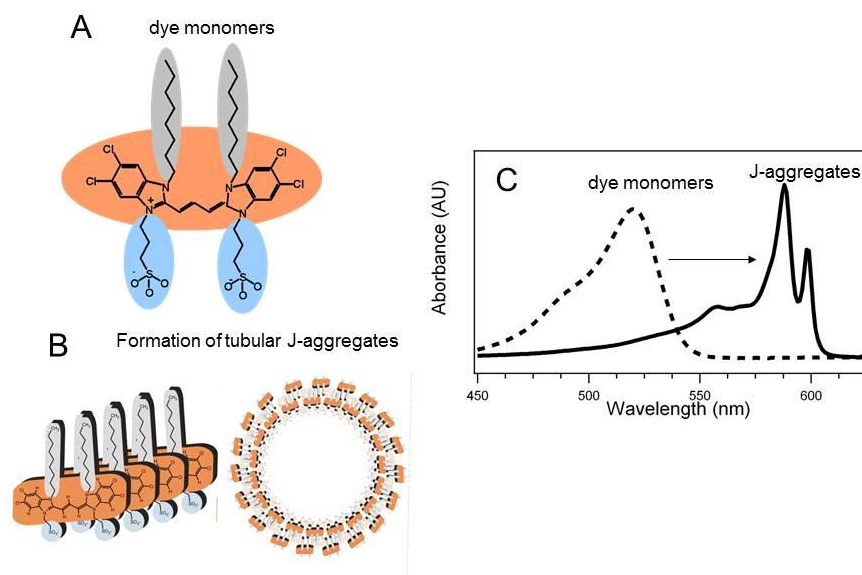
Figure 1: (A) 3,30 -bis(2-sulphopropyl)-5,50,6,60-tetrachloro-1,10 dioctylbenzimidacarbocyanine (C8S3) monomer **(B)** Schematic of the self-assembling process caused by superposition of the pi-pi-stacking of the dyes' chromophores and of the hydrophobic forces of the amphiphilic side chains resulting in a nanotube showing the double-walled structure with the alkyl chains at the interior of the bilayer. **(C)** Absorption spectra of the monomer's solution and the aggregate's solution showing the narrowed and redshifted transitions typical for J-aggregates.
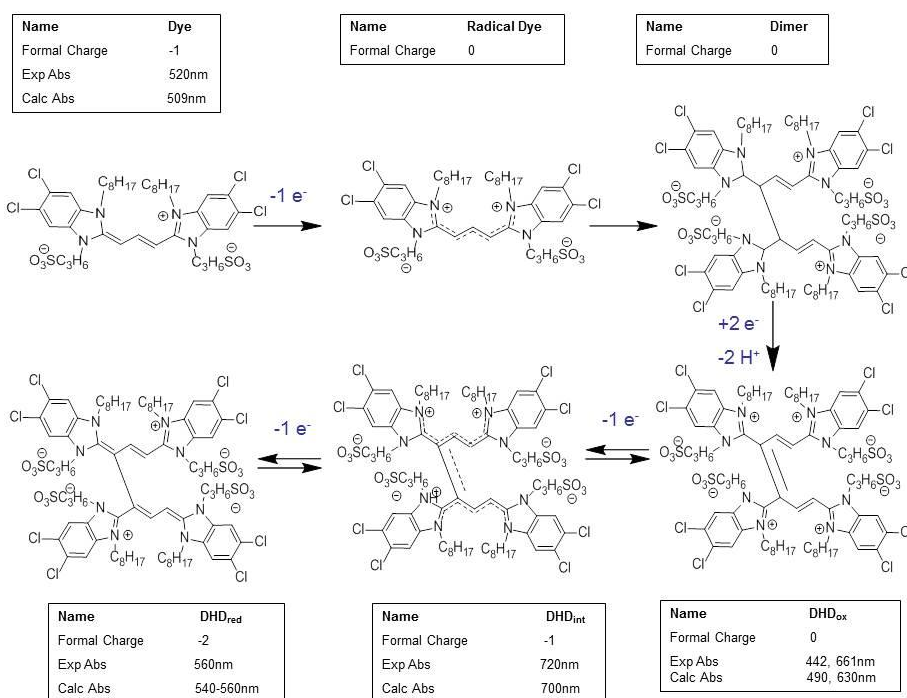
Scheme 1: Shows the electrochemical scheme by which the J-aggregate dye is oxidized from its monomeric form, dimerizes, and forms a new dehydrogenated dye complex free of the macromolecular aggregate. The maximum electronic absorbance is shown from experimentally extracted values compared to semi-empirically calculated absorbance values.

.
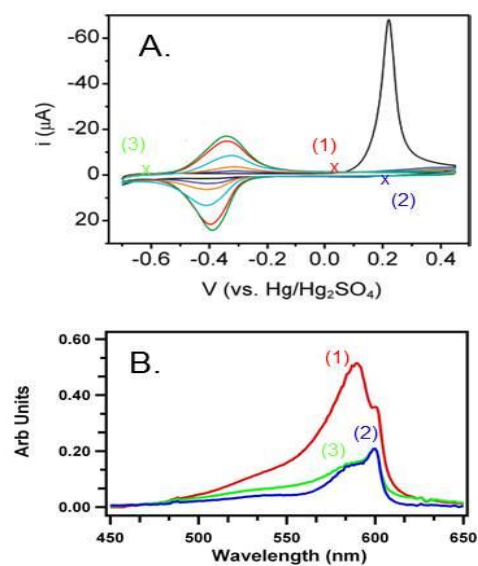
Figure 2. (A) Cycylic voltamagram of the oxidation of monomer dye, resulting in the dimer which has a unique reduction oxidation couple see scheme 1. With specific emphasis placed on 3 regions. **(B)** Representative spectra from the three regions of interest are shown. (1) is the original dye absorption septrum, (2) is the DHD_{OX} absorption spectrum, and (3) is the DHD_{RED} absorption spectrum.

.

41
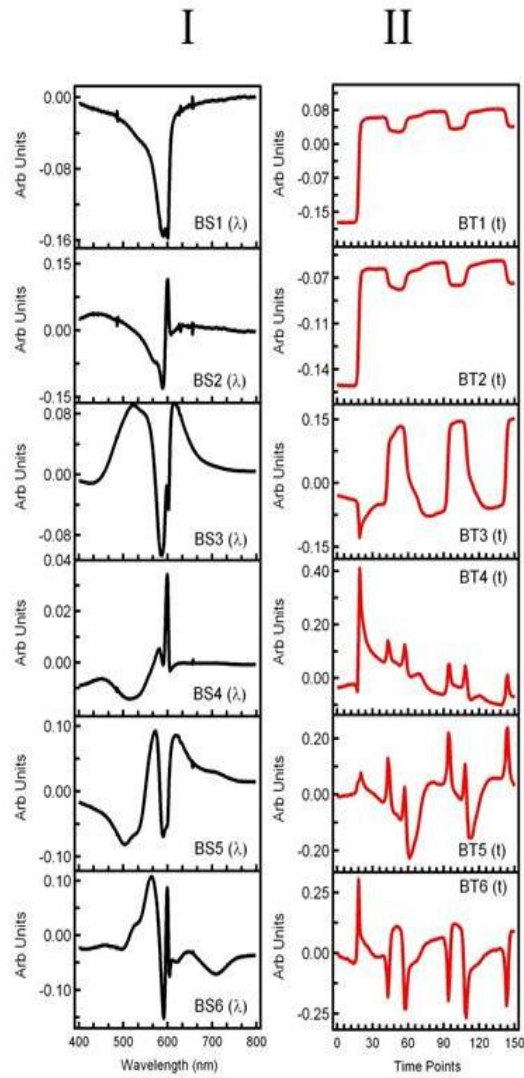
Figure 3. The unaltered SVD output of the six statistically most significant basis elements after deconvolution. Column I is the spectral feature and column II is the time dependent amplitude of that feature. The ranking of the elements decreases down each column.

42
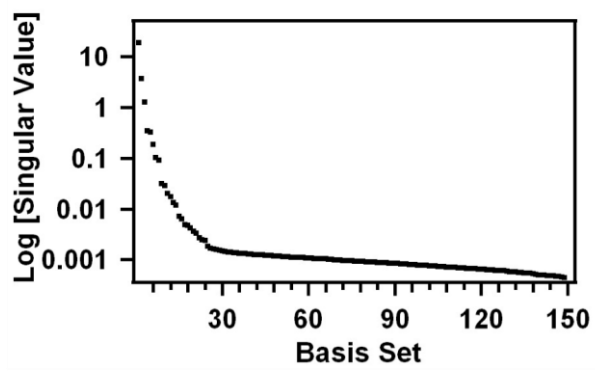
Figure 4. Plot of the singular values of each basis element, ordered from most representative to least.
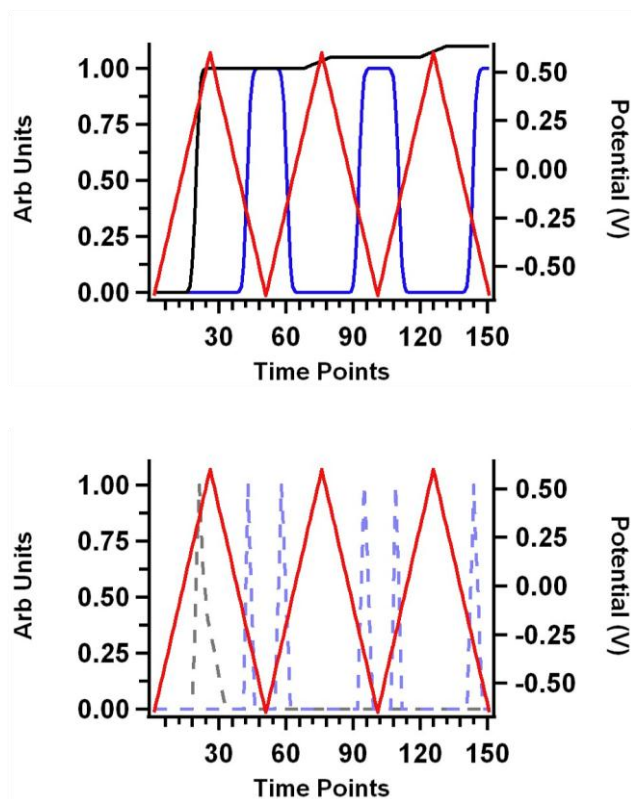
Figure 5. The integrated electrochemical current shown as a function time. The current was integrated over a linearly changing potential (red) to create the model system. All plots are shown based on time instead of voltage, for clarity. Initial irreversible oxidation in the black; secondarily reversible redox is blue, while the intermediate is shown dotted and below.
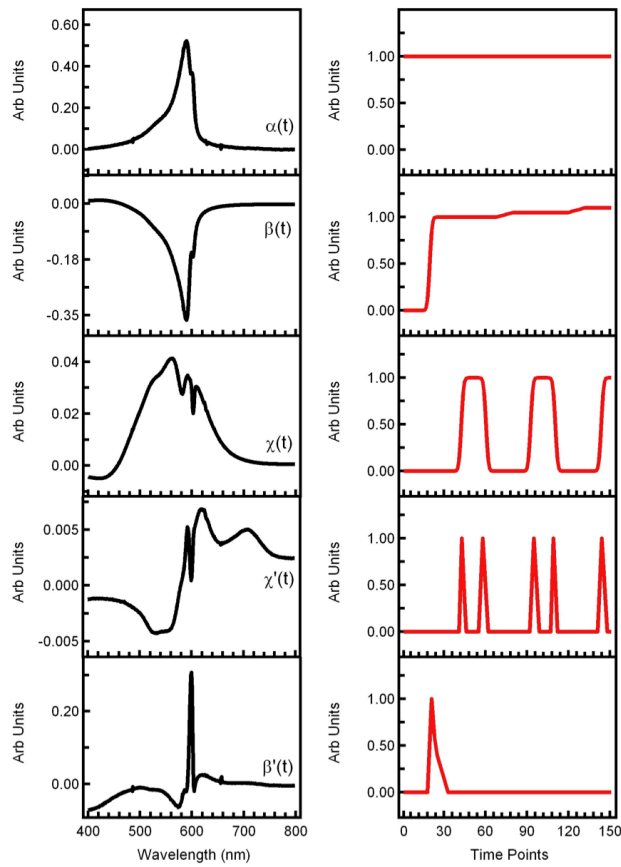
Figure 6. After modeling, the entire data is best represented with the five spectra show their modeled changes with respect to time are shown in the right and left columns.

45
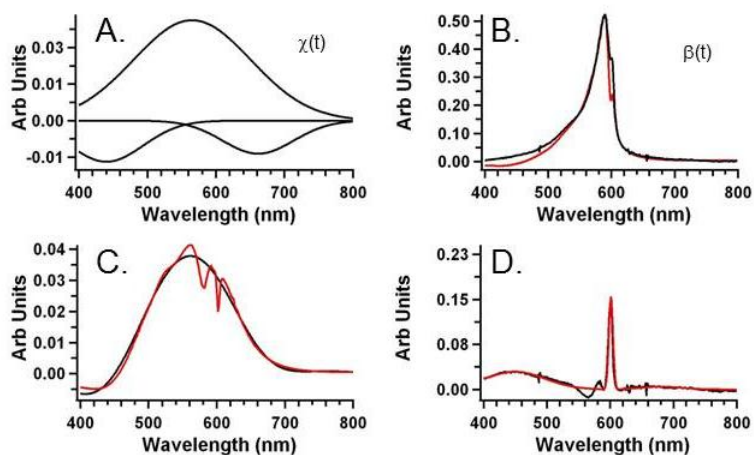
Figure 7. (A.) Shows the Gaussian representation of $\chi(t)$ spectral feature this process which is the modeled redox couple of the loss of DHD_{OX} and simultaneous increase in DHD_{RED}. **(B.)** Shows the $\beta(t)$ spectral feature as deconvolved via SVD. The SVD was modeled as the loss of the monomer species and single step creation of DHD_{OX}. The black spectra show the SVD spectra while the red is best fit of aggregated monomer and DHD_{OX}. **(C.)** Shows the Gaussian fit of loss of DHDOX and gain of DHDRED compared to the data as extracted from SVD. **(D.)** Shows the residual error of fitting $\beta(t)$ spectral feature where the red is the residual error and the black intermediate spectra $\beta'(t)$.

REFERENCES

(1)   Lehn, J. M. *Supramolecular Chemistry: Concepts and Perspectives*; VCH: Weinheim, Germany, 1995.

(2)   Lehn, J. M. *Science* **2002**, *295*, 2400.

(3)   Hoeben, F. J. M.; Jonkheijm, P.; Meijer, E. W.; Schenning, A. *Chemical Reviews* **2005**, *105*, 1491.

(4)   Elemans, J. A. A. W.; Van Hameren, R.; Nolte, R. J. M.; Rowan, A. E. *Advanced Materials* **2006**, *18*, 1251.

(5)   Eisele, D. M.; Knoester, J.; Kirstein, S.; Rabe, J. P.; Vanden Bout, D. A. *Nat. Nanotechnol.* **2009**, *4*, 658.

(6)   Eisele, D. M.; von Berlepsch, H.; Böttcher, C.; Stevenson, K. J.; Vanden Bout, D. A.; Kirstein, S.; Rabe, J. P. *J. Am. Chem. Soc.* **2010**, *in press*.

(7)   Weber, C.; Eisele, D. M.; Rabe, J. P.; Liang, Y.; Feng, X.; Zhi, L.; Müllen, K.; Lyon, J. L.; Williams, R.; Vanden Bout, D. A.; Stevenson, K. J. **2010**, in press.

(8)   Lyon, J. L.; Eisele, D. M.; Kirstein, S.; Rabe, J. P.; Vanden Bout, D. A.; Stevenson, K. J. *J. Phys. Chem. C* **2008**, *112*, 1260.

(9)   Scholes, G. D.; Rumbles, G. *Nat. Mater.* **2006**, *5*, 683.

(10)   Hill, J. P.; Jin, W. S.; Kosaka, A.; Fukushima, T.; Ichihara, H.; Shimomura, T.; Ito, K.; Hashizume, T.; Ishii, N.; Aida, T. *Science* **2004**, *304*, 1481.

(11)   Yamamoto, Y.; Fukushima, T.; Suna, Y.; Ishii, N.; Saeki, A.; Seki, S.; Tagawa, S.; Taniguchi, M.; Kawai, T.; Aida, T. *Science* **2006**, *314*, 1761.

(12)   Jin, W.; Yamamoto, Y.; Fukushima, T.; Ishii, N.; Kim, J.; Kato, K.; Takata, M.; Aida, T. *J. Am. Chem. Soc.* **2008**, *130*, 9434.

(13)   Yamamoto, Y.; Fukushima, T.; Saeki, A.; Seki, S.; Tagawa, S.; Ishii, N.; Aida, T. *J. Am. Chem. Soc.* **2007**, *129*, 9276.

(14)   Cacialli, F.; Wilson, J. S.; Michels, J. J.; Daniel, C.; Silva, C.; Friend, R. H.; Severin, N.; Samori, P.; Rabe, J. P.; O'Connell, M. J.; Taylor, P. N.; Anderson, H. L. *Nat. Mater.* **2002**, *1*, 160.

(15)   Kaiser, T. E.; Wang, H.; Stepanenko, V.; Wurthner, F. *Angew. Chem. Int. Ed.* **2007**, *46*, 5541.

(16)   Lin, H. Z.; Camacho, R.; Tian, Y.; Kaiser, T. E.; Würthner, F.; Scheblykin, I. G. *Nano Letters* **2010**, *online ASAP*.

(17)   Roger, C.; Miloslavina, Y.; Brunner, D.; Holzwarth, A. R.; Wurthner, F. *J. Am. Chem. Soc.* **2008**, *130*, 5929.

(18)   Lang, E.; Sorokin, A.; Drechsler, M.; Malyukin, Y. V.; Kohler, J. *Nano Letters* **2005**, *5*, 2635.

(19)   Lohr, A.; Wurthner, F. *Angew. Chem. Int. Ed.* **2008**, *47*, 1232.

(20)   Lohr, A.; Wurthner, F. *Chemical Communications* **2008**, 2227.

(21)   Hara, T.; Furukawa, K.; Nakamura, T.; Yamamoto, Y.; Kosaka, A.; Jin, W. S.; Fukushima, T.; Aida, T. *Journal of the Physical Society of Japan* **2008**, *77*, 034710.

(22)   Harris, K. D.; Xiao, S.; Lee, C. Y.; Strano, M. S.; Nuckolls, C.; Blanchet, G. B. *J. Phys. Chem. C* **2007**, *111*, 17947.

(23)   Fukushima, T.; Jin, W.; Aida, T. *Journal of Synthetic Organic Chemistry Japan* **2007**, *65*, 852.

(24)   Aida, T.; Fukushima, T. *Philosophical Transactions of the Royal Society a-Mathematical Physical and Engineering Sciences* **2007**, *365*, 1539.

(25)   Didraga, C.; Pugzlys, A.; Hania, P. R.; von Berlepsch, H.; Duppen, K.; Knoester, J. *J. Phys. Chem. B* **2004**, *108*, 14976.

(26)   von Berlepsch, H.; Kirstein, S.; Hania, R.; Pugzlys, A.; Böttcher, C. *J. Phys. Chem. B* **2007**, *111*, 1701.

(27)   von Berlepsch, H.; Kirstein, S.; Bottcher, C. *J. Phys. Chem. B* **2004**, *108*, 18725.

(28)   Knoester, J.; Daehne, S. *Int. J. Photoenergy* **2006**, 1.

(29)   Spitz, C.; Knoester, J.; Ouart, A.; Daehne, S. *Chem. Phys.* **2002**, *275*, 271.

(30)   Womick, J. M.; Miller, S. A.; Moran, A. M. *J. Phys. Chem. B* **2009**, *113*, 6630.

(31)   Womick, J. M.; Miller, S. A.; Moran, A. M. *J. Phys. Chem. A* **2009**, *113*, 6587.

(32)   Milota, F.; Sperling, J.; Nemeth, A.; Kauffmann, H. F. *Chem. Phys.* **2009**, *357*, 45.

(33)   Nemeth, A.; Milota, F.; Sperling, J.; Abramavicius, D.; Mukamel, S.; Kauffmann, H. F. *Chem. Phys. Lett.* **2009**, *469*, 130.

(34)   Oostergetel, G. T.; Reus, M.; Chew, A. G. M.; Bryant, D. A.; Boekema, E. J.; Holzwarth, A. R. *Febs Letters* **2007**, *581*, 5435.

(35)   Linnanto, J. M.; Korppi-Tommola, J. E. I. *Photosynthesis Research* **2008**, *96*, 227.

(36)   de Sa, R. J.; Matheson, I. B. C. *Methods Enzymol.* **2004**, *384*, 1.

(37)   Shafer, M. W.; McKee, G. R.; Schlossberg, D. J. *Rev. Sci. Instrum.* **2008**, *79*, 10F534/1.

(38)   Stamatopoulos, V. G.; Karras, D. A.; Mertzios, B. G. *Meas. Sci. Technol.* **2009**, *20*, 104021/1.

(39)   Zhao, Y.; Schmidt, M. *J. Appl. Crystallogr.* **2009**, *42*, 734.

(40)   Halgren, T. A. *Journal of Computational Chemistry* **1996**, *17*, 520.

(41)   Halgren, T. A.; Nachbar, R. B. *Journal of Computational Chemistry* **1996**, *17*, 587.

(42)   Halgren, T. A. *Journal of Computational Chemistry* **1996**, *17*, 616.

(43)   Halgren, T. A. *Journal of Computational Chemistry* **1996**, *17*, 490.

(44)   Halgren, T. A. *Journal of Computational Chemistry* **1996**, *17*, 553.

(45)   Schmidt, M. W.; Baldridge, K. K.; Boatz, J. A.; Elbert, S. T.; Gordon, M. S.; Jensen, J. H.; Koseki, S.; Matsunaga, N.; Nguyen, K. A.; Su, S.; Windus, T. L.; Dupuis, M.; Jr, J. A. M. *Journal of Computational Chemistry* **1993**, *14*, 1347.

(46)   Zerner, M. C.; Loew, G. H.; Kirchner, R. F.; Mueller-Westerhoff, U. T. *J Am Chem Soc* **1980**, *102*, 589.

(47)   Ridley, J.; Zerner, M. *Theoretical Chemistry Accounts: Theory, Computation, and Modeling (Theoretica Chimica Acta)* **1973**, *32*, 111.

(48)   Runge, E.; Gross, E. K. U. *Physical Review Letters* **1984**, *52*, 997.

(49)   Lyon, J. L.; Eisele, D. M.; Kirstein, S.; Rabe, J. P.; Vanden Bout, D. A.; Stevenson, K. J. *J. Phys. Chem. C* **2008**, *112*, 1260.

(50)   HyperChem™, Hypercube, Inc., 1115 NW 4th Street, Gainesville, Florida 32601, USA; unpublished data. B. L. Iverson

(51)   Lenhard, J. R.; Hein, B. R. *The Journal of Physical Chemistry* **1996**, *100*, 17287.

49

Chapter 3: Molecular Weight Effect on the formation of Beta Phase poly (9,9'−dioctylfluorene) in a poor solvent

CHAPTER SUMMARY

The effect of molecular weight on the formation of β phase poly (9,9'−dioctylfluorene) (PF8) was studied. Temperature dependent fluorescent experiments of unique synthetic batches as well as size excluded single batches of polyfluourene were studied. Each batch had unique characteristics, molecular weight, tetrahedral defect concentration and polydispersity index (PDI). Two phases of polyfluorene were observed which exhibit distinct electronic transition signatures and the affect that molecular weight has on the secondary phase was experimentally studied using dilute samples. Langevin simulations were performed to calculate the temperature dependence of the radius of gyration for a bead-and-spring homopolymer. Results suggest that size affects the average end to end distance corresponding to increases in secondary electronic absorption. In this report we find that interchain interactions which increase with molecular weight are required to form β phase for isolated chains of polyfluorene in a poor solvent.

INTRODUCTION

Organic semiconducting materials offer great potential as a new electronic material due to the ability to chemically tailor their properties through synthesis. In addition, organic materials, polymeric materials in particular, have demonstrated properties that can also vary strongly with morphology. [1-3] An excellent example of this is polyfluourene (PF) which is a polymerized blue emitting dye with a high quantum yield, as such it is the basis for an entire class of organic electronic materials. [4-8] Such

materials have had been synthetically altered by copolymerization to modulate the conjugated electronic backbone or the addition of soluble side chains to tune the material properties to specific usages. Morphologically polyfluorene presents two distinct phases in both films and solution. The α phase of polyfluorene is the most common phase, achieved when the polymer is well solvated and in a random coil shape. [9-11] The secondary phase of polyfluorene is referred to as the β phase and has been reported to offer improved electronic properties. [11-15] As the β phase exhibits a lower energy excited state, the structure is believed to have adopted a planar zigzag structure with an extended conjugation length. [5, 16-19] This new phase of PF was first reported by Grell as the onset of lower energy absorption and narrowed emission in pure poly(9,9'dioctylfluorene) (PF8), and PF8 dispersed in polystyrene. [20, 21] There have been many other ways in which the β phase of polyfluorene has been observed experimentally, such as varying the concentration and temperature, using poor solvents, thermal and vapor annealing, high boiling point solvents as solution additives and nanofibers formed from porous alumina network templates. [13, 16, 22, 23] While there have been many studies of this secondary phase both in films and solution, the mechanism of formation is still poorly understood. [17] While in many instances β phase formation has been associated with polymer aggregation, but also shown to form in dilute polymer solutions. [23] Previously it has been shown the temperature dependence of the β phase formation depends on the solvent quality. [24] This suggests that for dilute chains in solution β phase formation may be related to collapse of the polymer chains. This paper will examine how molecular weight affects the formation of the β phase and correlate those changes with the affect molecular weight have on polymer collapse.

The interconversion from α to β phase is directly observable from the appearance of a new feature in the absorption spectrum at 437nm associated with the β phase.

51

Initially, in a good solvent the spectrum of a dilute PFO will be free of β phase. If the temperature is lowered, the β phase peak will grow in. Although the exact amount of conversion for each batch is dependent on molecular weight, defects, solvent and other experimental variables, the temperature of greatest change is easily calculated. This mid-point temperature can then be compared with the theoretical θ temperature of the polymer in solution associated with collapse of the polymer chains.

The collapse of a homopolymer from a coil to globule can generally be understood through the concept of a θ temperature, in which the repulsive and attractive monomer interactions of the polymer chain effectively cancel out resulting in a negligible excluded volume (e.g., resembles the ideal chain). At temperatures greater than θ (good solvent regime), the polymer tends to form an expanded coil as a result of prevailing repulsive interactions between the monomers of the polymer chain. At temperatures less than θ (poor solvent regime), the polymer adopts a collapsed globule conformation as a result of prevailing attractive interactions between the monomers of the polymer chain.

If the formation of the β phase is correlated to the collapse of polymer in solution then the temperature of β phase formation and the θ temperature exhibit the same trends with respect to molecular weight. In the limit of an infinite chain, the θ temperature should be independent of the molecular weight. However for finite length one would expect the θ temperature to depend on chain length. While it would be possible to study this collapse directly with light scattering scatting techniques, this is not possible with the PF solutions as they rapidly aggregate upon cooling. Here, the dependence of the θ temperature on molecular weight was examined theoretically through simulations of a simple bead-and-spring homopolymer of finite chain length (N≤200).

EXPERIMENTAL SECTION

For this research four unique synthetic batches of Poly (9,9'–dioctylfluorene) were utilized that had all been synthesized via a Suzuki coupling reaction. [25] The hexamer oligomer was purchased from American Dye Source and used without further purification. All batches were characterized using gel permeation chromatography (GPC) to determine the average molecular weight and polydispersity index (PDI). It has been shown that shorter conjugation lengths lead to longer wavelength absorption maximum. [26] Tetrahedral defects were estimated using UV-VIS where the number of defects is related to the length of the maximum energy absorption.

GPC was used to characterize individual polymer batches, while also creating a physically separate distribution of molecular weights which were then be collected into individual fractions and analyzed using temperature dependent fluorescence measurements. The solvent was evaporated and remaining size excluded polymer solvated in a poor solvent with low freezing point, methyl-cyclohexane (MCH).

A modified SPEX Flourolog 1 from Horiba Jobin Yevon with a 450W xenon lamp was used for all temperature dependent measurements. The instrumentation was controlled via a custom labview program. All excitation spectra were collected from 350 to 450 nm for emission at 475 nm.

For each measurement a dilute sample was prepared (50uL of 1% by weight PF8 in MCH) in a standard rectangular fluorescent cuvette with a screw top. The molecular weight separated samples were diluted to fill 3mL sample cuvette as the samples had been diluted substantially during GPC analysis. All samples measured had concentration less than 10^{-3}% PF8 by weight percent.

For each temperature dependent fluorescent experiment the solution was heated to remove all aggregated polymer species and cooled to room temperature. The sealed

cuvette was placed in a Janis ST-100 optical cryostat and Lakeshore temperature controller was used to cool the cryostat to desired temperature. Once the sample had reached the desired temperature it was allowed to equilibrate for 15 minutes before optical measurements were taken. At low temperatures the experiments were limited by the formation of larger polymer aggregates which lead to large intensity spikes in the emission as well as visibly inhomogeneous samples. Every run was considered complete when large nonreversible aggregates were formed.

The temperature dependence of the beta-phase formation for each batch was probed by observing changes in the excitation spectra of the polymers in dilute solution. All samples were created highly dilute (50uL of 1 weight percent PF8/MCH stock solution, with 3mL of MCH added) every sample run was considered complete after the formation of large aggregates was observed in the emission spectra as detected by spikes in the fluorescence intensity. All samples analyzed had this observed phenomena with the exception of PF8 batches D and E in which the solvent freezing point was reached before the formation of large aggregates.

Simulation model and methods

Langevin simulation of bead-and-spring homopolymer model.

The polymer model consists of $N+1$ beads of mass m connected by N harmonic springs. The interaction between consecutive bonded beads separated by a distance r is described by a harmonic potential:

$$V_{bonded} = \tfrac{1}{2} k_{bonded} (r - \sigma)^2$$

while the interaction between non-bonded beads is described by a Lennard-Jones potential:

$$V_{non-bonded} = 4\varepsilon \left((\sigma/r)^{12} - (\sigma/r)^{6} \right)$$

where σ is the equilibrium bond distance, ε is the characteristic energy scale, and the spring constant was taken to be $k_{bonded} = 100\varepsilon/\sigma^2$. The dynamics of each bead is governed by the Langevin equation:

$$m\frac{\partial^2 \mathbf{r_i}(t)}{\partial t^2} = -\frac{\partial V}{\partial \mathbf{r_i}} - \xi\frac{\partial \mathbf{r_i}(t)}{\partial t} + \mathbf{R_i}(t)$$

where $\mathbf{r_i}(t)$ is the position of the bead, V is the total interaction potential, ξ is the frictional coefficient, and $\mathbf{R_i}(t)$ is the random force satisfying the fluctuation-dissipation theorem. Simulation data is reported in reduced form of the units of length, energy, and time, which are σ, ε, and $\tau = (m\sigma^2/\varepsilon)^{1/2}$, respectively. Polymer chains of lengths N=20, 40, 60, 80, 100, 120 and 120 were investigated in this study.

Characterization of transition from coil to globule.

Simulations of the bead-and-spring model were performed at constant values of temperature ranging from $T = 0.2\varepsilon/k_B$ to $T = 5.0\varepsilon/k_B$.

For a given fixed value of temperature, the mean radius of gyration $\langle R_g \rangle$ was computed for the polymer chains under thermal equilibrium. This was performed to obtain the temperature dependence of the mean radius of gyration for different chain lengths.

The conformational state of the bead-and-spring model was characterized by the scaling relation $\langle R_g \rangle \sim N^\nu$, where the scaling exponent assumes the values $\nu = 1/3$ and $\nu \approx 0.588$ for the collapsed globule and swollen coil, respectively. The scaling exponent of $\nu = 1/2$ corresponding to the ideal chain is used in this study to define the collapse transition temperature. [27] This is accomplished by plotting $\langle R_g \rangle N^{-1/2}$ vs. temperature and extrapolating to the temperature at which the curves representing different chain lengths intersect (e.g., the collapse transition temperature). Furthermore, the θ temperature for a particular chain length was estimated by extrapolating the temperature dependence of the

mean radius of gyration from simulation data and locating the point of intersection with the radius of gyration of the ideal chain.[27] It should be noted that the θ temperature corresponds to the aforementioned collapse transition temperature strictly in the limit of $N \rightarrow \infty$.

RESULTS AND DISCUSSION

Standard polymer characterizations were performed using GPC to determine the average molecular weight and polydispersity index (PDI) for each PF8 batch used. Table 1 shows the summary of the experimentally determined physical properties. Average molecular weight ranged from 6,500 to100,000 kDal (16 to 225 repeat units) and every PDI value was above 2.0 except the exceedingly low molecular weight polymer. For clarity: A refers to the largest polymer, D refers to the smallest polymer, and Batch E refers to the oligomer sample which never shows secondary phase absorption under any conditions. Sazuki coupling polymerizations are known to have a large polydispersity index (PDI) and be susceptible to tetrahedral defect creation along the conjugated backbone of the repeated unit. [28]

The presence of β phase can be detected by the formation of a new absorption band at 437nm. Excitation spectra are recorded for dilute solution rather than absorbance spectra in more concentrated solutions to avoid interchain aggregation. The amount of β phase formed was estimated by the percentage of primary absorption at 390nm compared to the secondary absorption at 437 nm. The onset, mid, and final temperatures are unique to each batch of PF. Figure 1A shows a typical increase in secondary absorption as a function of temperature. In Figure 1B the percentage of β phase is plotted as the temperature decreased. As the change in the spectrum as a function temperature contains

overlapping absorption and singular value decomposition was used to quantify the change in absorption.

Singular value decomposition (SVD) is a numerical technique that provides the minimal number of spectral features required to completely represent data sets [29-31] in this case it was used to quantify the amount of β phase and spectral features associated with the beta absorption. SVD was performed on the data set and it was found that the two spectral species represent each polymer data set. Each experiment was treated individually rather than combining all the data set in one set due to defects in the α phase from defects, and conjugation lengths. While SVD results vary with experiment yielded unique curvatures and maxima, key results were conserved and not different in any substantive form. The SVD allows for the extraction of the spectral features associated with β phase absorption. As Figure 2 shows the spectral features are more complex than the most obvious peak at 437nm. There is a vibronic progression of peaks which are similar to the results seen previously and extracted using subtraction. The results from SVD can be compared to previous results reported by Chunwaschirasiri et al, who modeled the β phase optical properties as a more ordered conjugated backbone and performed quantum mechanical calculations, yield satisfactory results. [32]

At each point along the experimental cooling curve, the percent of β phase does not change as function of waiting time. Moreover, if the temperature is returned to a previous value of percentage β phase is reproduced. This indicates the system is at equilibrium at every temperature measured. However, at low temperatures macroscopic aggregates begin to form that disrupt the experiment irreversibly. Therefore the lowest reported temperature is before the onset of aggregation formation. Then the absorbance maximum of the β phase is different to but easily relatable to the mid-point to determine due to the curvature of the response.

The mid-point temperature is the point at which the solvent-polymer and polymer-polymer energy of interaction are equivalent, also corresponding to the point of maximum interconversion between phases. This is trivial to estimate using finite difference methods on both the experimental and theoretical data as long there is suitable data points and signal.

The temperature mid-point of β phase formed was measured for each batch of PF8. Figure 3 shows the mid-point temperature as a function of average repeat units (squares). Results clearly do not correlate strictly with molecular weight. The highest temperature is polymer B but the largest molecular weight is polymer A. However, each synthetic batch of polymer has both a different molecular weight and defect concentration. Polymer A has the largest molecular weight but did not have the highest transition temperature or the largest amount of β phase formed. The number of defects in the different polymer batches can be estimated from the maximum of the primary α absorption as the defects tend to break the extended conjugation and shift the absorption to higher energy (see supporting information). Polymer B has least number of defects as judged from it having the lowest energy absorption. It also has the highest transition temperature and most β phase observed (see SI).

To isolate the molecular weight effect on the formation of the β phase in PF8 a system containing similar concentration of defects must be studied. A single batch of PF8 was physically separated using GPC. The concentration of tetrahedral defects along a conjugated backbone of PF8 should remain constant as the defects are a product of reaction conditions. Generally it is polymers systems with large PDIs (x > 2.0) are poor systems, however in this case they are extremely useful as it allows for large variation in the molecular weights of the sample collected after GPC analysis. The physical separation of polymers based on size was performed on PF8 batch A. Figure 4 shows the

temperature dependence of percent β phase for three distinct fractions for polymer A. Three distinct fractions were created by collecting five separate aliquots and analyzing the largest, smallest, and intermediate samples (inset of Figure 4). Figure 4 also shows full batch data (full diamonds). The highest molecular weight fraction has the highest mid-point temperature. The lowest molecular weight fraction has the lowest mid-point temperature. The average fraction has a similar mid-point temperature to that of the ensemble average.

This shows a clear dependence on the molecular weight of PF8 on the formation of β phase absorption in solution. Molecular weight dependence is subtle in contrast to the contribution of defects, which can dominate the trend. As can be seen in the supporting information for the GPC fractioned portions of polymer B, all of the mid-point temperatures are within the experimental noise.

The results of the physical separation of a single polymer batch show that the mid-point temperature of any polymer depends on the molecular weight. The experimental data as the molecular weight decreases the mid-point temperature increases. This agrees with theoretically predicted trend for molecular weight dependence on the temperature of collapse of chains with finite length.

To examine the molecular weight dependence on chain collapse, Langevin dynamics were performed on bead-and-spring polymer chains of various lengths. The mean radius of gyration of the chain is plotted as a function of temperature in Figure 5 shows a phase transition that was weakly chain length dependent. At fixed temperature values of $T = 0.2\varepsilon / k_B$ and $T = 5.0\varepsilon / k_B$, the mean radius of gyration exhibited a power law dependence on chain length with scaling exponents of $\nu = 0.34$ and $\nu = 0.56$, respectively. This is in excellent agreement with the expected scaling for the collapsed globule at low temperature and in reasonable agreement with the expected scaling of the

59

swollen coil at high temperature. The slight deviation from the expected scaling of the swollen coil is likely attributed to not exploring higher temperatures. Furthermore, the collapse transition temperature where the mean radius of gyration exhibits a chain length dependence of $N^{1/2}$ was found to be $T = 3.56\varepsilon/k_B$. Likewise, the θ temperature for different chain lengths was plotted in Figure 6. This weak dependence on chain length is found to gradually decrease with increasing chain length and is expected to disappear in the limit of $N \rightarrow \infty$ where the θ temperature converges to the collapse transition temperature and is independent of chain length.

When the results from the theory and experiment are directly compared there is strong correlation in size to θ temperature. As temperature is modulated in either method, it results in either decrease in calculated radius of gyration or to an increase in the amount of β phase optically observed. There is discrepancy between simulation beads and monomer units in the real polymer chain and how to interconvert between them.[1] Regardless of whether the conversion is literal (1bead :1monomer) or as the simulation as a miniaturization to aid with scale up (2.5bead:1monomer); polymer collapse temperature and length are always directly correlated. When the conversion is made between theoretical monomer units and polymer repeat units is set to 2.5beads:1monomer the agreement between temperatures is quite good. 100 repeat units (the average of batch B) has an observed mid-point temperature of 192K where the simulation has an observed θ temperature 2.6 (temperature units). The smallest fraction has an observed temperature of 180K. Were the trend to be exact this would predict the simulation should have transitin at a temperature of 2.4. The corresponding theoretical simulation has a mid-point temperature of 2.3 (temperature units). The largest fraction has an observed mid-point temperature 200K which would scale to a temperature of 2.7. The corresponding theoretical simulation has a θ temperature of 2.8 (temperature units). This agreement

between collapse of polymer and formation of the β phase in polyfluorene is very encouraging for establishment of a direct connection between the two previously unrelated phenomena.

In this report we observe a secondary solution phase of polyfluorene in dilute solutions. The β phase was observed in dilute solutions of isolated polymer chains to avoid intermolecular interactions and isolate the intrachain interactions. Excitation measurements were taken at equilibrium so that a phase transition could be observed. Multiple batches with unique characteristics (average molecular weight, polydisperiity index and tetrahedral defect concentration) were measured. There is also a strong dependence on the length of the polymers and the total amount of β phase formed which is expected because longer polymers have a larger number of available conformations; however, this effect is not as pronounced as the dependence on defect concentration. As defect concentration helps to define the amount of β phase possible for any given batch of polyfluorene, as the polymer with the lowest defect concentration shows the largest percentage of β phase formed.

The θ point in each experiment is the point at which the energetics of polymer-polymer and polymer-solution are evenly balanced. If the β phase arose only from a planarization of the polymer chain, the physical separation based on molecular weight results should all be within the experimental error as planarization is only a polymer-solvent interaction and does not depend on intrachain interactions. This is clearly not the case as the data shows a trend that is dependent on molecular weight. This supports the idea that interchain interactions are required to form β phase for isolated chains of solution phase polyfluorene.

CONCLUSIONS

In conclusion, β phase formation in polyfluorene is dependent on many specific factors. While higher molecular weight can be related to higher theta temperatures, the defect concentration determines the amount of β phase possible. The mid-point and θ point in each experiment is the point at which the energetics of polymer-polymer and polymer-solution are evenly balanced. If the β phase arose only from a planarization of the polymer chain, the physical separation based on molecular weight results should all be within the experimental error as planarization is only a polymer-solvent interaction and does not depend on intrachain interactions. This implies that the β phase of polyfluorene is driven by collapse of the polymer from solution. Langevin dynamics simulations show a dependence on molecular weight when the polymer is in the small length regime and weaker as chain length increases. In this paper we have shown the correlation between polymer collapse, defects and secondary phase of polyfluorene using temperature dependent fluorescence measurements and simulations.
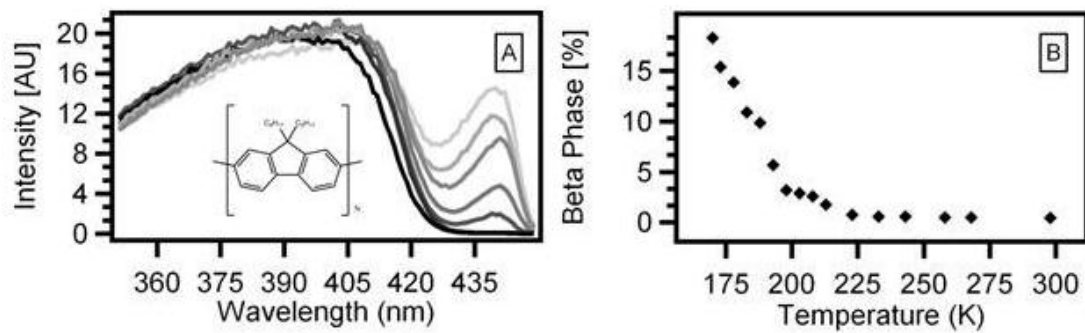
Figure 1. (A.) The spectra as a function of temperature of a dilute solution of PF8 in THF. The chemical structure of polyfluorene is shown in the inset. **(B.)** The calculated % of β phase is shown for each temperature.
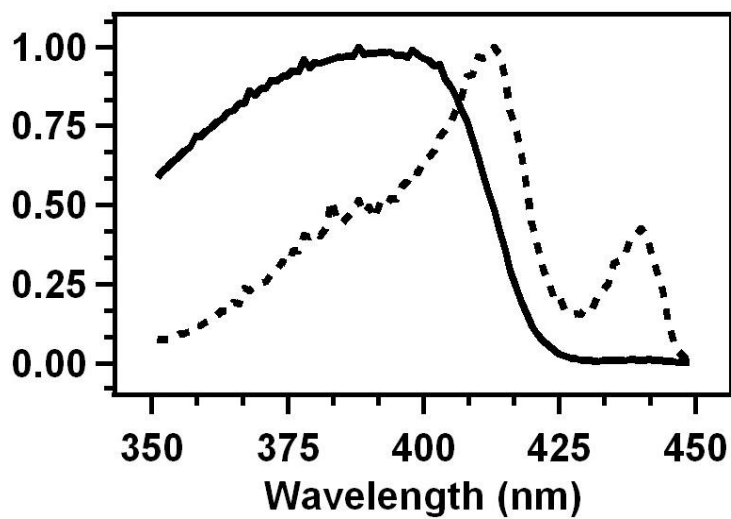
Figure 2. Shows the two most important spectral features which were extracted from a single series of temperature measurements using singular value decomposition. The solid line corresponds to the calculated α phase absorption while the dotted line corresponds to the calculated β phase absorption.

Name	Molecular Weight (kDal)	Polydispersity Index (PDI)	Average Monomer Units
A	100,000	2.56	216
B	76,000	2.38	164
C	30,000	2.5	65
D	6,500	1.47	13
E	2,500	1.00	5

Table 1. Summary of the physical characteristics of the different PF8 batches.
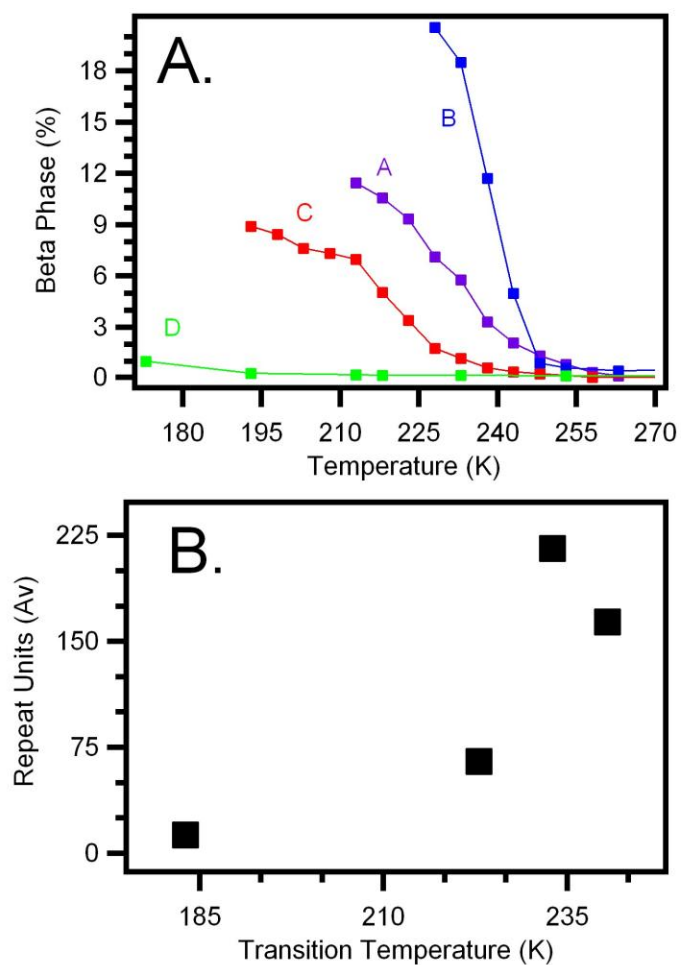
Figure 3. (A.) Shows the cooling curves for four different batches of polyfluorene as a function of β phase formation as the temperature is cooled. **(B.)** Comparison of the results where molecular weight is compared to the measured transition temperature observed in A.

66
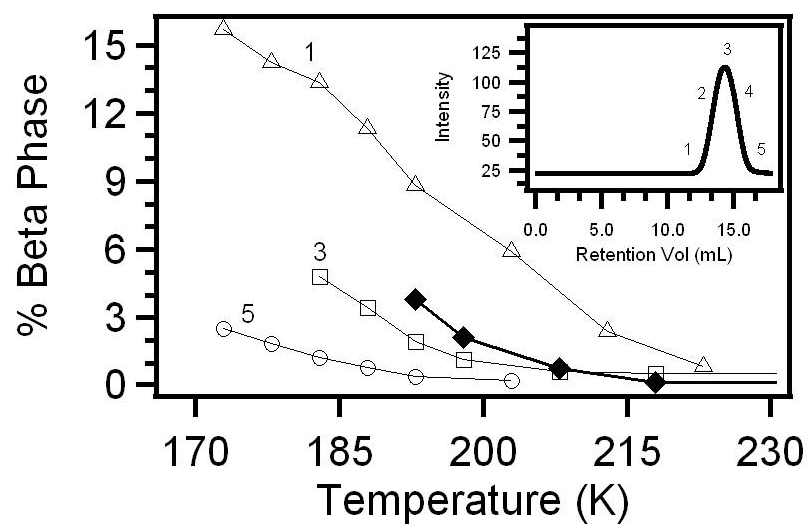
Figure 4. Batch that has been fractioned β phase cooling curves in methylcylcohexane inset shows gel permeation chromatograpy data from which molecular weight dependent samples were created.
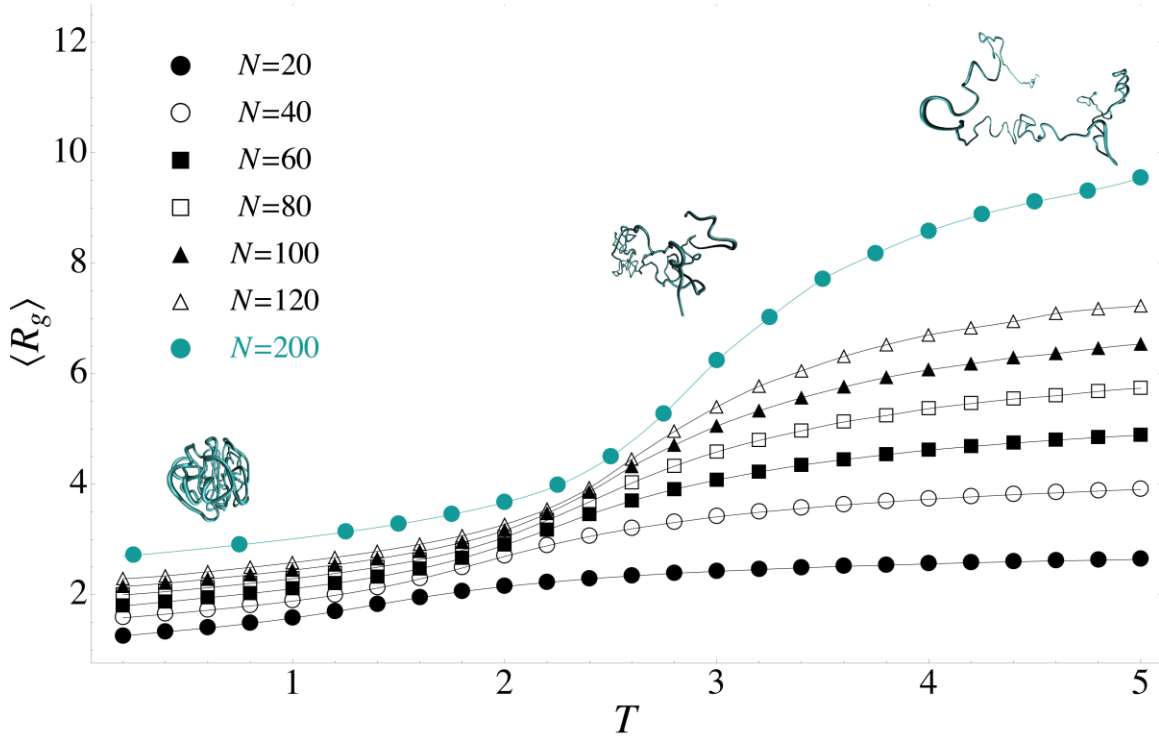
Figure 5. The radius of gyration for varying polymer lengths exhibited a transition from a globule, collapsed form to a swollen form at the θ temperature. The snapshots inset in the figure were of the N=200 polymer chain at T=0.25, T=2.75, and T=5.00, respectively.
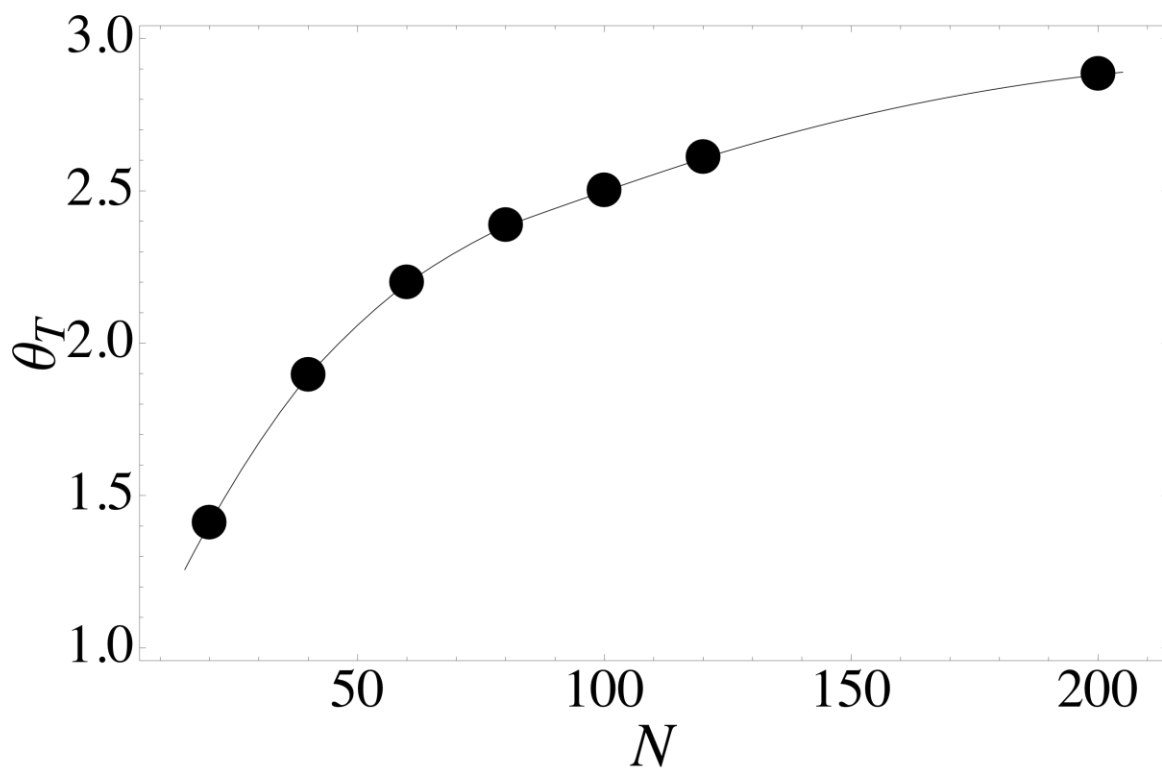
Figure 6. The θ temperature was found to exhibit a gradually weakening dependence on chain length. Note that the dependence should be nonexistent in the limit of $N \rightarrow \infty$.

REFERENCES

1. Hu, D.; Yu, J.; Wong, K.; Bagchi, B.; Rossky, P. J.; Barbara, P. F., *Nature* **2000,** *405* (6790), 1030-1033.

2. Barbara, P. F.; Gesquiere, A. J.; Park, S.-J.; Lee, Y. J., *Accounts of Chemical Research* **2005,** *38* (7), 602-610.

3. Rozanski, L. J.; Cone, C. W.; Ostrowski, D. P.; Vanden Bout, D. A., *Macromolecules* **2007,** *40* (13), 4524-4529.

4. Sims, M.; *Journal of Physics: Condensed Matter* **2005,** *17* (41), 6307.

5. Kilina, S.; Batista, E. R.; Yang, P.; Tretiak, S.; Saxena, A.; Martin, R. L.; Smith, D. L., *ACS Nano* **2008,** *2* (7), 1381-1388.

6. Zhu, B.; Han, Y.; Sun, M.; Bo, Z., *Macromolecules* **2007,** *40* (13), 4494-4500.

7. Janietz, S.; Bradley, D. D. C.; Grell, M.; Giebeler, C.; Inbasekaran, M.; Woo, E. P., *Applied Physics Letters* **1998,** *73* (17), 2453-2455.

8. Weinfurtner, K. H. F. A. U. F. H.; Fujikawa, H. F. A. U. T. S.; Tokito, S. F. A. U. T. Y.; Taga, Y., *Applied Physics Letters* **2000,** *76* 2502.

9. Leclerc, M., *Journal of Polymer Science Part A: Polymer Chemistry* **2001,** *39* (17), 2867-2873.

10. Kim, Y.; Vanden Bout, D., *Applied Physics A: Materials Science & Processing* **2009,** *95* (1), 241-247.

11. Klaerner, G.; Miller, R. D., *Macromolecules* **1998,** *31* (6), 2007-2009.

12. Ryu, G.; *Journal of Physics: Condensed Matter* **2007,** *19* (5), 056205.

13. Da Como, E.; Becker, K.; Feldmann, J.; Lupton, J. M., *Nano Letters* **2007,** *7* (10), 2993-2998.

14. Prins, P.; Grozema, F. C.; Nehls, B. S.; Farrell, T.; Scherf, U.; Siebbeles, L. D. A., *Physical Review B* **2006,** *74* (11), 113203.

15. Azuma, H.; Kobayashi, T.; Shim, Y.; Mamedov, N.; Naito, H,. *Organic Electronics* **2007,** *8* (2-3), 184-188.

16. Tsoi, W. C.; Charas, A.; Cadby, A. J.; Khalil, G.; Adawi, A. M.; Iraqi, A.; *Advanced Functional Materials* **2008,** *18* (4), 600-606.

17. Peet, J.; Brocker, E.; Xu, Y.; Bazan, G. C., *Advanced Materials* **2008,** *20* (10), 1882-1885.

18. Caricato, A. P.; Anni, M.; Manera, M. G.; Martino, M.; Rella, R.; Romano, F.; Tunno, T.; Valerini, D., *Applied Surface Science* **2009,** *255* (24), 9659-9664.

19. Bright, D. W.; Dias, F. B.; Galbrecht, F.; Scherf, U.; Monkman, A. P., *Advanced Functional Materials* **2009,** *19* (1), 67-73.

20. Grell, M.; Bradley, D. D. C.; Inbasekaran, M.; Ungar, G.; Whitehead, K. S.; Woo, E. P., Intrachain ordered polyfluorene. *Synthetic Metals* **2000,** *111-112*, 579-581.

21. Grell, M.; Bradley, D. D. C.; Long, X.; Chamberlain, T.; Inbasekaran, M.; Woo, E. P.; Soliman, M., *Acta Polymerica* **1998,** *49* (8), 439-444.

22. Cheun, H.; Tanto, B.; Chunwaschirasiri, W.; Larson, B.; Winokur, M. J., *Applied Physics Letters* **2004,** *84* (1), 22-24.

23. Caruso, M. E.; Anni, M., *Physical Review B* **2007,** *76* (5), 054207.

24. Kitts, C. C.; Vanden Bout, D. A., *Polymer* **2007,** *48* (8), 2322-2330.

25. Miyaura, N.; Suzuki, A., *Chemical Reviews* **1995,** *95* (7), 2457-2483.

26. Song, J.; Liang, W. Z.; Zhao, Y.; Yang, J., *Applied Physics Letters* **2006,** *89* (7), 071917-3.

27. Wittkop, M.; H^lzl, T.; Kreitmeier, S.; G^ritz, D., *Journal of Non-Crystalline Solids* **1996,** *201* (3), 199-210.

28. Brookins, R. N.; Schanze, K. S.; Reynolds, J. R., *Macromolecules* **2007,** *40* (10), 3524-3526.

29. Shafer, M. W.; McKee, G. R.; Schlossberg, D. J., *Rev. Sci. Instrum.* **2008,** *79* (10, Pt. 2), 10F534/1-10F534/4.

30. Zhao, Y.; Schmidt, M., *J. Appl. Crystallogr.* **2009,** *42* (4), 734-740.

31. Stamatopoulos, V. G.; Karras, D. A.; Mertzios, B. G., *Meas. Sci. Technol.* **2009,** *20* (10), 104021/1-104021/9.

32. Chunwaschirasiri, W.; Tanto, B.; Huber, D. L.; Winokur, M. J., *Physical Review Letters* **2005,** *94* (10), 107402.

Chapter 4: Effect of Film Morphology on the Energy Transfer to Emissive Green Defects in Di-alkyl Polyfluorenes

CHAPTER SUMMARY

The formation of a ketone defect at the 9-site along the backbone of di-alkyl polyfluorenes has been shown to be directly involved in the degradation of the polymer's emission from blue to an undesirable green. Films of poly(9,9'-dihexylfluorene) (PFH) with and without ketone defects were annealed above their liquid crystalline phase transition in an inert argon atmosphere and their emission spectra were collected in order to study the effect of morphology on the energy transfer to ketone defects. The annealing was performed in situ in the fluorometer allowing for a direct comparison of the absolute changes in the emission spectra. Annealing of the films resulted in regions of highly aligned polymer chains as confirmed by atomic force microscopy. After annealing, the fluorescence spectra of pristine films (without ketone defects) exhibited no green emission, indicating the lack of thermal oxidation in the inert atmosphere. However, these films did show an increase in fluorescence quantum yield revealing that high polymer order does not lead to interchain electronic species that quench the excited states. Annealing of partially photobleached PFH films revealed that an increase in the polymer chain order of a film containing a few defects resulted in an increase in green emission and decrease in blue without the creation of further defects. The increase in green emission combined with the decreased blue can only be the result of increased energy transfer from pristine chromophores to ketone sites, as the aligned polymer chains increase exciton diffusion. PFH films containing defects that were annealed beneath the LC temperature of the polymer did not result in any spectral changes, indicating that

alignment of polymer chains was necessary for the increased energy transfer to the defect sties.

INTRODUCTION

Polyfluorenes (PFs) and their copolymers are one class of semiconducting conjugated polymers that show promise for use in various electronics such as light emitting devices (LEDs),[1-5] photovoltaics[6-8] and field effect transistors.[9-10]   Polyfluorene in particular is one of few available blue-emitting conjugated polymers; its high quantum yield and thermal stability[11] make it quite promising as an active material in optoelectronic devices. Unfortunately, it has been observed that polyfluorene-based LEDs degrade with use, producing an overall decrease in emission intensity and undesirable red shift in wavelength towards a green emission.[12-15]   While this low energy emission band was initially believed to be from interchain species such as aggregates or excimers,[16-19] others have presented evidence that the emission was directly related to oxidative defects formed along the polymer backbone.[20-27,29-32]   Synthetic fluorene/fluorenone copolymers with fluorescence emission that matched that of degraded films further supported the relation between these ketone defects and green emission.[25-27]

Yet there is still debate over the exact nature of this green emission; Sims et al. proposed a new theory that an excimer between ketone defects was required for green emission.[28]   This new idea has ignited a fresh debate over the exact nature of the green peak, with recent papers testing the ketone-excimer theory.   Thorough examination of model fluorene/fluorenone oligomers and single molecule studies of similar copolymers refute the ketone excimer theory, demonstrating that a singular defect in the presence of

73

pristine chromophores is enough to produce green emission.[29-32] However, other papers that have studied the photodegredation of PFO isolated between nanoparticles claim that the intermolecular interactions are necessary for green emission.[33] A recent electrochemical study has also found another green emission band that is distinct from that observed in the fluorene/fluorenone copolymer that is assigned to crosslinked fluorenes.[34] A clear understanding of the green emission is further complicated by the role of morphology and energy transfer and the quantification of the green emission. Most studies have not examined film morphology, making a direct comparison between the different studies difficult. Comparisons are also complicated because quantification of the green emission is often done by comparing the ratio of the emission peaked at 440 nm to that at 550 nm. Since the appearance of the green emission coincides with a decrease in the blue, this ratio can often be misleading, thus a better means of quantifying green emission is to measure changes in both this ratio as well as in the absolute intensity.

In previous papers a combination of polarization Near-field Optical Scanning Microscopy (NSOM) and Atomic Force Microscopy (AFM) were used to infer the degree of polymer order between poly(di-alkylfluorenes) of varying side-chain lengths.[17,35-37] The shorter sidechain of poly(9,9'-dihexylfluorene) (PFH) displayed a higher degree of order after annealing to its liquid crystalline (LC) temperature than the longer side-chain poly(9,9'-dioctylfluorene) (PFO) more commonly seen in the literature, so PFH has been the focus of these studies in order to show the greatest effect of intermolecular interaction with defect sites. In the previous measurements it appeared that increasing the chain

74

order led to an increase in green emission that could be attributed to intermolecular interactions.[17,35-37] This was particularly the case in the PFH.[17] However, given the dramatic changes that were observed, it is possible that some of the annealing in inert atmospheres may have in fact, not been completely free of oxygen or water vapor. It has been demonstrated that thermal annealing in the presence of oxygen led to ketone defects,[21] therefore it is possible that the annealing led to changes in both film morphology and the number of ketone defects. If this was the case, what then is the role, if any, for film morphology? NSOM studies of pristine films not subjected to thermal treatment also showed a trend in which increased polymer order led to an increase in the green emission.[37] The effect of morphology cannot be discounted, as intensive research and modeling on conjugated polymers has shown the influence of film morphology on charge transport within films, where polymer chain orientation can increase charge transport.[39-44] Since ketone sites appear to behave as low energy traps,[29-32] increased transport within the film will enhance their quenching effect. Whether increased ordered leads to longer exciton diffusion distances is an open question. Studies in PPV derivatives have shown that a reduction in energetic disorder improves exciton diffusion. However, there is a simultaneous reduction in excited state lifetime.[45] In annealed MEH-PPV films this shortened lifetime has been attributed interchain species that quench the excited state that form as a result of increased ordering of the polymer chains.[46] The next effect, is that while ordering of the polymer may lead to increased exciton diffusion, the ordering may also lead to an increase in interchain species that shortened lifetime and reduce the net diffusion distance.[45]

In this paper, the role of morphology on the green emission in PFH will be examined by comparison of the emission from films before and after annealing to their liquid crystalline phase transition temperature. In order to make a quantitative comparison, the annealing was performed in situ in the fluorometer so the samples could be probed under identical conditions and film orientations. This was due to the sensitivity of the instrument, where small differences in topography, film thickness, or angle relative to the incident excitation beam have a substantial effect on the fluorescence intensity. Great care was taken to control the inert atmosphere for annealing to prevent the oxidation of the films while heating. To study the role of morphology of films with ketone defects, films were photochemically bleached before annealing. The measurements all show that when carbonyl defects are initially present within the polymer film, an increase in the alignment of the polymer chains led to an increase in the green emission, the result of increased exciton diffusion to ketone sites; without the generation of further defects.

EXPERIMENTAL SECTION

Poly(9,9-dihexylfluorene) from the Dow Chemical Company was used without further preparation. Two types of films were made: 100 nm thin films for fluorescence measurements were spincast from 1% (w/w) solutions in chloroform onto cleaned glass or quartz substrates, and ~1 micron thick films were dropcast onto aluminum-coated silicon wafer for FTIR measurements. FTIR spectra were taken on a Thermo Mattson Infinity Gold FTIR with a Pike Technologies Veemax II variable angle grazing accessory at 60˚ incident angle; thick films were treated in an identical manner as the thin films used for in situ measurements. In situ fluorescence measurements were taken in a SPEX DM3000 Fluorometer in front-face mode using a homemade holder with gas purging

capability and a thermocouple-regulated heat source. Thin films spincast on quarts substrates were sealed within the holder so that the film could be purged with dried argon; the excitation light went through the quartz substrate to excite the polymer film, minimizing surface roughness effects. With the exception of films annealed in air, all films were purged with dried argon for one hour prior to heating to ensure thorough removal of oxygen, and continued to be purged after annealing until they returned to room temperature. All annealed films were heated for two hours, within ± 1° C of the temperature mentioned. Absorbance spectra were collected on a Cary 5000 UV-VIS NIR spectrometer before and after annealing, and underwent baseline correction. Topography measurements were taken on a Digital Instruments Multimode AFM in tapping mode.

RESULTS AND DISCUSSION

As has been shown previously in literature, di-alkyl polyfluorene films can be damaged photo-oxidatively as well as thermally in air to produce the expected[21,22] cyclic ketone carbonyl stretch in FTIR spectra around 1720 cm^{-1}. Fewer defects are formed thermally, producing a much weaker peak in the IR compared to photobleaching of the films (supporting information), and films annealed under nitrogen gas showed an increase in the green peak fluorescence without any evidence of carbonyl defects in the IR spectrum. This was indicative that a few defects, beneath the detection limit of the FTIR instrument, had a considerable effect on the fluorescence emission (supporting information). Since water vapor in the gas is a potential source of oxygen for ketone defects, dried argon gas was used to purge films to prevent the creation of ketone defects

from air or water vapor. FTIR studies were performed on PFH films to ensure that defects were created within the films used for the morphology studies.

In order to directly compare the spectra before and after annealing, the heating of the sample was performed in situ in the fluorometer using a homebuilt heat cell designed to be purged with inert gas. In situ data for a PFH thin film annealed under dried argon for two hours is shown in Figure 1, exhibiting the structured blue emission characteristic of all poly(di-alkylfluorenes), with maxima at 426 nm, 450 nm and 480 nm. Direct comparison of the intensities of the emission before and after annealing requires a correction for the absorbance of the film at the excitation wavelength. Absorbance spectra taken before and after annealing (supporting information) showed a slight decrease in overall absorbance after annealing, likely due to the film forming ordered domains that have polarized absorption. Once the emission spectra were adjusted to account for the difference in the absorbance of the film at the excitation wavelength, the annealed emission was slightly higher than the pristine emission, indicating a slight increase in the quantum yield (Φ) upon annealing, as has been reported previously.[38] Figure 1 (Inset) shows the pristine and annealed spectra normalized to have the intensity at 426 nm. The two spectra are indistinguishable, indicating no defects were created after prolonged annealing under the inert atmosphere. The increase in quantum yield also demonstrates that unlike the PPV systems, an increase in polymer order does not lead to interchain species that quench the excited state. Rather, the annealing seems to remove some non-radiative decay paths and the excited state lifetime is enhanced.

78

For comparison, the effect of defects on polyfluorene emission was also examined in situ for films annealed in air. The emission spectra, adjusted for the differences in the film's absorbance at the excitation wavelength, are shown in Figure 2. The creation of ketone defects after annealing is evident in the growth of a new, small broad peak at 525 nm, coupled with a pronounced decrease in intensity of the structured blue peaks. Annealing of the films in air changes both the order of the film and the number of defects (seen by the carbonyl peak in FTIR). Since these in situ spectra show the absolute change in the film emission, it is apparent that the defects formed are highly effective at quenching blue emission, yet are not very emissive in of themselves, as only a minimal amount of green emission is produced after the creation of defects. Normalization of the two spectra to the first vibrational peak, shown in the inset of Figure 2, places emphasis on the green peak, showing its slightly greater intensity compared to the remainder of the blue peaks. Without a direct comparison of the spectra, this normalization to the first peak gives the impression that an extensive amount of green emission is produced, rather than an overall decrease in emission, seen by the in situ spectra.

As there is no evidence of defects created when films are annealed under dry argon, it was possible to study the role of morphology on films already containing a small number of defects. To generate a few ketone defects, films were photobleached under a UV lamp for forty minutes; enough to create a new broadened green peak at 520 nm in the spectrum, while not significantly quenching the blue peaks. Adjustment of the spectra for changes in absorbance did not change the final annealed emission; these spectra are shown in Figure 3. Prior to annealing, the spectrum retains much of the

79

original blue intensity, with the green peak barely noticeable. Once annealed, the intensity of the blue emission decreased by half with a concomitant, but less intense, increase in the green emission. The absolute intensity changes of this in situ data can be compared directly, and it is seen that the green emission has grown in intensity while the blue emission has decreased much more dramatically in comparison. No new defects were created as the annealing of the partially bleached film proceeded under dried argon, so this increase in the green peak must relate only to increased energy transport in the form of excitons to ketone defect sites as the polymer chains reorder into tightly-packed domains. This increase cannot be explained by an increase in quantum yield, as that would have led to an increase of emission over the entire spectrum. The only explanation for the simultaneous decrease in blue emission and increase in green is that the high energy blue excited state is funneled more efficiently to the lower energy defect sites after annealing, as no new defects have been created. Others have shown highly efficient intrachain energy transfer from pristine chromophores to defects on a single chain,[29-32] evidence that the ketone defect behaves as a low-energy trap. Although Dias *et al.*[32] examined the intermolecular energy transfer between polyfluorene and polyfluorene-fluorenone copolymers in solution, concluding that intermolecular energy transfer was inefficient, polymer chains in films are not isolated from neighboring chains as they are in solution, and increases in intermolecular energy transfer is seen when chains are well ordered and packed together.[47-49] The increase in green emission is likely not from newly formed excimer species in the annealed film; studies on similar rigid-rod PPE polymers

have shown that the ordered polymer chains minimized the unfavorable close contacts required for excimers.[50]

The degree of order within these films was examined by anisotropy measurements, which measure the degree of polarization; taken for all of the films (supporting information). Pristine films have an anisotropy of roughly 0.04, due to energy transfer among the disordered polymer segments that almost entirely washes out any polarization. Annealed PFH films have an increased degree of order, with anisotropy values of 0.14 for films annealed in air or under dried argon. The green emission in the partially bleached film annealed under dried argon has the largest film anisotropy (0.2). The large anisotropy value remains constant over the green emission, implying that the green emission is polarized in the same direction as the absorbance. This also indicates that energy transfer to the defects occurs predominately within ordered domains where the polymers have the same orientation. The anisotropies for the argon-annealed films contain a large peak on the blue edge of the spectrum that results from emission from the highest energy chromophores. These sites can only be populated by direct excitation, rather than through energy transfer, so they exhibit the highest degree of polarization.

Model spectra were created using singular value decomposition (SVD)[52] to quantitatively compare the spectra before and after annealing. The SVD was performed on the basis set of all of the spectra acquired. The SVD results indicated that the entire data set could be well represented by two basis spectra. A blue emission spectrum and green emission spectrum were created from this basis set, with one basis spectrum as essentially the blue spectrum, and the green spectrum generated by adding a sufficient

amount of the first basis spectrum to the second so that it had a positive value for all wavelengths. These two spectra were then used to fit all the acquired data simply by varying their relative amplitudes. Figure 4 shows the fit with the blue and green spectra for a PFH film bleached for forty minutes under a UV lamp prior to annealing (A), and after annealing (B). The generated full spectrum, created through the addition of the two spectra, is shown overlaid with the experimental data in the inset of both graphs of Figure 4; the excellent fit allows for quantification of the blue and green emission. Prior to annealing under dried argon, the ratio of the blue emission to the green emission in Figure 5 is 5.12, this ratio drops to 1.31 after annealing. Since both the blue and green emission change by different amounts, a comparison of the fits of just the blue or green emission reveals that the area of the blue intensity decreased 48.8% after annealing, whereas the area of the green intensity increased 103%. From these numbers alone it appears that the green emission has grown dramatically to have a higher intensity than the blue emission, however, taking into account that the blue emission was five times as large as the green emission initially, the decrease in blue was considerably larger than the increase in green. The overall emission intensity decreased by 24.4% after annealing.

The increase in green emission has been attributed to an increase in energy transfer that results from the increased order of polymer chains, and to show that the aligned polymer chains were the source of increased green emission, a partially photobleached film was annealed at a temperature below the liquid crystal (LC) temperature of 250°C for PFH. Heating the films at 150°C for the same amount of time as the LC temperature annealed films provides heating of the film without ordering the

82

chains into a liquid-crystalline phase. The emission spectra for the low-temp annealed partially-bleached PFH films, adjusted for their differences in absorption at the excitation wavelength, are shown in Figure 5. Similar to PFH annealed at its LC temperature, the emission spectra increases slightly in intensity after annealing under dried argon, showing a small increase in quantum yield. However, the inset in Figure 5 shows that the overlay of the annealed and the pristine emission spectra are completely indistinguishable, therefore the increase in quantum yield did not lead to a change in the ratio of the blue to green emission.

Unlike the PFH film annealed at the LC temperature, the film heated at the lower temperature does not show any birefringence under cross polarized illumination in a microscope, indicating a lack of micron-sized ordered domains in the film. Atomic force microscopy (AFM) images allow a comparison of the nanoscale ordering of the films. Figure 6 shows the AFM images of a film annealed at 150°C and a film annealed at the liquid crystalline phase transition temperature. The topography of the lower-temperature heated film is very similar to that of the pristine film (supporting information), with both the pristine and the lower-temperature annealed films having a rough, disordered topography. This is in stark contrast to the topography of the film annealed at the LC temperature, which exhibits bundles of aligned ribbon-like structures that extend over many microns. Near-field scanning optical microscopy studies have demonstrated that these ribbon-like features are composed of aligned polymer chains.[33] Therefore it is apparent that the increase in the green emission in the LC annealed and partially-bleached film resulted from an increase in polymer order, allowing for more efficient energy

transfer to the defect sites.[39,44]   Without this alignment the only change is the slight increase in quantum yield with no increase in green emission.

CONCLUSIONS

In situ annealing of PFH films allowed for direct comparison of the absolute changes in emission spectra, and these changes were quantified using SVD basis spectra. Films annealed under dried argon showed no evidence of ketone defect formation, thus it was possible to monitor the effect of increased film order on emission of a film already containing defects.   An increase in green emission was seen in annealed films containing defects, evidence that increased polymer order led to increased diffusion of excitons from pristine chains to trapping defect sites.   Quantification of the amount of blue and green emission supported this evidence, showing that energy from the blue emission was transferred more efficiently to the defect sites to produce more green emission.   The increase in polymer chain order was definitively found to be the source of the increase in green emission and decrease in blue emission for films annealed to the LC temperature, thus the reordering of polymer chains into tightly-packed domains is required for the increased exciton diffusion to the few defect sites in the film.   These results should be generic for other conjugated polymer systems in that increase order should lead to more efficient energy transfer.   The caveat being that in some systems such as PPV derivatives increased order can also shorten the excited state lifetime.[45-46]   The results have important implications for polymer photovoltaics, as initial steps for generating charges within a polymer photovoltaic requires efficient exciton transport to heterojunctions.[53]   The morphologies in these polymer solar cells are often limited as the exciton diffusion length is roughly 10 nm or less.[54]   Thus the use of aligned polymer chains can increase the

exciton diffusion distances if interchain species can be minimized, allowing for more efficient movement of excitations to the charge separation heterojunctions.
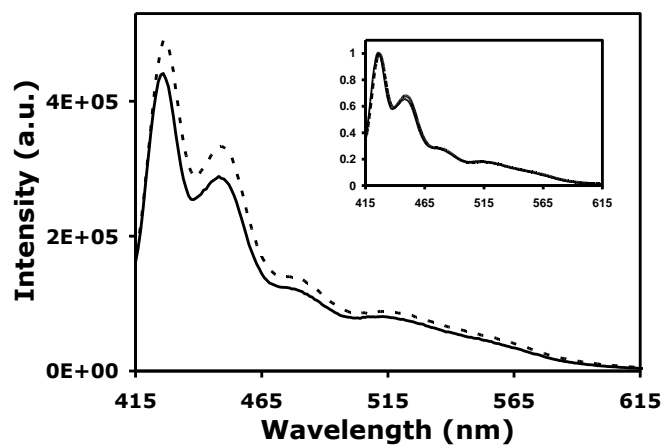
Figure 1: Pristine PFH emission (solid line) and after annealing under dried argon (dashed line). Both spectra normalized to the 426 nm blue peak (inset) showing no increase in green emission.
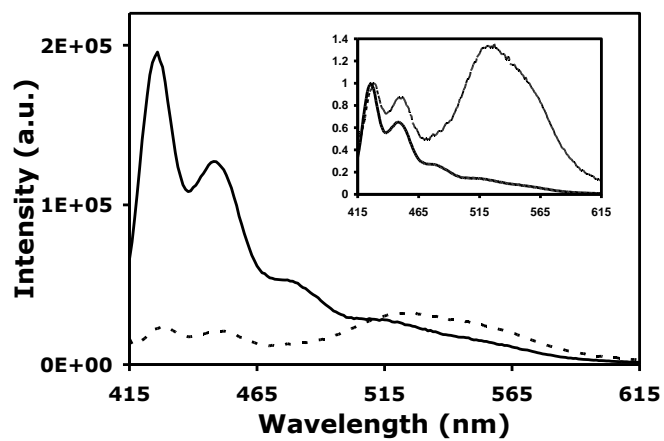
Figure 2. Pristine PFH film emission (solid line) and emission after film was annealed in air (dashed line). The spectra are normalized to the first blue peak, illustrating the increase in green emission (inset).

.
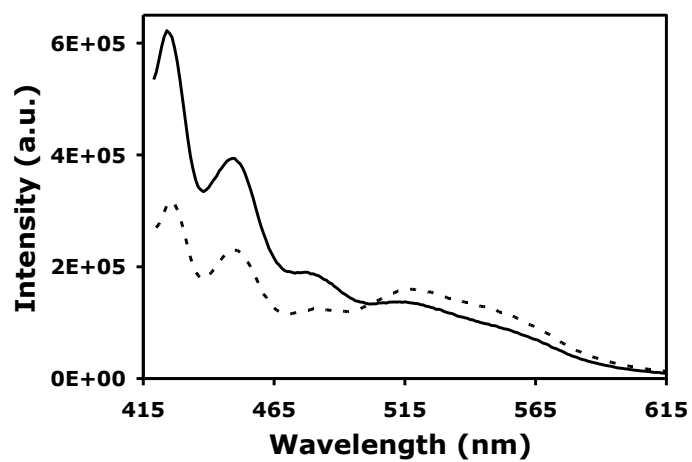
Figure 3. In situ emission spectra of a partially photobleached PFH film prior to annealing (solid line), and after annealing (dashed line). The intensity of the blue emission decreased, and a slight growth in the green emission was also observed.
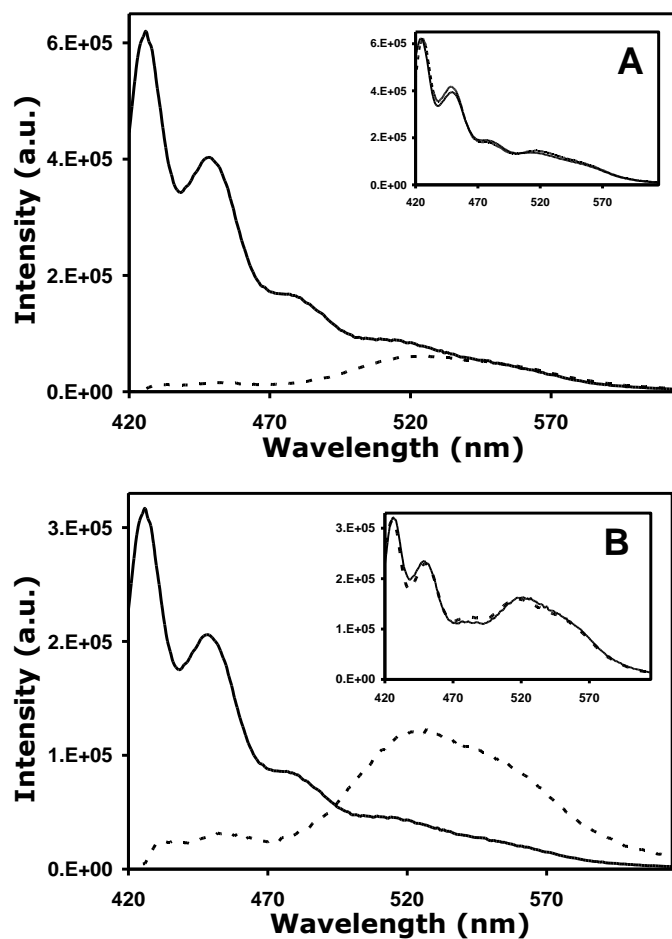
Figure 4. Model spectra for the partially bleached PFH film prior to annealing (A), and after annealing (B). For both, the generated blue spectrum (solid line) and green spectrum (dashed line) are combined (inset, dashed line) and overlaid with the actual emission spectrum (inset, solid line), with nearly identical overlay.
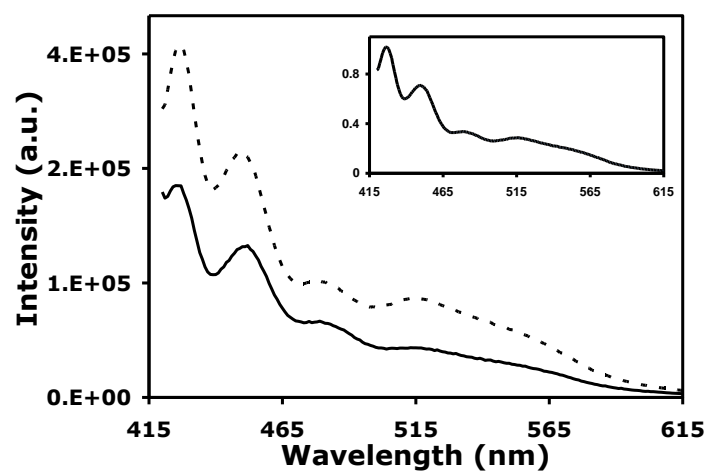
Figure 5. Partially bleached PFH film emission (solid line) and emission after heating to 150˚C for 2 hours (dashed line). Both spectra normalized to the initial blue peak, showing an identical overlay.
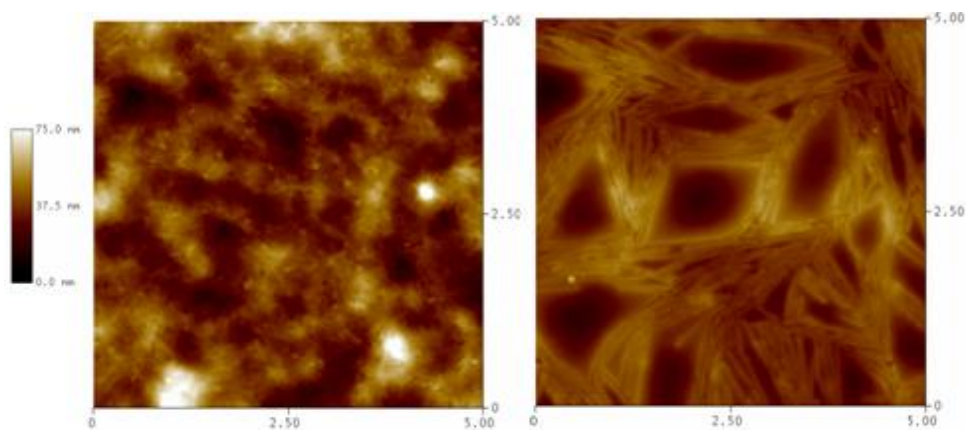
Figure 6. 5x5 µm AFM scans of PFH films annealed at 150˚C (left) for two hours and 250˚C (right) for two hours. The film annealed at 250˚C has its polymer chains reordering into long ribbon-like structures.

REFERENCES

(1) Friend, R. H.; Gymer, R. W.; Holmes, A. B.; Burroughes, J. H.; Marks, R. N.; Taliani, C.; Bradley, D. D. C.; Dos Santos, D. A.; Bredas, J. L.; Logdlund, M. L.; Salaneck, W. R. *Nature* **1999**, *397*, 121.

(2) Nakazawa, Y. K.; Carter, S. A.; Nothofer, H. −G.; Scherf, U.; Lee, V. Y.; Miller, R. D.; Scott, J. C. *Appl. Phys. Lett.* **2002**, *80*, 3832.

(3) Grice, A. W.; Bradley, D. D. C.; Bernius, M. T.; Inbasekaran, M.; Wu, W. W.; Woo, E. P. *Appl. Phys. Lett* **1998**, *73*, 629.

(4) Bernius, M. T.; Inbasekaran, M.; O'Brian, J.; Wu, W. *Adv. Mater.* **2000**, *12*, 1737.

(5) Leger, J. M.; Carter, S. A.; Kuhstaller, B.; Nothofer, H. G.; Scherf, U.; Tillman, H.; Horhold, H.H. *Phys. Rev. B.* **2003**, *5*, 4209.

(6) Arias, A. C.; MacKenzie, J. D.; Stevenson, R.; Halls, J. J. M.; Inbasekaran, M.; Woo, E. P.; Richards, D.; Friend, R. H. *Macromolecules* **2001**, *34*, 6005.

(7) McNeill, C. R.; Frohne, H.; Holdsworth, J. L.; Dastoor, P. C. *Nano Lett.* **2004**, *4*, 2503.

(8) Kietzke, T.; Neher, D.; Kumke, M.; Montenegro, R. *Macromolecules* **2004**, *37*, 4882.

(9) Chua, L.; Zaumseil, J.; Chang, J.; Ou, E. C.-W.; Ho, P. K. −H.; Sirringhaus, H.; Friend, R. H. *Nature* **2004**, *434*, 194.

(10) Sirringhaus, H.; Wilson, R. J.; Friend, R. H.; Inbasekaran, M.; Wu, W.; Woo, E. P.; Grell, M.; Bradley, D. D. C. *Appl. Phys. Lett.* **2000,** *77*, 406.

(11) Millard, I. S. *Synth. Met.* **2000**, *111-112*, 119.

(12) Bliznyuk, V. N.; Carter, S. A.; Scott, J. C.; Klärner, G.; Miller, R. D.; Miller, D. C. *Macromolecules* **1999**, *32*, 361.

(13) Weinfurtner, K. H.; Fujikawa, H.; Tokito, S.; Taga, Y. *Appl. Phys. Lett.* **2000**, *76*, 2502.

(14) Lee, J. I.; Klaerner, G.; Miller, R. D. *Synth. Met.* **1999**, *101*, 126.

(15) Pei, Q. B.; Yang, Y. *J. Am. Chem. Soc.* **1996**, *118*, 7416

(16) Lemmer, U.; Heun, S.; Mahrt, R. F.; Scherf, U.; Hopmeier, M.; Siegner, U.; Göbel, E. O.; Müllen, K.; Bässler, H. *Chem. Phys. Lett.* **1995**, 373.

(17) Teetsov, J.; Vanden Bout, D. A. *Langmuir* **2002**, *18*, 897.

(18) Grell, M.; Bradley, D. D. C.; Ungar, G.; Hill, J.; Whitehead, K. S. *Macromolecules* **1999**, *32*, 5810.

(19) Cimrová, V.; Scherf, U.; Neher, D. *Appl. Phys. Lett.* **1996**, *69*, 608.

(20) List, E. J. W.; Guentner, R.; de Freitas, P. S.; Scherf, U. *Adv. Mater.* **2002**, *14*, 374.

(21) Gong, X.; Iyer, P. K.; Moses, D.; Bazan, G. C.; Heeger, A. J.; Xiao, S. S. *Adv. Funct. Mater* **2003**, *13*, 325.

(22) Hintschich, S. I.; Rothe, C.; Sinha, S.; Monkman, A. P.; de Freitas, P. S.; Scherf, U. *J. Chem. Phys.* **2003**, *119*, 12017.

(23) Lupton, J. M.; Craig, M. R.; Meijer, E. W. *Appl. Phys. Lett.* **2002**, *80*, 4489.

(24) Zojer, E.; Pogantsch, A.; Hennebicq, H.; Beljonne, D.; Bredas, J. L.; de Freitas, P. S.; Scherf, U.; List, E. J.W. *J. Chem. Phys.* **2002**, *117*, 6794.

(25) Gong, X.; Moses, D.; Heeger, A. J.; Xiao, S. *Synth. Met.* **2004**, *141*, 17.

(26) Dias, F. B.; Maiti, M.; Hintschich, S. I.; Monkman, A. P. *J. Chem. Phys.* **2005**, *122*, 054904.

(27) Romaner, L.; Pogantsch, A.; de Freitas, P. S.; Scherf, U.; Gaal, M.; Zojer, E.; List, E. J. W. *Adv. Funct. Mater.* **2003**, *13*, 597.

(28) Sims, M.; Bradley, D. D. C.; Ariu, M.; Koeberg, M.; Asimakis, A.; Grell, M.; Lidzey, D. G. *Adv. Funct. Mater.* **2004**, *14*, 765.

(29) Pogantsch, A.; Zaami, N.; Slugovc, C. *Chem. Phys.* **2006**, *322*, 399.

(30) Becker, K.; Lupton, J. M.; Feldmann, J.; Nehls, B. S.; Galbrecht, F.; Gao, D.; Scherf, U. *Adv. Funct. Mater.* **2006**, *16*, 364.

(31) Chi, C.; Im, C.; Enkelmann, V.; Ziegler, A.; Lieser, G.; Wegner, G. *Chem. Eur. J.* **2005**, *11*, 6833.

(32) Dias, F. B.; Knaapila, M.; Monkman, A. P.; Burrows, H. D. *Macromolecules* **2006**, *39*, 1598.

(33) Aharon, E.; Albo, A.; Kalina, M.; Frey, G. L. *Adv. Funct. Mater.* **2006**, *16*, 980.

(34) Montilla, F.; Mallavia, R.; *Adv. Funct. Mater.* **2007**, *17*, 71.

(35) Teetsov, J; Vanden Bout, D. A. *J. Am. Chem. Soc.* **2001**, *123*, 3605.

(36) Teetsov, J; Fox, M. A. *J. Mater. Chem* **1999**, *9*, 2117.

(37) Teetsov, J; Vanden Bout, D. A. *J. Phys. Chem. B* **2000**, *104*, 9387.

(38) Asada, K.; Kobayashi, T.; Naito, H. *Jpn. J. Appl. Phys.* **2006**, 45, L247.

(39) Hennebicq, E.; Pourtois, G.; Scholes, G. D.; Herz, L. M.; Russel, D. M.; Silva, C.; Setayesh, S.; Grimsdale, A. C.; Müllen, K.; Bredas, J-L.; Beljonne, D. *J. Am. Chem. Soc.* **2005**, *127*, 4744.

(40) Sreearunothiaj, P.; Morteani, A. C.; Avilov, I.; Cornil, J.; Beljonne, D.; Friend, R. H.; Phillips, R. T.; Silva, C.; Herz, L. M. *Phys. Rev. Lett.* **2006**, *96*, 117403.

(41) Nguyen, T-Q.; Yee, R. Y.; Schwartz, B. J. *J. Photochem. Photobiol. A.* **2001**, *144*, 21.

(42) Nguyen, T-Q.; Schwartz, B. J. *J. Chem. Phys.* **2002**, *116*, 8198.

(43) Schwartz, B. J. *Annu. Rev. Phys. Chem.* **2003**, *54*, 141.

(44) Wong, K. F.; Bagchi, B.; Rossky, P. J. *J. Phys. Chem. A* **2004**, *108*, 5752.

(45) Markov, D. E.; Tanase, C.; Blom, P. W. M.; Wildeman, J. *Phys. Rev. B* **2005**, *72*, 045217-1.

(46) Nguyen, T. Q.; Martini, I. B.; Liu, J.; Schwartz, B. J. *J. Phys. Chem. B* **2000**, *104*, 237.

(47) Prins, P.; Grozema, F. C.; Nehls, B. S.; Farrell, T.; Scherf, U.; Siebbeles, L. D. A. *Phys. Rev. B.: Condens. Matter Mater. Phys.* **2006**, *74*, 113203/1.

(48) Chou, H.; Lin, K.; Fan, Y.; Wang, D. *J. Polym. Sci., Part B: Polym. Phys.* **2005**, *43*, 1705.

(49) Lee T. and Ok, O. Park *Adv. Mater.* **2000**, *12*, 801.

(50) Bunz, U. H. F.; Imhof, J. M.; Bly, R. K.; Bangcuyo, C. G.; Rozanski, L.; Vanden Bout, D. A. *Macromolecules* **2005**, *38*, 5892.

(51) Zhao, W.; Cao, T.; White, J. M. *Adv. Funct. Mater.* **2004**, *14*, 783.

(52) Henry, R.; Hofrichter, J. *Methods in Enzymology* **1992**, *210*, 129.

(53) Snaith, H. J.; Friend, R. H. *Thin Solid Films* **2004**, *451*, 567.

(54) Ramsdale, C. M.; Bache, I. C.; MacKenzie, J. D.; Thomas, D. S.; Arias, A. C.; Donald, A. M.; Friend, R. H.; Greenham, N. C. *Physica E* **2002**, *14*, 268.

Chapter 5: Twist Induced Charge Transfer Molecular Rotors used to Report on Local Dynamics of Self-Assembled Block Copolymer Materials

CHAPTER SUMMARY

Local molecular dynamics within phase segregated block copolymer films were studied through synthetic placement of a molecular rotor dye into specific locations along the block co-polymer chain. Temperature dependent fluorescence measurements of the dye were utilized to measure local glass transition temperatures in thin films of the different block copolymer systems. The dynamics of the covalently bound probe placed precisely at the interface of the polymer blocks was found to show two transitions, distinct from either bulk material.

INTRODUCTION

Block copolymer systems are the basis for a wide array of applications including drug delivery systems, microfluidic devices, molecular electronic energy materials and photonic systems. The advantage of block copolymer systems is their ability to self-assemble into well-defined nanostructures, the morphology of which can be controlled via synthesis of the polymer.[1,2] The dynamics within block copolymer systems is unique compared to bulk phase segregated polymer films, as the two blocks are covalently bound at the interface and thus confined to heterogeneous nano-scale regions.[3] This nano-scale confinement of materials has been demonstrated to result in large perturbations of their physical properties. The confinement of chains to small spatial regions, exposed surfaces, and substrate interfaces all have been shown to cause large deviations from the bulk glass transition temperature (T_g).   This deviation from the bulk thermal properties can range

from less than 1 degree to tens of degrees.[4-7] Without a thorough understanding of the heterogeneous, morphological dependent behavior of these materials when organized as thin films, material properties, polymer behavior and device functionality are extremely difficult to optimize.[8-11] This challenge is compounded further when block copolymers are studied, as an additional interface has been created where the blocks meet.

Previous research has utilized the temperature dependence of fluorescent probes to locate the glass transition of single or multi-layer thin films.[12-15] Here we utilize a twisted intramolecular charge transfer (TICT) dye as a molecular rotor to report on local dynamics. Molecular rotors show a direct relationship between their local environment and their emissive properties as a result of competing pathways for relaxation upon photoexcitation.[16-19] One route involves intramolecular charge transfer coupled with a molecular rotation, making radiative relaxation substantially less probable. This path is favored in low viscosity environments where free rotation can occur. The second path is a radiative emission that occurs if the aforementioned free rotation is restricted, as is the case in highly viscous environments. Previously, solvatochromic properties of TICT dyes have been used to report on the local heterogeneities of complex materials.[20-22] However, studies have not involved dye covalently bound to specific locations within a block copolymer chain with the degree of control presented here.

EXPERIMENTAL SECTION

Synthetic Methods

A series of polynorbornene based copolymers were synthesized containing two, roughly equal sized polymer blocks with different glass transition temperatures. These polymers were synthesized through ring-opening metathesis polymerizations using 1st

96

generation Grubbs' catalyst.[23] One block (B) has a benzyl pendant group and exhibits a higher T_g while the other block (O) has octyl pendant chains. Three different block copolymers were synthesized which have the TICT probe covalently polymerized into different locations along the polymer chain. As can be seen in Figure 2, the dye (T) is either within the benzyl block poly(BTBO), within the the octyl block poly(BOTO), or directly at the interface of the two blocks poly(BTO). These three polymers were then dropcast onto glass substrates and solvent annealed with o-DCB to allow phase segregation.

Experimental Measurements

Topography images acquired with an atomic force microscope (AFM) were used to identify the extent of lateral phase segregation. All films showed increased order upon solvent annealing, as the average domain size obtained via AFM decreased in size for all samples over longer timescales.

A modified SPEX Flourolog 1 from Horiba Jobin Yevon with a 450W xenon lamp was used for all temperature dependent measurements. The instrumentation was controlled via a custom labview program.

RESULTS AND DISCUSSION

Figure 3 shows the temperature dependent fluorescence intensity of poly(BTBO). As the temperature is raised, the fluorescence intensity of the film decreases. As mentioned, the quantum yield of the TICT dye is strongly dependent on its ability to twist in the excited state. Thus, as the temperature is raised the polymer has greater conformational freedom and the dye is more able to twist into its non-radiative conformation which decreases fluorescence. However, the extent of fluorescence

97

decrease with temperature increase is not constant. At a particular temperature, there is a discontinuity in the slope of the temperature dependent fluorescence, which has been shown to correlate with the T_g of the polymer. [20] This is a result of the thermal expansion coefficient of the glassy polymer being different from that of the rubbery state, above T_g. For poly(BTBO) only one T_g is observed as the probe is only located with the benzyl block. The lack of a transition corresponding to the octyl block indicates that the dye is not influenced by the octyl block and thus the film is well segregated. In order to accurately determine the temperature point at which the slope changes, a finite difference method was used in which a running average and standard deviation were calculated for the slope starting from the high and low temperature ends of the data. Sequential points were compared with this data set, and when the next data point did not fall within the standard deviation of the previous data, it was deemed to be the start of a transition. Through application of the method to both high and low temperature sides of the data, the transition temperature range was determined. This defines the temperature range at which the probe molecule is experiencing significantly changing environments.

Poly(BTBO) and poly(BOTO) exhibit distinct T_g from each other using this method. This is a clear indication of self-assembly into ordered, phase segregated domains in the block copolymer films, as in either film the dye dynamics are not affected by the opposite block. For this to occur ordered regions within the films are required. If the film was not sufficiently ordered, both the poly(BOTO) and the poly(BTBO) samples would show similar dynamics. The agreement between the spectroscopically determined local dynamics and bulk measurement using differential scanning calorimetry (DSC) confirms the ordering and accuracy of the spectroscopic properties.

The material which provides the most insights at the molecular level is poly(BTO), in which the dye is covalently bound at the interface between the two blocks.

In this location the dye shows two transition temperatures. The temperature of both transitions (-25±6C and 15±4C) is not far from the DSC values of T_g for the bulk (-25and15 C). The fact that there are two transitions implies that the probe is not only covalently bound between a B and O molecule but is physically located at an interfacial bulk region and thus is affected by dynamic changes to either block. In other words, the dye is affected by the T_g of both blocks. This means that heterogeneous dynamics exist where nanoscale confinement of the two blocks is present within the film. The fact that both T_g's measured with the dye are at lower temperatures than the T_g of pure B and O, provides molecular insight into what is occurring at the interface. The shift of the transitions to lower temperatures at the interface of the blocks indicates that this is the area with the highest enthalpy and thus is the first to melt. This is most likely a result of the larger free volume that exists at the interface, as the material is less ordered than areas composed entirely of only one block.

This proves the dynamics measured at the interface are different than the bulk dynamics within the copolymerized blocks. Of a greater interest is the length scale of this effect. Using the synthetic method and analysis techniques outlined in this paper it is possible to measure local dynamics with lateral resolution greater than current imaging techniques, with theoretical resolution through monomer unit control of ~ 0.6 nm. However, despite the synthetic placement of the dye at specific locations along the polymer chain, the physical conformation of the polymer complicates the measurement as a distribution of distances from the interface is now to be expected due to distribution of polymer conformations within a thin film. This may limit the resolution.

CONCLUSIONS

In conclusion, we have a demonstrated the capabilities of a molecular rotor fluorescent dye to be incorporated at specific locations within a block copolymer system to report on local film dynamics. These local measurements differ substantially from bulk measurement techniques. Specific insights into the interfacial region are provided via a self-assembling block copolymer system. The depression of T_g at the interface shows the lateral heterogeneity with the bulk material which has great promise for elucidating local dynamics of a variety of block copolymer materials, specifically interfaces.
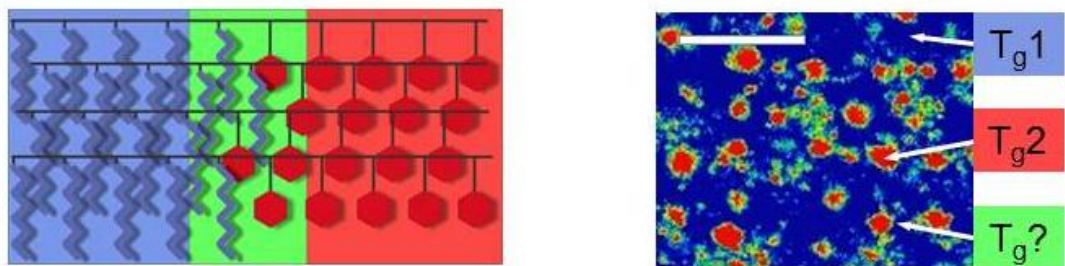
Figure 1. Schematic representation of interfacial regions within the block copolymer thin film. An AFM topography image of a solvent annealed film is used to articulate the chemical composition of different regions within in the film.
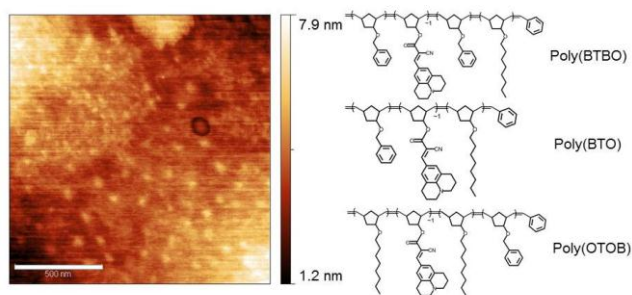
Figure 2. The AFM topography image of the poly(BOTO) film on glass that has been solvent annealed for one day. Beside the micrograph the chemical structures are shown for the block copolymers studied..
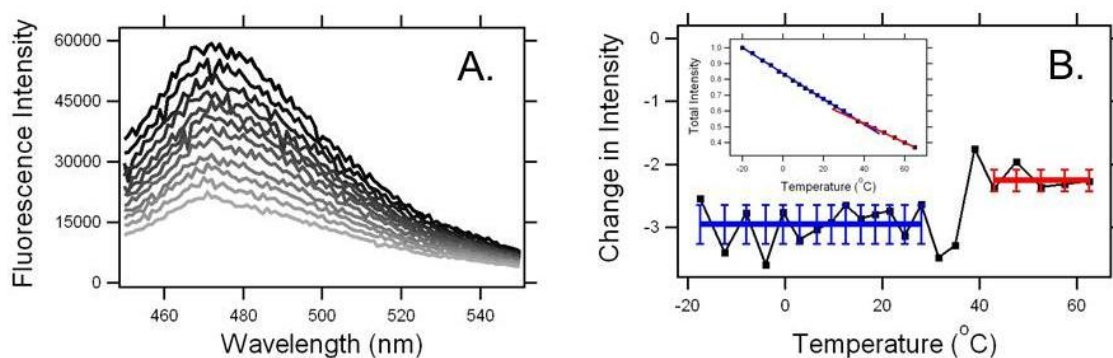
. **Figure 3. (A.)** The total fluorescence of poly(BTBO) as a function of temperature is shown. The total quantum yield decreases as the temperature is increased. **(B.)** The change in total fluorescence intensity is shown. T_g was determined to be $35C \pm 5$. The blue line indicates the running average and standard deviation for below the glass transition temperature. The red line indicates the region above the T_g. The inset shows the total intensity with the two linear regressions applied to the change in the rate of fluorescence.
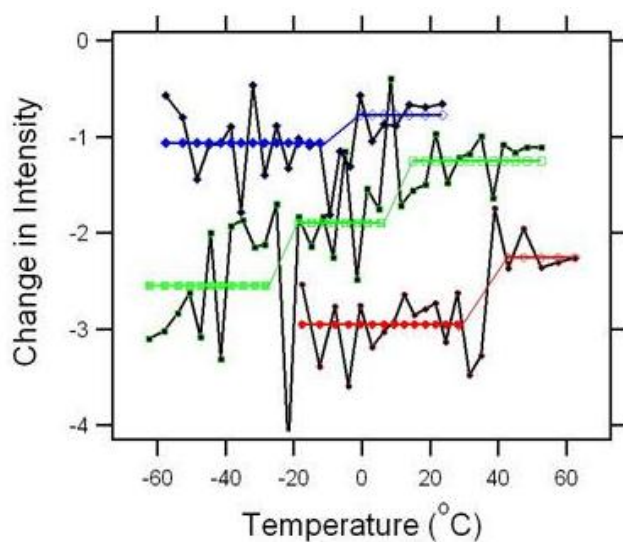
Figure 4. The change in total fluorescence and the calculated average of the change in total fluorescence is shown for the three polymers. The dye bound between benzyl groups poly(BTBO) is shown in red; and the dye bound between octyl substituent groups poly(BOTO) is shown in blue. When the dye is specifically bound at the interface of the two blocks poly(BTO) is shown in green.

REFERENCES

(1)   Jenekhe, S. A.; Chen, X. L. *Science* **1999**, *283*, 372-375.

(2)   Leibler, L. *Macromolecules* **1980**, *13*, 1602-1617.

(3)   Alcoutlabi, M.; McKenna, G. B. *J. Phys.: Condens. Matter* **2005**, *R*.

(4)   Abetz, V. *Block Copolymers I*; Springer-Verlag: Berlin, 2005; Vol. 189.

(5)   Mok, M. M.; Kim, J.; Marrou, S. R.; Torkelson, J. M. *Eur. Phys. J. E: Soft Matter Biol. Phys.* **2010**, *31*, 239-252.

(6)   Kim, S. D.; Torkelson, J. M. *Macromolecules* **2002**, *35*, 5943-5952.

(7)   Kim, S.; Roth, C. B.; Torkelson, J. M. *J. Polym. Sci., Part B: Polym. Phys.* **2008**, *46*, 2754-2764.

(8)   Ellison, C. J.; Ruszkowski, R. L.; Fredin, N. J.; Torkelson, J. M. *Phys. Rev. Lett.* **2004**, *92*, 095702/1-095702/4.

(9)   Harrats, C. G., G. *Micro- and Nanostructured Multiple Polymer Blend Systems: Phase Morphology and Interfaces*; Taylor & Fancis: New York, 2006.

(10)   Kim, S.; Hewlett, S. A.; Roth, C. B.; Torkelson, J. M. *Eur. Phys. J. E: Soft Matter Biol. Phys.* **2009**, *30*, 83-92.

(11)   Shiraishi, Y.; Inoue, T.; Hirai, T. *Langmuir* **2007**, ACS ASAP.

(12)   Ellison, C. J.; Torkelson, J. M. *Nat. Mater.* **2003**, *2*, 695-700.

(13)   Roth, C. B.; Torkelson, J. M. *Macromolecules* **2007**, *40*, 9.

(14)   Ellison, C. J.; Torkelson, J. M. *J. Polym. Sci., Part B: Polym. Phys.* **2002**, *40*, 2745-2758.

(15)   Mok, M. M.; Kim, J.; Wong, C. L. H.; Marrou, S. R.; Woo, D. J.; Dettmer, C. M.; Nguyen, S. T.; Ellison, C. J.; Shull, K. R.; Torkelson, J. M. *Macromolecules* **2009**, *42*, 7863-7876.

(16)   Ramalingam, A.; Sivaram, B. M.; Palanisamy, P. K.; Masilamani, V. *Spectrochim. Acta, Part A* **2000**, *56A*, 1205-1210.

(17)   Haidekker, M. A.; Theodorakis, E. A. *Org. Biomol. Chem.* **2007**, *5*, 1669-1678.

(18)   Jones, G., II; Jackson, W. R.; Choi, C. Y.; Bergmark, W. R. *J. Phys. Chem.* **1985**, *89*, 294-300.

(19)   Zhu, D.; Haidekker, M. A.; Lee, J.-S.; Won, Y.-Y.; Lee, J. C. M. *Macromolecules* **2007**, *40*, 7730-7732.

(20)   Priestley, R. D.; Ellison, C. J.; Broadbelt, L. J.; Torkelson, J. M. *Science* **2005**, *309*, 456-459.

(21)   Rittigstein, P.; Torkelson, J. M. *J. Polym. Sci., Part B: Polym. Phys.* **2006**, *44*, 2935-2943.

(22)   Rittigstein, P.; Priestley, R. D.; Broadbelt, L. J.; Torkelson, J. M. *Nat. Mater.* **2007**, *6*, 278-282.

(23)   Trnka, T. M.; Grubbs, R. H. *Accounts of Chemical Research* **2001**, *34*, 11.

Chapter 6: Effect of Long Range Order on Measurements of Novel Block Copolymers Dynamics using a Local Reporter

CHAPTER SUMMARY

In this report we present the synthesis and characterization of a novel system of block copolymers with a covalently bound twist intermolecular charge transfer (TICT) dye that reports on the local dynamics of the material specifically the glass transition temperature. The synthesis of a block copolymer system that contains functional pendant groups covalently bound to the backbone, the two functional backbones have very different glass transition temperatures and phase segregate. A TICT dye was selectively placed within each phase of the block copolymer system to report on the local dynamics within specific regions of a thick (several microns) free standing film. Temperature dependent fluorescent measurements were performed to directly observe the material dynamics. The results showed that covalently bonding dye into the backbone affects the temperature dependence of the fluorescence of the TICT dye. Order within the film shifts the observed glass transition temperatures closer to the bulk material experimental values.

INTRODUCTION

The use of block copolymer systems are the fundamental building block for several exciting fields of research. Block copolymers have been used for drug delivery systems, microfluidic devices, molecular electronic energy materials and photonic systems. [1-6] These very diverse fields utilize the morphological and dynamic properties of block copolymers which are tailored to the specific material need. Such a system has been proposed with organic solar cells in a triblock system where morphology, dynamics and

intermixing all play an intimate role. [7-12]Dynamics of block copolymer systems, specifically the glass transition temperature, is of interest to condensed matter physics and are poorly understood. Block copolymer research currently focuses on polystyrene/polymethylmethacrylate systems. The first step toward creating organic devices where the donor/acceptor are bound together is accomplished by characterizing a more simple block copolymer system before functional materials are incorporated.

Glass transition is the change from crystalline to glassy state which is as the temperature where a system moves on a laboratory scale (on the order of seconds) instead of that of a solid (order of hours). For block copolymer systems (AB) where region A has a significantly different transition temperature from that of the region B, if the materials segregate it will act as independent phases, as is diagramed in Figure 1. Of interest is the interface region between well-defined AB regions. Does the region feel one transition between that of region A and region B or two different transitions. [13] Based on previous research it is ambiguous which circumstance happens. [14, 15] But there is of great interest and research related to the persistence length, the length scale on which the effect persists, where the mere presence of another material being in contact. Such a scenario is cooperatively rearranging regions (CRR). [14, 16, 17]Published reports of such persistence length vary from 1-4nm to x>100nm in systems with highly attractive substrate where the ordering within the system. It is the poor understanding of both the nature of the glass transition of mixed materials as well as the interface that motivates this research.

Confining semi-crystalline polymers on the order of the nanoscale, results in large perturbations of their physical properties and dynamics. Glass transition temperatures

(T_g) of confined polymers have been heavily characterized as this attribute macroscopic property is related to the polymer's physical local environment. [17, 18] Confining the mobility of individual chains by grain boundries on the order of chain length, exposed surfaces, and substrate energetics modulation have all been shown to cause large deviations from the bulk material T_g. [19] This deviation from the bulk thermal properties can range from less than 1 degree to greater than 50 degrees. [20, 21]

This change in the physical properties of the polymer can have large effects on applications which utilize polymer or block copolymer films such as microelectronics. Without a thorough understanding of the behavior of polymers when organized as thin films, material properties, polymer behavior and device functionality are extremely difficult to improve upon. This challenge is compounded further when block copolymers are studied, as an additional interface has been created where the blocks meet or a mix of the two blocks has been created if the material does not phase segregate. In order to design copolymers which self-assemble into particular morphologies and possess useful properties, close attention must be paid to the respective T_g that is expected for each block when self-assembled into films with long range order. [22]

Linear diblock copolymers of the form AB have been shown to form a litany of equilibrium microphase morphologies which are dependent upon both the ratio of A and B and the energetic interaction of A and B. Thus, predicting the interactions between polymer blocks and their expected morphology, is at the very least phonological. Tight control over phase separation is truly a prerequisite to designing and creating effective devices based on multiblock polymers. [18, 23]

Initially, Keddie et al. was able to demonstrate deviations in the T_g of polystyrene films. Ellipsometry was used to measure film thickness as a function of temperature, allowing a characterization of the T_g of films supported by silica. [24]   This work was advanced and supported by Ellison and Torkelson, when they were able to show that the deviation in T_g is seen as a function of the distance from the free surface as well as the substrate. Furthermore, they were able to randomly dope or specifically label polystyrene films with a fluorophore and detect changes in the emissive intensity as the temperature was modulated with results where the polymers stopped behaving as a solid. [14, 17, 25]   Other methods of probing local polymer dynamics, including T_g measurements that have been attempted include: Brillouin scattering, X-ray reflectivity, dielectric spectroscopy, differential scanning calorimetry (DSC), and solid state nuclear magnetic resonance. [26-28, 29]

Synthetically novel block copolymers are of interest as the march toward studying functional materials can be bridged by such intermediates. Previous research utilizing twist intermolecular charge transfer dyes (TICT) have found the quantum yield and emission energy is dependent on the local environment of the dye. [30, 31] As such, TICT dyes have had their solvatachromic properties used to report on the local heterogeneities of complex samples. TICT dyes have been used to report on the glass transition temperatures as the region affects the emission energy and total emission of the dye. Research has found that the reported glass transition from fluorescent methods can be modulated by several factors. Deviations from bulk T_g values have been observed in polymer films previously based on several factors. Factors such as thickness,

crystallinity, intermixing, nano confinement, edge effects, hardness, absorbed water and free volume are determined implicitly by decreasing the effect until it becomes the bulk value. Factors such as thickness, edge effects, and absorbed water can be quantified and corrected for using spectroscopic elipsometery which allows these parameters to be directly modeled. [3, 27, 28, 32] However, none of the past methods of local T_g measurements, fluorescent or otherwise, have utilized emissive reporters covalently bonded to a specific region with monomer placement precision to report on the local dynamics of the film. Heterogeneity of the system and accuracy of the method can directly verified with DSC, for a block copolymer system in solution there are two phase transitions measured. [33, 34] By modulating the spatial orientation of a local reporting dye molecule within the block copolymer system it possible to come to more meaningful conclusions about block copolymer properties on and distributions of the properties than with more commonly used bulk techniques.

Studying the interface of block copolymers is important for a tri block copolymer energy harvesting material. The interface is of specific consequence for charge separation in photovoltaic materials. [7, 11, 13, 29, 35-43] The persistence length of one material on a phase segregated material is essential for charge extraction away from interfaces as well. Using a similar polymer backbone from ring opening metathesis polymerization (ROMP) where the pendent groups conduct and have analogous solvation groups could be utilized as a covalently bonded tri block solar cell material. Once an excited state has been spilt into free carriers the mobility of the carrier through the material limits the collection efficiency. The more pure the material the larger the mobility, the degree of phase

111

segregation of block copolymer films created via solvent methods is also important. The amount of mixing in organic photovoltaic devices has been shown to affect device performance. We were able to modulate the amount of phase segregation within the films by solvent annealing the films for twenty four hours. Solvent annealing allows for solvent to absorb and desorb repeatedly which increases the amount of ordering within the films. The increased order within films affects the observed dynamics as T_g is directly related to the phase segregation of the material. As the amount of phase segregation increase the T_g observed by the report will trend toward the bulk T_g value measured by more standard techniques that are only capable of measuring the bulk values of a material.

We have synthesized a group of novel block copolymers with a TICT dye covalently bonded at selected points within the AB region. This work answers the question of when a local fluorescence reporter which is bonded within a specific region of a block copolymer does the response of the TICT dye as a function of temperature report on the local dynamics.

EXPERIMENTAL SECTION

Materials.

All chemicals were purchased from commercial suppliers and were used as received. Solvents were dried using Pure-Solv 400 solvent purification system and reactions were performed under inert atmosphere using standard Schlenk techniques except where otherwise noted. Column chromatography was carried out on Silicyle® SiliaFlash® F60, 40-63 mm 60Å or neutral activated alumina, Brockmann I. Thin layer chromatography was performed on precoated silica gel F254 plates with fluorescent indicator or on precoated aluminum oxide IB-F plates. Visualization of non-

fluorescent/non-quenching molecules was done in an I_2 chamber or through a potassium permanganate dip. Deuterated solvents were purchased from Cambridge Isotope Laboratories and used without further purification.

Typical Polymerization.

For poly(BTBE), equimolar stock solutions, 0.25 M, of the benzyl monomer and ethylhexyl monomer were made in dry CH_2Cl_2. Additionally, stock solutions of the TICT(juliodene) monomer (0.023 M) and 1st generation Grubbs' catalyst (0.012 M) were made in dry CH_2Cl_2. A 5 mL vial was charged with a stir bar and 500 μL of benzyl stock solution was added. With stirring a 40 μL injection of catalyst was made. After 3 hours of stirring, 50 μL of TICT stock solution was added. After another 30 minutes of stirring, 500 μL of the benzyl stock solution was added. After 3 hours, a 1.00 mL of injection of the ethylhexyl solution was added. The reaction was quenched after another 3 hours with ethyl vinyl ether. After 30 minutes of stirring, the polymer was precipitated into excess MeOH, filtered, and thoroughly rinsed with additional MeOH.

Sample preparation.

Samples were prepared by dropcasting 20mg/mL of polymer in ortho-dichlorobenzene onto a glass cover slip cleaned by sonication in acetone. Dropcast films were then desiccated immediately by vacuum system for 5 hours. Solvent annealed films were dropcast, then allowed to remain in a solvent rich environment for 24 hours and then vacuum pumped for five hours.

Instrumentation.

Fluorescent measurements were collected in front face mode using a Spex Fluorolog 1 (Horiba Jobin Yuvan) modified with a Labview operating system. Films were placed in a Janus ST-100 Cryostat which was cooled for 1 hour at the lowest

reported temperature and allowed to equilibrate at each temperature for 15 min at each temperature point before an emission scan was collected. Emission scans were collected and summed to create total intensity as a function of temperature. Break points were determined by minimizing the error resulting from linear regression of the total intensity as a function of temperature.

AFM images were created using a Veeco™ multimode atomic force microscope in tapping mode. Samples that were used to create images were also used for temperature analysis where possible.

RESULTS AND DISCUSSION

To verify that the synthesized dye was sensitive to the environment the dye was mixed with glycerol: ethylene glycol. As the viscosity of the solvent system changed the quantum yield of the dye changed proportional to the change in solvent viscosity. Mixtures of 7:3, 6:4, 4:6, and 3:7 glycerol: ethylene glycol were used to test the sensitivity of the dye to environmental conditions. The decrease in fluorescence as the viscosity decreaes can be seen in Figure 2. Not only does the quantum yield decrease as the viscosity decreases, but the most probable emitted photon energy shifted to lower energy as well. Not only is total quantum yield dependent on the environment but the emission energy is as well. This is due to the drastically changed conformational change the juliodene monomer is capable of undergoing when unhindered by the solvent environment. The twisted excited state conformation is less radiant than the planar excited state as it has less wavefunction overlap. The photophysical properties of the dye as the solvent is changed shows that interaction with the environment changes the emission properties with reproducible results.

114

The most basic measurement of T_g measurement via local fluorescent reporter are the dye and homo polymer co deposited in a thick film. The bulk glass transition was measured for homopolymers and block copolymers using differential scanning calorimetery. The homopolymers showed only one transition, 21 C for poly(B) and -42 C for poly(E).   The block copolymers showed two glass transitions as the sample is thermally annealed to begin the measurement. For the block copolymers the average value for each transition was -44.1+/- 2.4 C for the poly(E) rich region and 20.2 +/- 3.4 C for the poly(B) rich region. This is the average of the bulk value taken over five different batches of individually polymerized material. This is the value that the individual fluorescent reporter temperatures will be compared to and deviations based off of. As can be seen in Figure 3A and 3B when the TICT dye is present within the matrix of polymer E and polymer B there is a drastically different dependence on temperature observed for each system. The optical transition for dye in poly(B) is observed to be 54 C, a difference of +34C from the average reported bulk value. Whereas for the optical transition in poly(E) is observed at -16 which is a difference of +28C from the average reported bulk value. As expected from the DSC results the T_g point in polymer E is much lower than that of the polymer B. The observed Tg values are substantially differ from the bulk observed value. Large deviations, both positive and negative, from the bulk observed Tg have been observed for polymer materials as the repeat unit is confined on the nanoscale. Generally this deviation arises when the film thickness is decreased under 100nm but if the film is in some other way being inhibited in motion, such as bonding or tangled due to disorder such deviations is to be expected.

When the dye is covalently bonded with the host polymer matrix the observed T_g changes with respect to the previous measurements. As can be seen in Figure 4A and 4B for both systems the reported T_g is higher than the dye and host polymer matrix co

115

deposited. This shift in to higher temperature than the dye solvated in the homopolymer system is due to the removal of degrees of freedom in vibrational relaxation or the change in free volume surrounding the dye, however, the . Covalently bonding the dye along the backbone of the polymer does have an effect on the reported temperature because the dynamics being reported are convolved with the dyes position within the host which is perturbed by covalent bonding to the backbone rather than freely associated dye via codeposition. This point is important as the dye reports on the local environment as well as effects from the host matrix as a result of being bonded to the backbone of the polymer.

The transition from homo polymer bound covalently to the TICT to block copolymer system with TICT dye covalently bound should also provide a perturbation of the Tg values. The effect of covalently bonded dye compared to codeposited is pronounced so the modulation of reported T_g by changing from a homo polymer to block co polymer should be equivalently pronounced. Even though the dye is covalently bound in an poly($A_{75}T_1A_{75}B_{150}$) scheme, there will be disorder in the films due to the drop cast (unordered) nature of the film. The disorder within the film should create an increase in the free volume due to the mismatch of fit between the interpenetrating block polymer networks; the increased free volume available to the dye should alter the dynamics reported as a function of temperature. This can be seen as the value of T_g that are reported for the dropcast films of block copolymer are shifted compared to the films containing only homo polymers. The change in reported values from homo polymer to block copolymer can be seen Figure 4A and 4B. Both the poly($E_{75}T_1E_{75}$ B_{150}) and poly($B_{75}T_1B_{75}E_{150}$) reported dynamics shift from the homo polymer values toward an average of the two pure matrix values. Also the poly(ETEB) has two observed transitions, one that is closer to the average temperature and the other is that of the pure

116

system E, indicating that there is some complicated type of phase segregation occurring and the dye is experiencing two different local environments. Figure 5A and 5B both include the results for poly(BTE) which is of interest as the dye is located at the exact interface between the B and E blocks. However the results for this material are complicated as the reported temperature is far too high when compared to any previous result. This is not surprising as we have previously speculated that the dropcast material is a random interpenetrated copolymer network so the interface between these two is unclear and not well defined. Therefor the environments are highly random and the dye is very sensitive to minor fluctuations in local density and chain mobilities thus the dye reports a much more complicated temperature dependence than traditional methods which measures the bulk value of the glass transition temperature. The fact that the reported T_g is higher than any reported value is an indication of a disordered environment due to the mixed environment that surrounds the dye. When the environment is a mixture rather than assembled into blocks an average of both the high and low T_g material. Which means that as the degree of phase segregation increase, the T_g observed trends toward bulk T_g values.

There are substantial disagreements between the DSC and fluorescent methods for disordered films. If the disordered nature of the material is responsible for the disparity between the values reported by values then substantial ordering of the material should affect the T_g reported by the fluorescent method. To show that ordering was occurring during solvent annealing atomic force micrographs were taken of films of each material that had been both dropcast and solvent annealed. Figure 6 shows films characteristic of each material on length scale where the features and repetition are apparent. The AFMs show that the material is clearly changing due to the one day spent in the solvent saturated environment. In the micrographs of the phase image it is assumed that the

117

region which induces a shift in the phase of the forced feedback loop driving the AFM tip is the region containing the benzyl group. As this is the more crystal pendent group; therefore, it will cause a larger perturbation of the phase then less crystaline regions, as has been seen in other AFM characterization experiments. Also the effect of solvent annealing can be seen in each material as the characteristic length scale of morphological features decreases for each material.

The ordering of the material was performed by solvent annealing for twenty four hours. Solvent annealing has been shown to order films as the solvent saturated environment allows for the solvent to repeatedly absorb and desorb which allows the energetic minima to be approached. Twenty four hours was chosen to anneal the films as it was long enough to allow ordering but still remain practical. Figure 6A, 6B, and 6C show the dependence of the quantum yield on temperature for each material that was dropcast or dropcast and then solvent annealed. One of the trends from the comparison of film treatment conditions is that the amount change observed is substantially less. This is due to the ordering as it affects the attenuation of the change. If the film is closer packed (higher density) the change in the amount of change observed will be minimal. For the dropcast films the observed values for T_g of each material was shifted towards the DSC observed (bulk) value. After ordering the T_g of the films are closer to the values returned by DSC. Both of the materials in which the dye is imbedded in a specific block shift away from the previous averaged result and now tend to report a local T_g much closer to the bulk average or that observed in the homo polymer. This indicates that as the intermixing of blocks is decreased the local dynamics tend towards that of the pure phase.

The most important result is that of the material poly(BTE), where the dye is fixed to the interface of the two regions. When randomly cast from solution the T_g temperature was far too indicating some sort of lowering of the free volume and changes

118

in local densities; however, now that the material is better packed the poly(BTE) material shows two distinct transitions. These transitions are close to that of the dye in each individual homo polymer. This means that the dynamics of the interface are contingent on both blocks if the material is sufficiently ordered. This has been observed previously and a numerical value attached to the persistence length of 1-1000nm depending on the conditions attached to the effect.

The observed temperature of the glass transitions within a block copolymer that was annealed, dropcast, polymerized and solvated shows a wide distribution of local dynamics when compared to the bulk measurement. The observed glass transition temperatures for each sample and treatment were compared to the bulk averaged value in Figure 7. Solvent annealing of the film shifts all of the observed glass transition temperatures closer to the bulk indicating that are less disruptions in the system that were shifting the local dynamics in nonsolvent annealed films.

However there is still large scale disorder as can be seen in the AFMs as there is a distribution of sizes of features. Small angle x-ray scattering (SAXS) and grazing incident- small angle x-ray scattering (GI-SAXS) measurements of all preparations of all methods of all films show general amorphous scatter. These are both common techniques to quantify the regular feature size, they fail for this application due to disorder in the films due to incomplete ordering and size distributions created during synthesis. While the ordering has increased due to solvent annealing it has not increased enough to create regular features that create coherent x-ray scatter.

In this report we have detailed dynamic measurements of polymeric materials using a TICT molecule placed within the material in the solid phase. As a polymer material undergoes a glass transition the movements of the material stop happening on the time scale of seconds and move to hours. Depending on whether the material has a

constructive or destructive effect it will affect the change in the change in quantum yield of the dye, it will monotomically decrease as a function of temperature otherwise. Using freely solvated dye co deposited with a homo polymer the temperature of the T_g measured were both shifted higher than the value reported DSC determination for the homopolymer alone. (54 vs 25 C for B and -16 vs -46 C for E) This increase in reported shift of T_g temperature shows that the reported temperature is not exactly measuring the dynamics but it does qualitatively describe the material traits. The exact disagreement is related to the free volume limits of dye that is not exactly intercalated into the homopolymer.

When the TICT dye is covalently incorporated into a homopolymer the results again do not agree exactly. The shift to higher temperature than reported by DSC has increased with covalent incorporation into the backbone of the polymer. (84 vs 25 C for poly(BTB) and -4 vs -46 C for poly(ETE)). This is due to the increased loss in degrees of freedom for the dye to completely incorporate in to the polymer matrix and accurately report the dynamics. However, the qualitative trended noted for the freely solvated dye is still present for the high and low T_g materials.

Instead of a homopolymer a block copolymer system can be studied using a similar analysis. Conceptually the results for materials where the second block is separated (poly(BTBE) and poly(ETEB)) should have no effect on the results and the material of interest is when the reporter is at the interface (poly(BTE)). However, due to entropic contributions, specifically mixing, this is not true. The reported values of the material with a second block added differ substantially from the homopolymers (84 vs 25 C for poly(BTB), poly(BTBE) and -4 vs 12 C for poly(ETE), poly(ETEB)). Both of the values are averaged are shifted away from the homopolymer values because the dye is not surrounded by pure material instead the mix that surrounds the dye provides the muddled result. Also of note is that the poly(ETEB) has two clear transition points, this is

120

most likely due to partial and incomplete demixing of the blocks of the copolymer material during evaporation in the vacuum chamber used for removing solvent. As such, there are two distinct regions created, which vary in how concentrated the low T_g material is within the domain. So the low temperature corresponds to dye that located in a B rich phase and the high temperature transition corresponds to intermixed E and B regions. The material where the dye is bound to the interface provides an interesting result as it is higher temperature than that of any material. This material is not ordered so it most likely bound in an intermixed state far from equilibrium which skews the results away from being meaningful.

The amount of mixing for materials cast from solution can be changed using several methods. In this paper we chose to use solvent annealing as it does not affect the chemical properties and still orders the material reliably and consistently. The effects of solvent annealing can be seen using atomic force microscopy. The characteristic length of morphological properties decreases for each material. This shows that the domains are becoming more pure in material composition and therefore packing tighter and more evenly.

The solvent annealing affects the morphological features of each material, but what is the effect on the T_g as reported by the TICT dye for these materials? There is no reason to think that values should stay the same, and they do not. For each material where the reporter dye is bound to a specific region (poly(BTBE) and poly(ETEB)) the observed values for the glass transition temperature are substantially closer to that the homopolymers (poly(BTBE) and poly(ETEB)). This indicates that intermixing of the polymers affects the temperature at which phase transitions can be observed. This makes sense from a fundamental perspective if less one material is in proximity of the reporter

than it will have less of an affect. However, the values are not exact which is indicative of not complete phase segregation between blocks.

The most interesting result occurs for the temperature dependence of poly(BTE) occurs when it is solvent annealed. Instead of reporting at far too high a temperature from the non-equilibrium mixed state. Under the more order conditions two transitions are now observed. This implies that when the block copolymer material increases in demixing into two regions which are both more pure than dropcast methods and that the two regions both influence the phase behavior at the interface. This is the first step in determining the coherence length of one region on another as this system has demonstrated monomeric control over the placement of the reporter dye which is roughly 5.5 angstoms (the spacing of one repeat backbone unit) or on the order of the most sophisticated material characterization techniques.

We have shown the effect of ordering on block co polymer films glass transition temperature. Using a fluorescent reporter covalently bound to the block copolymer system, the local report provides insights that are not readily available through more traditional methods.

CONCLUSIONS

The dynamics of block copolymers has been integrated using covalent modulation of the location of a fluorescent reporter probe. TICT dyes report on the environment in which they are placed. We have shown that in high ("B") and low ("E") T_g material the temperature dependence of the quantum yield will reflect which that of the material. This was done by codeposition of the dye and polymer material. The act of incorporating the reporter dye into the backbone a polymer changes the observed T_g. This is due to the

reduction of degrees of freedom for the TICT molecule to replanarize, or free volume, or nanoconfinement. In both the B and E regions temperature dependence plots show a higher glass transition point than when freely solvated. When comparing the addition of a co polymerized block physically separated from the reporter molecule a presents a more complicated problem in that random deposition of material leads to intermixing of E and B regions. This causes the reported T_g values to shift closer to the average of the separate regions. The disorder of the material can be decreased by solvent annealing for 24 hours. The reported T_g values shift much closer to the values reported by differential scanning calorimetry. The increase in order can also be verified using atomic force microscope imaging to determine the characteristic morphology.
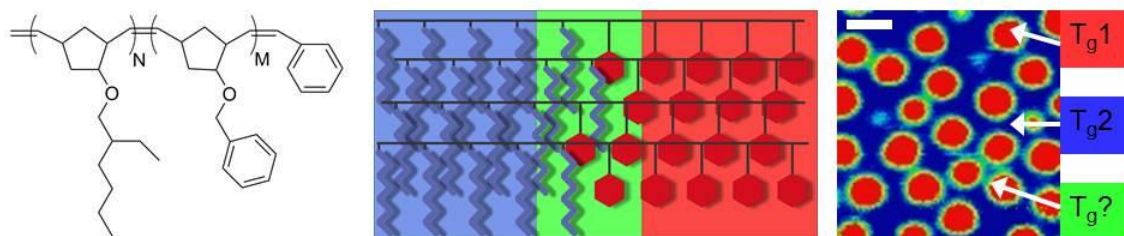
Figure 1. Shows the general schematic for the block copolymer system. The 2-ethylhexal substituent is shown in blue while the benzyl substituent is shown in red. Atomic force microscope image on the right show topography and phase are shown for a representative of the phase segregation.
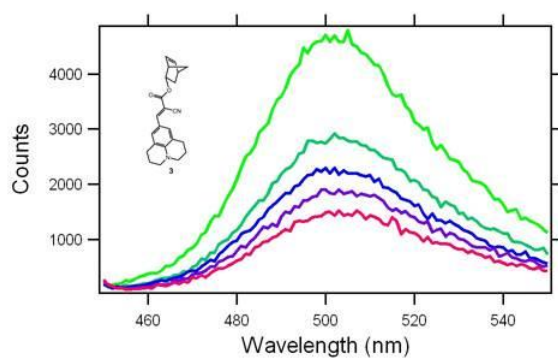
Figure 2. Shows the photophysics associated with the fluorescence of the TICT monomer in 3:7, 4:6, 5:5, 6:4, 7:3, mixture of glycerol and ethylene glycol at room temperature. The decrease in total fluorescence is correlated to the increase in viscosity.
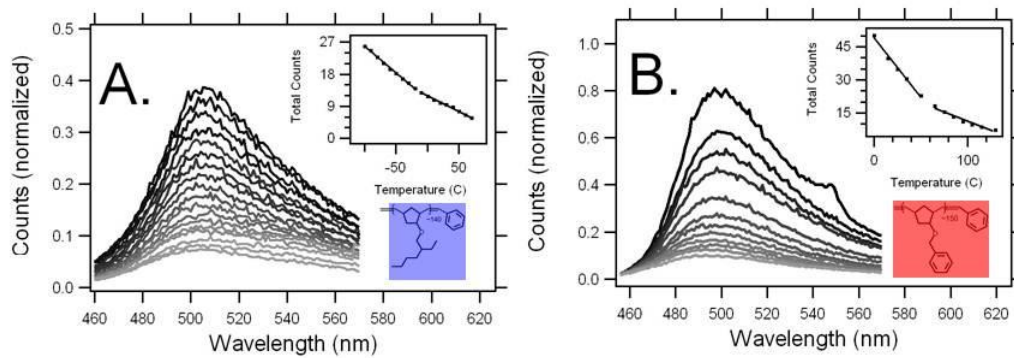
Figure 3. (**A**.) Shows the temperature dependence of fluorescence of TICT dye in the benzyl substituent. The inset shows the summed intensity as a function of temperature with linear fits. (**B**.) Shows the TICT dye fluorescence as a function of temperature. The inset shows summed intensity with linear fits.
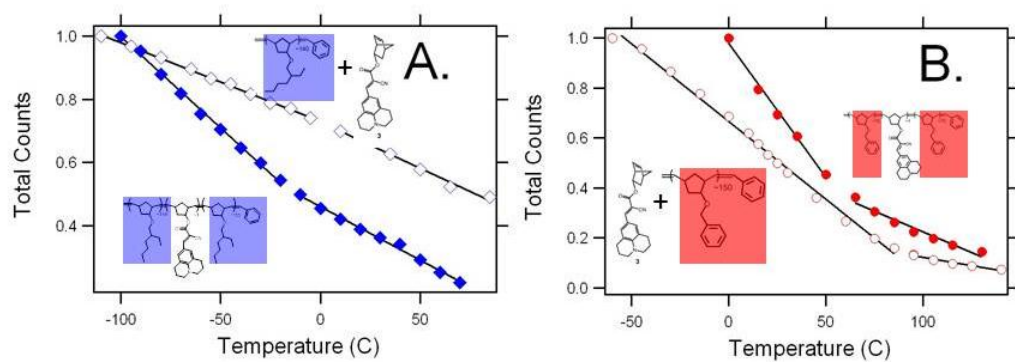
Figure 4. (A.) Shows the summed intensity of the fluorescence as function of temperature for the TICT dye dissolved in region poly(E), (open diamond) and copolymerized in poly(ETE), (closed diamond) (**B**.) Shows the summed fluorescence as a function of temperature for the dye dissolved in polymer poly(B), (open circles) and copolymerized as poly(BTB), (closed circles).
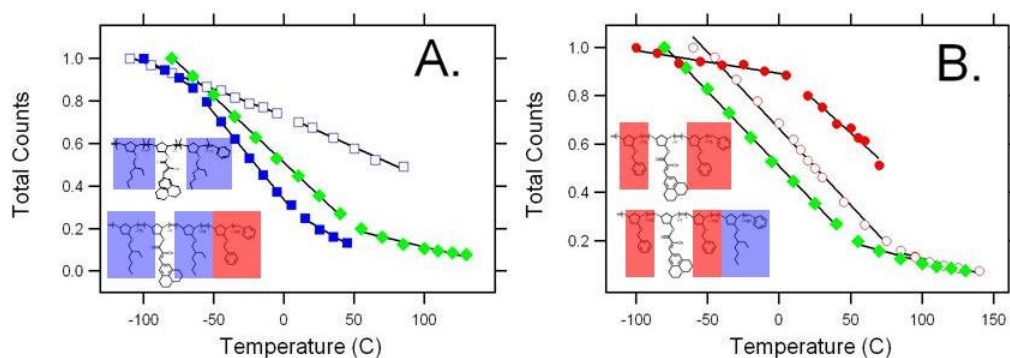
Figure 5. (**A**.) Shows the summed intensity of the fluorescence as function of temperature for the TICT dye polymerized in the "E" region. Poly(ETE), (open squares) and poly(ETEB), (closed squares) are compared to poly(BTE), (green). (**B.)** Shows the summed fluorescence as a function of temperature for the TICT dye polymerized in the "B" region. Poly(BTB), (open circles) and poly(BTBE), (closed circles) are compared to poly(BTE), (green) where the dye is covalently bound to the interface.
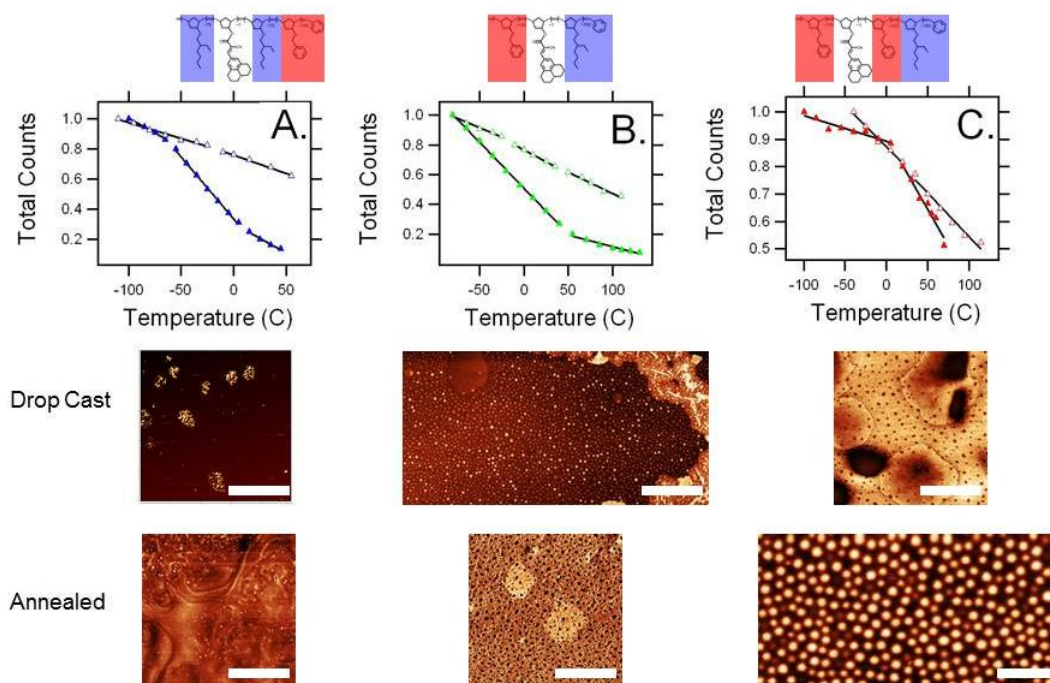
Figure 6. (**A**.) Shows the summed fluorescence as a function of temperature for dropcast (closed diamonds) and solvent annealed (open diamonds) for poly(ETEB). Solvent annealing orders the film and only one inflection point is observed as the film is increased in order. (**B.)** Shows the summed fluorescence as a function of temperature for dropcast (closed triangles) and solvent annealed (open triangles) for poly(BTE). (**C.)** Shows the summed for the TICT dye polymerized in the "B" region for dropcast and solvent annealed films. Dropcast (closed triangles) and solvent annealed (closed triangles) show the effect of order on the temperature dependence of fluorescence. AFM images are shown below temperature dependence graphs to image the ordering effect of solvent annealing.

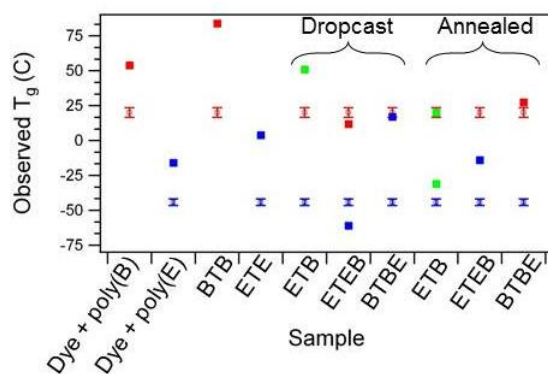**Figure 7.** Shows the observed glass transition measurements for both the bulk measurements from differential scanning calorimetery (open squares) and from the local fluorescent reporter (filled squares). Transitions associated with the B rich region are shown in red while the transitions associated with the E rich region is blue. Transitions observed specifically for the interface are shown in green.

REFERENCES

(1)   Lehn, J. M. *Supramolecular Chemistry: Concepts and Perspectives*; VCH: Weinheim, Germany, 1995.

(2)   Lehn, J. M. *Science* **2002**, *295*, 2400.

(3)   Hoeben, F. J. M.; Jonkheijm, P.; Meijer, E. W.; Schenning, A. *Chemical Reviews* **2005**, *105*, 1491.

(4)   Elemans, J. A. A. W.; Van Hameren, R.; Nolte, R. J. M.; Rowan, A. E. *Advanced Materials* **2006**, *18*, 1251.

(5)   Eisele, D. M.; Knoester, J.; Kirstein, S.; Rabe, J. P.; Vanden Bout, D. A. *Nat. Nanotechnol.* **2009**, *4*, 658.

(6)   Eisele, D. M.; von Berlepsch, H.; Böttcher, C.; Stevenson, K. J.; Vanden Bout, D. A.; Kirstein, S.; Rabe, J. P. *J. Am. Chem. Soc.* **2010**, *in press*.

(7)   Weber, C.; Eisele, D. M.; Rabe, J. P.; Liang, Y.; Feng, X.; Zhi, L.; Müllen, K.; Lyon, J. L.; Williams, R.; Vanden Bout, D. A.; Stevenson, K. J. **2010**, in press.

(8)   Lyon, J. L.; Eisele, D. M.; Kirstein, S.; Rabe, J. P.; Vanden Bout, D. A.; Stevenson, K. J. *J. Phys. Chem. C* **2008**, *112*, 1260.

(9)   Scholes, G. D.; Rumbles, G. *Nat. Mater.* **2006**, *5*, 683.

(10)   Hill, J. P.; Jin, W. S.; Kosaka, A.; Fukushima, T.; Ichihara, H.; Shimomura, T.; Ito, K.; Hashizume, T.; Ishii, N.; Aida, T. *Science* **2004**, *304*, 1481.

(11)   Yamamoto, Y.; Fukushima, T.; Suna, Y.; Ishii, N.; Saeki, A.; Seki, S.; Tagawa, S.; Taniguchi, M.; Kawai, T.; Aida, T. *Science* **2006**, *314*, 1761.

(12)   Jin, W.; Yamamoto, Y.; Fukushima, T.; Ishii, N.; Kim, J.; Kato, K.; Takata, M.; Aida, T. *J. Am. Chem. Soc.* **2008**, *130*, 9434.

(13)   Yamamoto, Y.; Fukushima, T.; Saeki, A.; Seki, S.; Tagawa, S.; Ishii, N.; Aida, T. *J. Am. Chem. Soc.* **2007**, *129*, 9276.

(14)   Cacialli, F.; Wilson, J. S.; Michels, J. J.; Daniel, C.; Silva, C.; Friend, R. H.; Severin, N.; Samori, P.; Rabe, J. P.; O'Connell, M. J.; Taylor, P. N.; Anderson, H. L. *Nat. Mater.* **2002**, *1*, 160.

(15)   Kaiser, T. E.; Wang, H.; Stepanenko, V.; Wurthner, F. *Angew. Chem. Int. Ed.* **2007**, *46*, 5541.

(16)   Lin, H. Z.; Camacho, R.; Tian, Y.; Kaiser, T. E.; Würthner, F.; Scheblykin, I. G. *Nano Letters* **2010**, *online ASAP*.

(17)   Roger, C.; Miloslavina, Y.; Brunner, D.; Holzwarth, A. R.; Wurthner, F. *J. Am. Chem. Soc.* **2008**, *130*, 5929.

(18)	Lang, E.; Sorokin, A.; Drechsler, M.; Malyukin, Y. V.; Kohler, J. *Nano Letters* **2005**, *5*, 2635.

(19)	Lohr, A.; Wurthner, F. *Angew. Chem. Int. Ed.* **2008**, *47*, 1232.

(20)	Lohr, A.; Wurthner, F. *Chemical Communications* **2008**, 2227.

(21)	Hara, T.; Furukawa, K.; Nakamura, T.; Yamamoto, Y.; Kosaka, A.; Jin, W. S.; Fukushima, T.; Aida, T. *Journal of the Physical Society of Japan* **2008**, *77*, 034710.

(22)	Harris, K. D.; Xiao, S.; Lee, C. Y.; Strano, M. S.; Nuckolls, C.; Blanchet, G. B. *J. Phys. Chem. C* **2007**, *111*, 17947.

(23)	Fukushima, T.; Jin, W.; Aida, T. *Journal of Synthetic Organic Chemistry Japan* **2007**, *65*, 852.

(24)	Aida, T.; Fukushima, T. *Philosophical Transactions of the Royal Society a-Mathematical Physical and Engineering Sciences* **2007**, *365*, 1539.

(25)	Didraga, C.; Pugzlys, A.; Hania, P. R.; von Berlepsch, H.; Duppen, K.; Knoester, J. *J. Phys. Chem. B* **2004**, *108*, 14976.

(26)	von Berlepsch, H.; Kirstein, S.; Hania, R.; Pugzlys, A.; Böttcher, C. *J. Phys. Chem. B* **2007**, *111*, 1701.

(27)	von Berlepsch, H.; Kirstein, S.; Bottcher, C. *J. Phys. Chem. B* **2004**, *108*, 18725.

(28)	Knoester, J.; Daehne, S. *Int. J. Photoenergy* **2006**, 1.

(29)	Spitz, C.; Knoester, J.; Ouart, A.; Daehne, S. *Chem. Phys.* **2002**, *275*, 271.

(30)	Womick, J. M.; Miller, S. A.; Moran, A. M. *J. Phys. Chem. B* **2009**, *113*, 6630.

(31)	Womick, J. M.; Miller, S. A.; Moran, A. M. *J. Phys. Chem. A* **2009**, *113*, 6587.

(32)	Milota, F.; Sperling, J.; Nemeth, A.; Kauffmann, H. F. *Chem. Phys.* **2009**, *357*, 45.

(33)	Nemeth, A.; Milota, F.; Sperling, J.; Abramavicius, D.; Mukamel, S.; Kauffmann, H. F. *Chem. Phys. Lett.* **2009**, *469*, 130.

(34)	Oostergetel, G. T.; Reus, M.; Chew, A. G. M.; Bryant, D. A.; Boekema, E. J.; Holzwarth, A. R. *Febs Letters* **2007**, *581*, 5435.

(35)	Linnanto, J. M.; Korppi-Tommola, J. E. I. *Photosynthesis Research* **2008**, *96*, 227.

(36)	de Sa, R. J.; Matheson, I. B. C. *Methods Enzymol.* **2004**, *384*, 1.

(37)	Shafer, M. W.; McKee, G. R.; Schlossberg, D. J. *Rev. Sci. Instrum.* **2008**, *79*, 10F534/1.

(38) Stamatopoulos, V. G.; Karras, D. A.; Mertzios, B. G. *Meas. Sci. Technol.* **2009**, *20*, 104021/1.

(39) Zhao, Y.; Schmidt, M. *J. Appl. Crystallogr.* **2009**, *42*, 734.

(40) Halgren, T. A. *Journal of Computational Chemistry* **1996**, *17*, 520.

(41) Halgren, T. A.; Nachbar, R. B. *Journal of Computational Chemistry* **1996**, *17*, 587.

(42) Halgren, T. A. *Journal of Computational Chemistry* **1996**, *17*, 616.

(43) Halgren, T. A. *Journal of Computational Chemistry* **1996**, *17*, 490.

(44) Halgren, T. A. *Journal of Computational Chemistry* **1996**, *17*, 553.

(45) Schmidt, M. W.; Baldridge, K. K.; Boatz, J. A.; Elbert, S. T.; Gordon, M. S.; Jensen, J. H.; Koseki, S.; Matsunaga, N.; Nguyen, K. A.; Su, S.; Windus, T. L.; Dupuis, M.; Jr, J. A. M. *Journal of Computational Chemistry* **1993**, *14*, 1347.

(46) Zerner, M. C.; Loew, G. H.; Kirchner, R. F.; Mueller-Westerhoff, U. T. *J Am Chem Soc* **1980**, *102*, 589.

(47) Ridley, J.; Zerner, M. *Theoretical Chemistry Accounts: Theory, Computation, and Modeling (Theoretica Chimica Acta)* **1973**, *32*, 111.

(48) Runge, E.; Gross, E. K. U. *Physical Review Letters* **1984**, *52*, 997.

(49) Lyon, J. L.; Eisele, D. M.; Kirstein, S.; Rabe, J. P.; Vanden Bout, D. A.; Stevenson, K. J. *J. Phys. Chem. C* **2008**, *112*, 1260.

(50) HyperChem™, Hypercube, Inc., 1115 NW 4th Street, Gainesville, Florida 32601, USA; unpublished data. B. L. Iverson

(51) Lenhard, J. R.; Hein, B. R. *The Journal of Physical Chemistry* **1996**, *100*, 17287.

Vita

Craig Cone was born in southwest Colorado to a close and wonderful family. He attended college at Regis University, in Denver, Colorado. He graduated in 2005 with a bachelor of science in chemistry and mathematics as well as general honors. It was in Denver that he also met his now wife with whom he graduated college. She was kind enough to agree to marry him and they were married in September 2007. They now make their home in Austin along with a mildly well behaved labrador/poodle mix named Ella who is never disappointed when you come home.

Permanent address: 11112 Liberty Farms Drive, Austin TX, 78754. Or at CraigCone@mail.utexas.edu

This dissertation was typed by Craig William Cone.